The hydrothermal system of the Miocene volcanic rocks of Western Lesbos, Greece

by
Alexis Imperial

A Thesis Submitted to
Saint Mary's University, Halifax, Nova Scotia
in Partial Fullfillment of the Requirements for
a Bachelor of Science, Honours Geology.

December 2017, Halifax, Nova Scotia

Approved: Dr. Georgia Pe-Piper
Professor of Geology

Date: December 2017

The hydrothermal system of the Miocene volcanic rocks of Western Lesbos, Greece

Alexis Imperial

Abstract

The Sigri Pyroclastic Formation in the western side of the island of Lesbos consists primarily of pumice flows, mud flows and stream conglomerate. Most of the pyroclastic rocks appear to be derived from a caldera near Vatoussa and shows extensive alteration and mineralization. The purpose of this study is to understand the hydrothermal system and determine the origin of the silica-iron-manganese mineralization. Samples were collected from the Jithra Ignimbrite, layered fine-grained sediments underlying the ignimbrite, a zoned nodule from a fault zone, and silicified wood samples from the Sigri Petrified Forest. Rock mineralogy and chemistry were investigated using a petrographic microscope, scanning electron microscope, electron microprobe, Laser Raman spectroscopy, and X-ray powder diffraction. Hydrothermal alteration minerals and assemblages identified from the altered ignimbrite were: (1) *K-feldspar +silica +illite +minor apatite, zircon, TiO_2 minerals*; (2) *jarosite +hematite +amorphous silica* and; (3) *Mn-oxide*. Three different horizons from the underlying sediments show identical mineral assemblage of *smectite +silica +TiO_2 minerals ±monazite, hematite*. The presence of hydrothermal quartz and K-feldspar, kaolinite and smectite are closely similar to the alteration assemblages found in the epithermal system of the Taupo volcanic zone which are created by different types of circulating groundwater. The hydrothermal veins and the zoned nodule are predominantly made up of *silica +iron +manganese* mineralization. The availability of manganese may be related to the decay of organic matter as the study area used to be forested with multiple tree horizons. While the amorphous silica-iron mineralization is mineralogically and chemically comparable to jaspers found in exhalative marine systems. This observation is interesting because there is no evidence for a nearby marine condition in Western Lesbos.

December 2017

ACKNOWLEDGEMENTS

I would like to thank my supervisor Dr. Georgia Pe-Piper for the opportunity to work on this project. Also to Dr. Basilios Tsikouras for his helpful feedback as an external reader. Thanks to Dr. D.J.W. Piper for his field work and aid with the many revisions of the thesis.

I would also like to thank Xiang Yang for the training and assistance with SEM analysis. Thanks to Randy Corney for helping me cut and prepare samples plus his constant help throughout the project. Thanks to Owen Brown for his assistance with the XRD sample slide preparation. Dan MacDonald for his help with the microprobe. Cathy Sedge for showing me how to work the RAMAN. Furthermore, I would like to thank the whole SMU Geology Department for the constant support and valuable advice I received for completing this project.

Research funding was provided by the NSERC Discovery Grant to Dr. Georgia Pe-Piper.

TABLE OF CONTENTS

List of Tables

List of Figures

List of Appendices

CHAPTER 1: INTRODUCTION

The island of Lesbos is located in the northeastern Aegean Sea, separated from Turkey just by the narrow Mytilini Strait. The Petrified Forest of Lesbos is preserved on the western side of the island of Lesbos in the Sigri Pyroclastic Formation (Fig 1.1). The forest was created about 20 million years ago when volcanic material covered and petrified the forest present at the time. The site is now a "Protected Natural Monument" because of its recognized importance to geological and paleontological value, (UNESCO Global Geoparks Network).

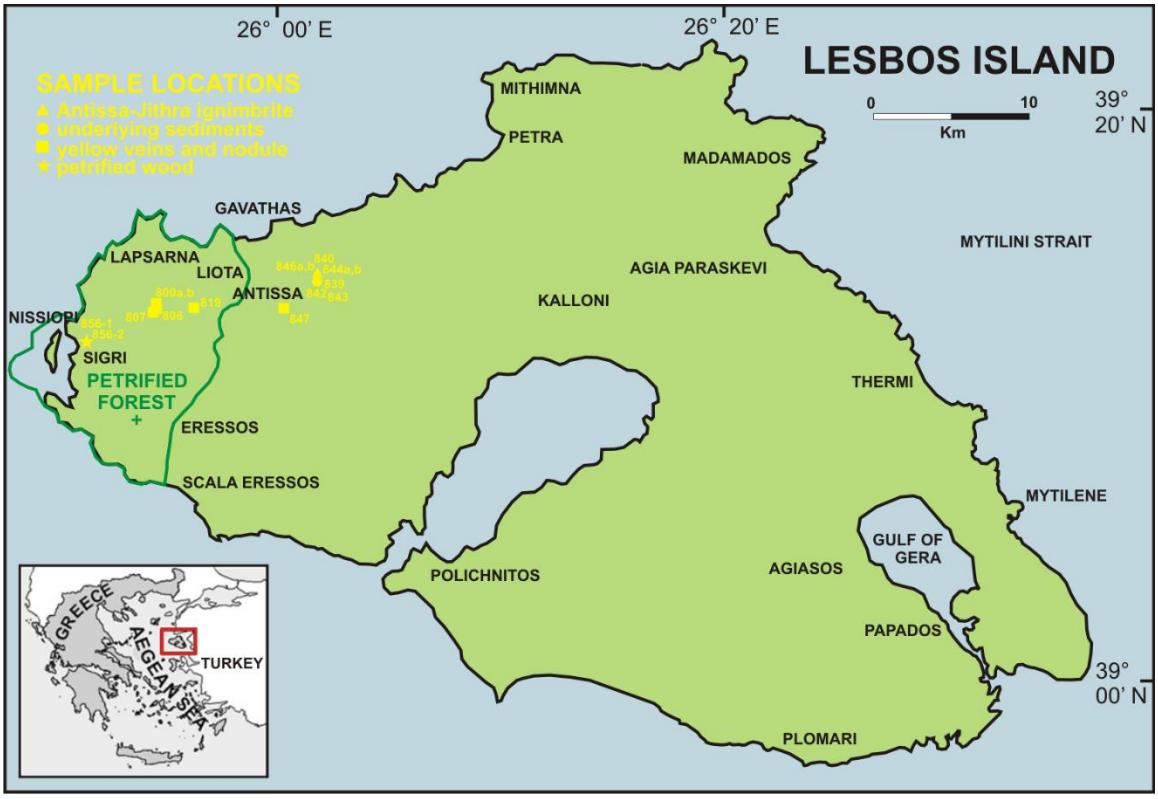

Figure 1.1. Locality map of the study area showing sample locations.

During the Miocene, the whole area of the Aegean was a continental land with intense calc-alkaline volcanic activity that formed a series of volcanoes due to the subduction of

the African tectonic plate under the Eurasian plate. When the products of the volcanic eruptions blanketed the plants of the forest, all the plant organs were covered and was petrified as a result. A huge forest covering the area was covered by volcanic ash and as a result, the trees and other living organic matter at the time were fossilized. The presence of the upright trees suggests that the forest was originally in the area when pyroclastic flows started to happen. This means that the fossilized trees were not moved or transported, but they were rather a native of the area. The petrified trees together with their host pyroclastic rocks exhibit light and dark mineralization and little to extreme alteration.

The objective of the study is to determine the nature of the hydrothermal system in the area and the origin of the silica-iron-manganese mineralization of the fossil trees and their host pyroclastic rocks. This objective was achieved by:

a) Determining what minerals are present in the fossil trees
b) Determining where else such minerals are found and what is their geological setting

In addition, investigation of silica polymorphs in the hydrothermal system was also determined using Raman Laser spectroscopy and the investigation of the differences in the colours of wood petrification was achieved by studying trace elements acquired using a scanning microscope energy dispersive spectroscopy (SEM-EDS) and an electron microprobe dispersive wavelength spectroscopy (EMP-WDS).

CHAPTER 2: GEOLOGICAL SETTING

The Petrified Forest of Lesbos is preserved in the Sigri Pyroclastic Formation on the western side of the island of Lesbos. The island's primary volcanic chain extends from the northeast to southwest and is mostly composed of thick Miocene volcanic rocks. These volcanic rocks overlie a Paleozoic metamorphic basement. The western side of the island consists principally of the Sigri Pyroclastic Formation where the Petrified Forest of Lesbos is preserved (Fig. 2.1). The forest comprises silicified tree fossils at multiple stratigraphic levels within the Early Miocene Sigri Pyroclastic Formation. Widespread andesite-dacite domes, the Eressos Formation, intrude and overlie a metamorphic basement and were previously dated near Eressos at 21.6±0.5 Ma (K-Ar, hbl; Pe-Piper & Piper, 1983).

Previous work has shown that the Miocene igneous rocks of the Lesbos Island have an abundance in K-feldspar and a scarcity of quartz, even in rhyolitic composition (Pe-Piper, 1978). The Sigri pyroclastics underlie the Polychnitos ignimbrite at the Vassilika and Nea Kidonia. The island was mapped by Hecht (1972-1976), who recognized the lower lava unit and the upper lava unit separated by felsic pyroclastics rocks. Small late basalt cones, regarded by Hecht as Pliocene were mapped in the east of the island. Pe-Piper refined the stratigraphic sequence using petrology and geochemistry to classify the lava units and by using paleomagnetic stratigraphy as a correlation tool.

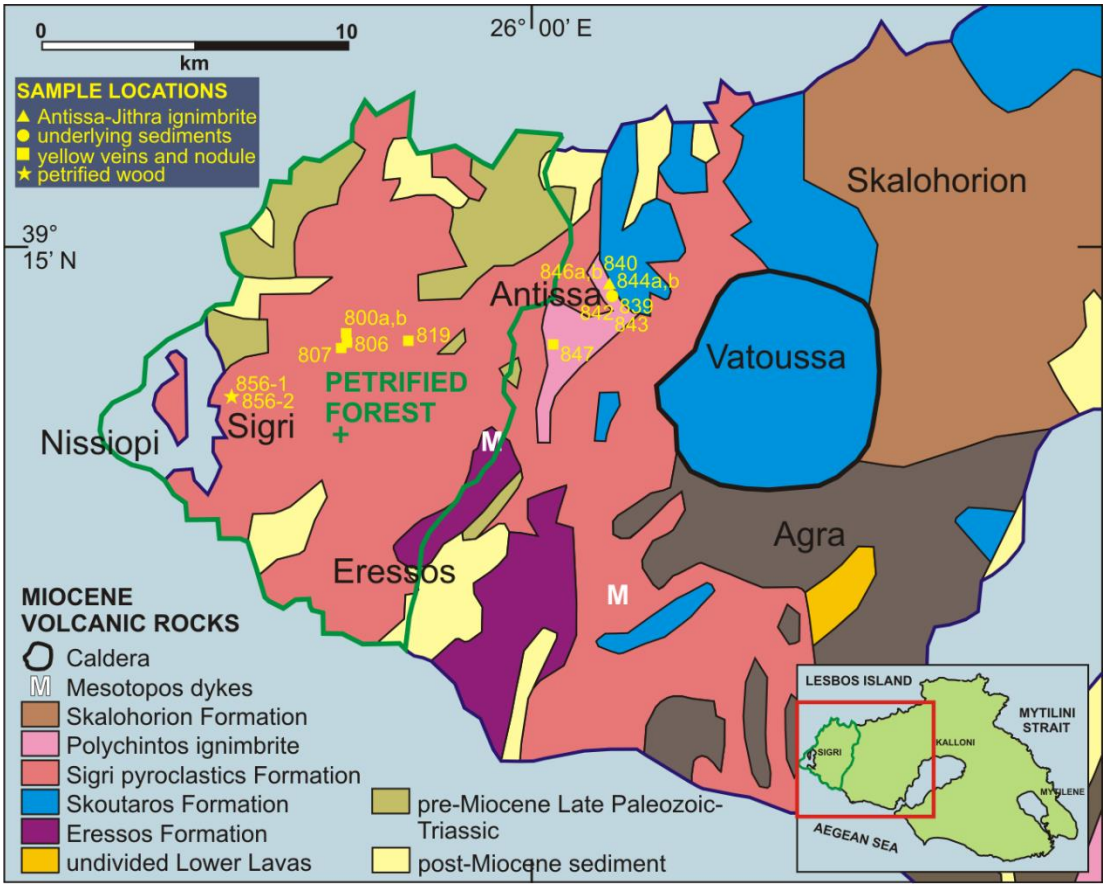

Figure 2.1. Geological map of the western side of the island of Lesbos (map modified from Pe-Piper & Piper, 1981).

The volcanic activity of the island can be summarized by the stratigraphic column in Fig. 2.2. The oldest rocks are mainly highly kaolinitized basalts and andesites known as the Lower Lava Unit. These are followed by shoshonitic andesites and dacites with plugs of rhyolite. On the flanks of the stratavolcanoes, the Lower Lava unit is overlain by agglomerates, tuff, and ashes of the Sigri Pyroclastic Fm. Highly welded ignimbrites overlie the Sigri Pyroclastic Fm. The rhyolites, ignimbrite and the Sigri Pyroclastic Fm. make up the Acid Volcanic Unit (Pe-Piper, 1980).

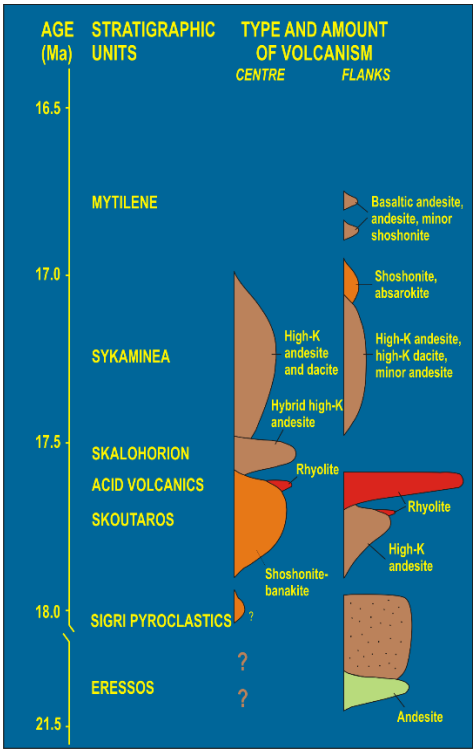

Figure 2.2. Volcanic stratigraphy of island of Lesbos (Pe-Piper and Piper, 1992)

CHAPTER 3: METHODS

Rock samples were collected from the Jithra ignimbrite, the underlying sediments of the ignimbrite, hydrothermal yellow veins cutting across pyroclastic rocks or tree horizons, and a sample from a fossilized tree from the Sigri Petrified Forest. Samples were selected based on the presence of alteration during field observation to identify hydrothermal mineral assemblages present in these rocks.

3.1: Sample Preparation

Sample preparation was mostly done in the geology lab in the Department of Geology at Saint Mary's University. All rock samples brought back from Lesbos were first optically examined to determine significant areas appropriate for cutting. The samples were cut using water and oil-cooled diamond blade rock saws and were sent to Vancouver Petrographics Ltd to be made as polished thin sections.

The polished thin sections of samples analyzed, using the scanning electron microscope (SEM) and the Electron Microprobe (EMP), were carbon coated using a Leica EM CED-030 carbon coater. In contrast, polished thin sections of samples analyzed using the Laser Raman spectroscopy microscope (LRM) were cleaned off of carbon coating by gently rubbing methanol soaked Kim Wipes on the surface of the polished thin sections.

Samples analysed for X-ray diffraction were prepared at Bedford Institute of Oceanography, in Dartmouth. The rock samples were crushed separately by placing them inside an iron crusher and by using a hammer to apply force until the materials were completely pulverized and ready for smear slides. Glass slides were cut into one inch

squares and labeled on the underside. A smear slide is produced by spreading each sample mixed with methanol thinly and evenly across the one inch glass slide. The slides were air-dried until the methanol completely evaporated.

3.2: Analytical Techniques

The samples were analyzed using a variety of techniques: (1) Scanning electron microscope (SEM) for chemical analyses, mineral identification and for textural relationships; (2) Electron microprobe (EMP) for quantitative chemical analyses of minerals; (3) Laser Raman spectroscopy (LSM) for crystal structure determination; and (4) X-ray powder diffraction (XRD) to determine bulk major mineral composition and clay mineral identification. The various analytical techniques used to analyze each samples is summarized in Table 3.1. Mineral abbreviations used in this thesis are after Whitney and Evans, 2010.

Table 3.1. Summary table of analytical techniques performed on the samples.

Group	Sample number	Field rock name	XRD	SEM	EMP	LSM
Hydrothermal veins cutting pyroclastic rocks	800a	yellow mineral		X		X
	800b	yellow mineral		X		
	806	brown vein	X	X		
	807	yellow mineral vein	X	X		
	819	yellow cement in sandstones	X	X		
	847	yellow vein in ignimbrite	X	X		
	846a	"Mn-oxide" veins	X	X	X	X
	846b	"Hematite" veins		X		
Fine-grained sediments	839	white clay	X	X		
	842	black clay	X	X		
	843	red clay	X	X		
Jithra ignimbrite	840a	black glassy ignimbrite		X		
	844a	white altered ignimbrite	X	X		
	844b	white altered ignimbrite	X	X		
Petrified wood	856-1	petrified wood		X		
	856-2	petrified wood		X	X	X

3.2.1: Scanning electron microscope (SEM)

SEM analysis was performed in the Regional Analytical Centre at Saint Mary's University using a TESCAN MIRA 3 LMU Variable Pressure Schottky Field Emission Scanning Microscope. The SEM is equipped with both a backscattered electron detector (BSE) and an INCA X-max 80mm^2 Silicon Drift Detector (SDD) Energy dispersive spectrometer which are able to provide qualitative elemental/phase information and semi-quantitative elemental information respectively about the sample being analyzed. The EDS system has a detection limit of < 0.1%. A pure cobalt plate was used as a standard to calibrate the beam for analysis. The beam has an average diameter of approximately <10 nm and has an X-ray production volume of ~10 μm (depending on the minerals). The

SEM has a maximum resolution of 1.2 nm at 30kV. All analyses were acquired using a power of 20kV.

The Oxford Instrument's INCA program is equipped with a QuantMap package which maps elements based on quantitative elemental compositional data. In this study, QuantMap was used for mapping oxides instead of elements because oxide concentrations are more useful and informative when identifying mineral phases compared to element compositions.

3.2.2: Mineral Identification

For mineral identification, all samples were analyzed using the SEM-EDS. However some minerals were seen to be either amorphous or mixtures of two or more different minerals and therefore it was difficult to identify specific mineral names. Table 3.2 shows various nomenclature used for the unidentified minerals or mixtures for this study.

Table 3.2. Summary table of nomenclature terms used for unidentified minerals or mixtures using the SEM.

Mixture Name	**Composition**	**Characterization**
Mixture 1	Si + Fe	all amorphous gel ± crystallites with a composition of SiO_2 + FeO (Si + Fe)
Mixture 2	Mn + Si ± Fe	all amorphous mixture ± crystallites with a composition of MnO + SiO_2 ± FeO (Mn + Si ± Fe)
Mineral Name		
Silica (Am)	SiO_2	all amorphous silica mineral
Silica (Mc)	SiO_2	all microcrystalline silica crystallites
Silica (Qz)	SiO_2	all silica minerals with noticeable crystal outline
K-feldspar	$K_2O + Al_2O_3 + SiO_2$	all K-feldspar minerals (orthoclase-sanidine)
"Fe-oxide"	Fe ± Si	All opaque minerals mainly of Fe composition with or without small amounts of SiO_2 impurities. However it is still uncertain if Fe is an oxide, hydroxide or a mixture of both
"Mn-oxide"	Mn ± Si ± Fe ± Ba	all minerals with appropriate physical properties and with a composition of Mn with or without Si or Fe, however it is still uncertain if Mn and Fe are either oxides, hydroxides or mixtures. Possible Mn minerals are: Romanechite, Hollandite, and Ferrihollandite

Volcanic glass versus K-feldspar:

Two means of separating volcanic glass and K-feldspar were used in this study. One approach is to look at their morphology and texture. Igneous K-feldspar have defined feldspar crystal outline and crystal habit. In contrast, volcanic glass form either spherulites or shards. However in this study, hydrothermal K-feldspar often replaces volcanic glass which at times would make the first approach unreliable. In this case, we used chemical analyses of fresh volcanic glass from sample 840 (Table 3.3) to separate glass chemically from hydrothermal K-feldspar.

Table 3.3. Representative EDS chemical analyses of fresh volcanic glass from the black glassy ignimbrite.

	SiO_2	TiO_2	Al_2O_3	FeO	MgO	CaO	Na_2O	K_2O	Cl	Total	A.Total
Glass	73.81		14.95	1.06	0.35	1	2.32	6.32	0.21	100	101
Glass	74.78	0.34	15.05	1.16		0.68	1.87	6.14		100	104
Glass	73.77		15.39	1.39	0.39	0.83	2.12	6.11		100	104
Glass	74.12		15.1	1.06	0.31	0.91	2.26	6.24		100	111
Glass	74.3		15.09	1.04		0.99	2.27	6.32		100	109
Glass	73.96	0.32	14.85	1.18	0.36	1	2.23	6.1		100	111
Glass	74.21	0.29	15.15	0.91		0.99	2.15	6.3		100	110
Glass	74.18	0.29	15.12	0.98		0.84	2.35	6.24		100	110
Glass	73.74	0.29	14.94	1.43		0.83	2.37	6.39		100	110
Glass	74.48	0.29	15	0.76		0.82	2.34	6.3		100	111
Glass	74.5		15.05	1.04		0.88	2.32	6.22		100	111
Glass	74.44	0.29	15	0.87		0.8	2.3	6.3		100	110
Glass	74.3	0.32	15.11	0.98		0.9	2.21	6.19		100	109
Glass	75.2		14.07	0.95		0.87	2.07	6.83		100	105
Glass	73.45	0.31	15.03	0.81		0.81	2.7	6.89		100	112
Glass	73.69		14.89	0.78	0.33	0.77	2.68	6.85		100	114
Glass	72.98	0.28	15.04	1.28		0.93	2.8	6.7		100	113
Glass	73.2	0.32	15.02	1.11		0.92	2.7	6.72		100	114
Glass	73.02		15	1.44		1.03	2.71	6.8		100	113
Glass	73.43		14.87	1		0.85	2.89	6.81	0.16	100	116
Glass	73.26		14.97	1.03		1.02	2.92	6.79		100	117
Glass	73.45		14.75	0.98		0.97	3	6.85		100	116
Glass	73.61		15.2	1.07		0.74	2.71	6.66		100	114
Glass	74.26	0.29	14.92	0.31		0.86	2.7	6.67		100	115
Glass	74.32		15.18	0.42		0.59	2.66	6.85		100	118
Glass	74.01	0.36	15.18	0.92		0.86	2.35	6.31		100	110
Glass	74.29	0.29	15.07	0.83		0.89	2.19	6.44		100	111
Glass	74.13	0.31	14.91	0.77		0.76	2.35	6.58	0.19	100	112
Glass	73.6		14.81	1.18		1	2.57	6.66	0.18	100	112
Glass	73.85		14.72	1.27		0.92	2.53	6.71		100	114
Glass	73.23	0.31	14.9	1.39		0.87	2.46	6.85		100	114
Glass	73.47	0.32	15.01	1.05		0.99	2.51	6.65		100	114
Glass	73.46	0.29	15.2	0.74		1.01	2.51	6.8		100	111
Glass	74.06		14.99	0.96		0.79	2.5	6.7		100	112
Glass	73.41		14.68	1.31	0.29	0.94	2.68	6.69		100	112
Glass	73.36	0.32	15.14	1.08		1.03	2.46	6.6		100	114
Glass	73.19		14.96	1.36		0.99	2.78	6.73		100	113
Glass	72.92	0.37	14.82	1.34		0.91	2.87	6.78		100	115
Glass	73.52		14.8	1.17		0.89	2.78	6.83		100	114
Glass	72.58	0.33	14.89	1.45		0.93	2.84	6.81	0.18	100	113
Glass	73.88	0.3	15.12	1.04	0.36	0.8	2.26	6.24		100	115
Glass	74.02	0.29	14.92	0.86	0.44	0.78	2.32	6.36		100	115

3.2.3: Electron Microprobe (EMP)

A petrified wood sample and another sample containing "Mn-oxide" were taken for analysis at the Regional Electron Microprobe Centre at Dalhousie University, in Halifax. Analysis was performed using a JEOL-8200 electron microprobe (EMP) which is equipped with a Noran 133 eV dispersive spectrometer and five wavelength spectrometers. The EMP is also equipped with a wavelength dispersive spectrometer (WDS) and gives more accurate chemical analyses for further precision. This provides a more careful identification of the "Mn-oxide" minerals and a more accurate trace element identification of the petrified wood sample. Separate set of standards were chosen for each of the two samples. The equipment was operated at 15 kV.

3.2.4: Laser Raman Microspectroscopy (LRM)

Laser Raman spectroscopy analyses for samples containing SiO_2 minerals were performed at the Regional Analytical Centre at Saint Mary's University using a Horiba Jobin-Yvon LabRam HR confocal instrument. The LRM uses a 100 mW 532 nm Nd-YAG diode laser from Toptica Phonotics and a Synapse charge-coupled device form Horiba Jobin-Yvon. The LRM uses a maximum of 100x Olympus MPlanN objective for image capture and analysis.

3.2.5: X-ray powder diffraction (XRD)

Quantitative X-ray diffraction analyses were performed at the Geological Survey of Canada (Atlantic) in Dartmouth. Previously prepared samples were carried out on a Siemens Kristaloflex diffractometer using Co Kα radiation. The air-dried samples were

scanned from 2-52 20, with a 0.2 step. Diffractograms were processed using EVA software. Minerals were identified from their characteristic d-spacing (Brown and Brindley, 1980). Table 3.5 summaries the d-spacing of the commonly found minerals in this study.

Table 3.4. Summary of the referenced d-spacing of the commonly found minerals in the study.

Silica									
Alpha quartz	4.26	**3.34***	2.46	2.28	1.80	1.60			
Cristobalite	**4.05***	3.14	2.84	2.49	2.47	2.12	1.87		
Tridymite	**4.30***	**4.09***	**3.80**	3.25	2.48	2.31			
Moganite	**4.43**	**3.39**	**3.34***	3.12	1.83	1.37			
Clay minerals									
Kaolinite	**7.2***	**4.37**	4.19	**3.58**	**1.62**	1.59	**1.59***		
Montmorillonite (smectite)	**15***	**5.01**	**4.50**	3.77	**3.02**	1.70	**1.50**	**1.49**	
Illite	**10***	4.90	**4.45***	**2.55***	1.98				
Feldspar									
Sanidine	**6.50**	**5.80**	4.55	**4.15***	3.90	**3.75***	3.60	3.50	**3.45**
	3.25*	3.20	**2.98**	**2.90**	2.76	**2.55**	2.17	**1.80**	
"Mn-oxide"									
Romanechite	3.47	2.88	2.42	**2.19***	1.82	1.56	1.39		
Hollandite	4.86	3.52	3.46	3.18	**3.14***	**3.10***	3.07		
Hausmannite	4.92	3.09	2.88	2.77	**2.49***	2.46	2.37	2.04	1.54
Todorokite	**9.65***	7.02	**4.82**	**4.48**	3.20	3.07	2.75	2.46	2.42
"Fe-oxide"									
Hematite	3.68	**2.7***	**2.52**	2.21	1.84	**1.69**			
Magnetite	4.85	2.97	**2.54***	2.42	2.10	1.71	1.62		

Notes: **bolded:** intensity = 50-80; **bolded*:** intensity = 90-100

CHAPTER 4: RESULTS

A variety of alteration products related to the Sigri Pyroclastic Formation were investigated from SEM analysis of polished thin sections and by X-ray diffraction. These include altered and fresh samples of the Jithra ignimbrite, at the top of the Sigri Pyroclastic Formation and immediately underlying fine grained sediments including a probable paleosol. Another paleosol at the base of the Sigri Pyroclastic Formation was investigated from island of Nissiopi. Veins and discontinuous nodules in fractures cutting pyroclastic rocks were also sampled and studied: these samples also provided information on the hydrothermal history of the host tuff. Finally, the mineralogical composition of silicified fossil wood was investigated.

In each case, the field setting of the samples is briefly presented, followed by the findings of the SEM-EDS analyses. The X-ray diffraction results and a detailed study of silica types based on Raman spectroscopy and electron microprobe are presented separately.

4.1: Jithra ignimbrite

The Jithra ignimbrite was seen in the field as both fresh (Fig. 4.1A) and highly altered (Fig. 4.1B). The fresh ignimbrite is dark and vitric with large crystals of feldspar and fragments of pumice (Fig. 4.1C), and is situated at the base of the altered Jithra ignimbrite. The altered ignimbrite appears to be bleached and kaolinitized (Fig. 4.1 D). It displays a dark mineral, “Mn-oxide” vein (Fig. 4.1E) and numerous “Fe-oxide” (hematite) veins cutting across it (Fig. 4.1F).

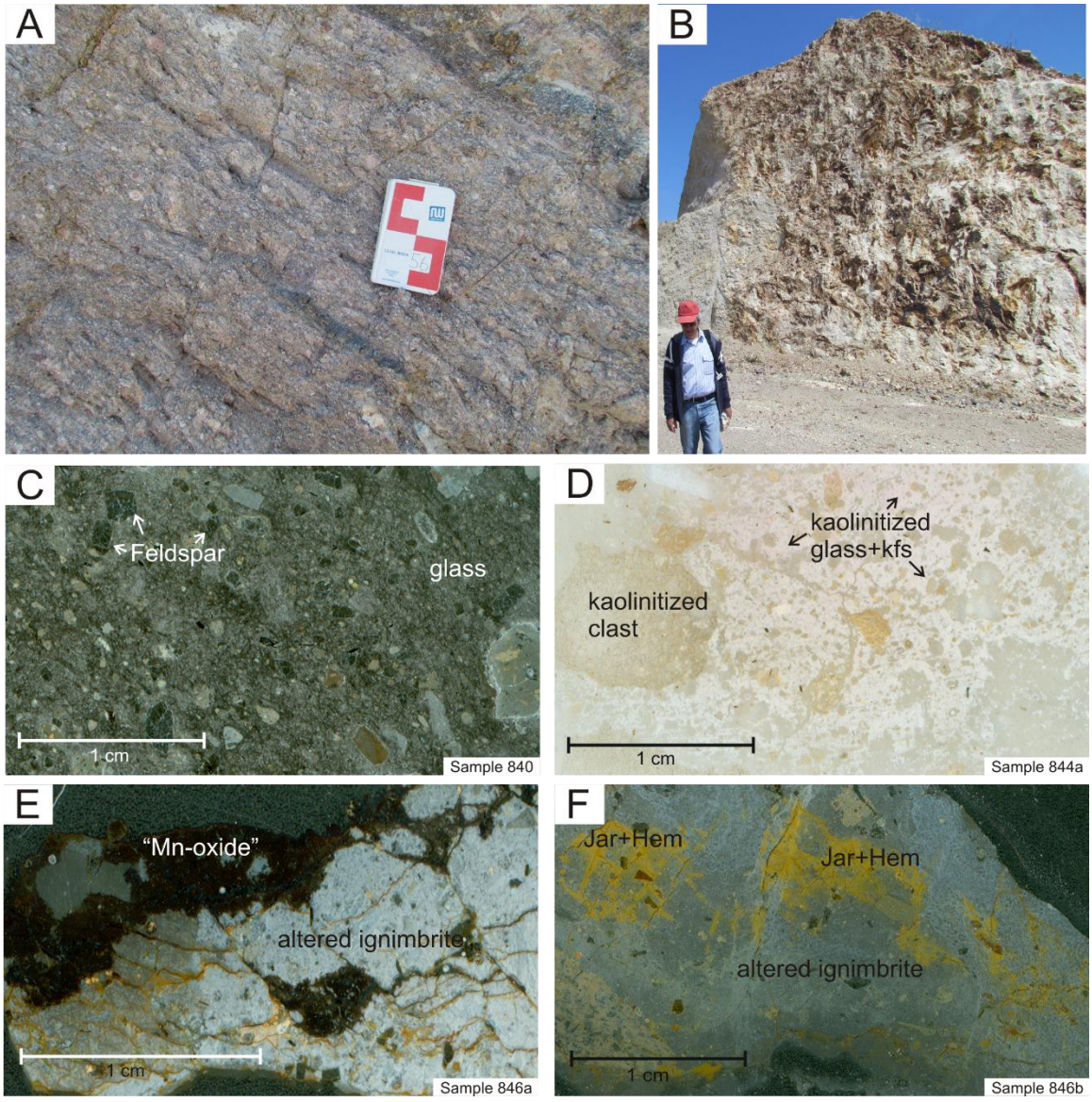

Figure 4.1. Field photographs and scanned thin section images of the fresh and altered Jithra ignimbrite. (A) Field photograph of the fresh, glassy Jithra ignimbrite (sample 840). (B) Field photograph of the bleached altered Jithra ignimbrite (sample 844) showing numerous cross-cutting mineralized veins (samples 846a, b). (C) Scanned thin section of sample 840 showing large crystals of feldspar in glass. (D) Scanned thin section of sample 844a showing the highly kaolinitized ignimbrite. (E) Scanned thin section of sample 846a showing a dark mineralized ("Mn-oxide") vein cutting across the altered white ignimbrite. (F) Scanned thin section of sample 846b showing "Fe-oxide" (jarosite + hematite) veins cutting across the white altered ignimbrite.

4.1.1: Fresh ignimbrite: Sample 840

Sample 840 is a fresh vitric-lithic-crystal ignimbrite situated directly at the base of the altered Jithra ignimbrite. The sample is mostly made up of fresh volcanic glass (Fig. 4.2A) and large crystals of feldspar (Fig. 4.2B). The feldspar are mostly plagioclase with minor K-feldspar. EDS chemical analyses of volcanic glass appear to be very uniform (App. 3, table 3.2). Rare biotite, zircon, apatite, ilmenite and rutile crystals were also present in the sample. Although the sample is predominantly fresh, it shows alteration to montmorillonite (Fig. 4.2C) and rare alteration of glass to barite and apatite (Fig. 4.2D). It also shows occasional alteration to silica and "Fe-oxide".

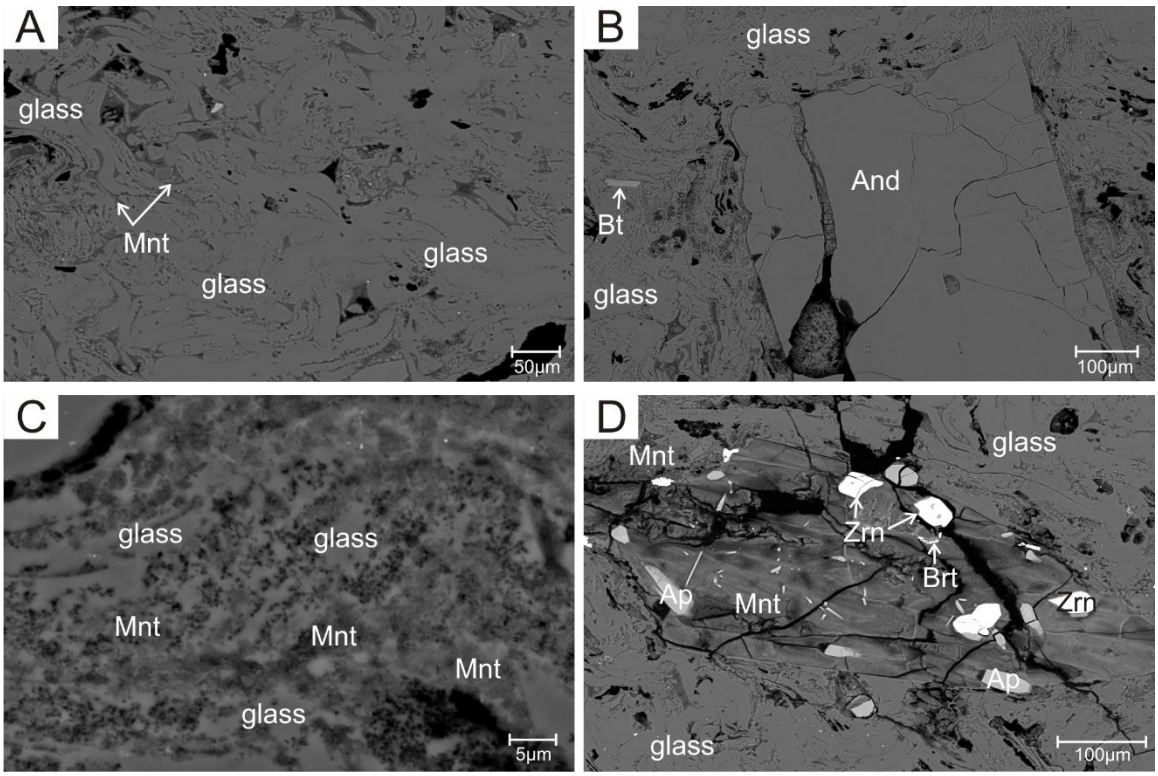

Figure 4.2. Representative BSE images of textures and minerals of the fresh Jithra ignimbrite (sample 840). (A) BSE image of the glassy fresh Jithra ignimbrite. (B) A large phenocryst of Andesine and a small crystal of biotite in glass. (C) Alteration of glass to montmorillonite. (D) Clay alteration (montmorillonite) with rare alteration of glass to apatite and barite.

4.1.2: Altered ignimbrite: Sample 844a, b

The altered Jithra ignimbrite is a highly kaolinitized vitric-lithic-crystal ignimbrite compared to sample 840. Bleaching of the ignimbrite may have been the result from the reduction of Fe ($Fe_2O_3 \rightarrow FeO$). Three main mineral assemblages of hydrothermal origin occurs in the altered Jithra ignimbrite: (1*) K-feldspar + silica + illite/kaolinite + minor apatite, zircon and* TiO_2; (2) *jarosite + hematite + amorphous silica* (sample 846b) and; (3) *"Mn-oxide"* (sample 846a).

The first assemblage mostly occurs as replacement of glass and minerals or direct deposition in fractures. This mineral assemblage was found in samples 844a and 844b. K-feldspar forms well expressed spherulites and is the only feldspar in this study classified as hydrothermal in origin. It appears to be clear of inclusions and seems to have been formed by replacement of volcanic glass.

The formation of these spherulites suggests previous existence of volcanic glass. The spherulites consist of various K-feldspar and amorphous silica proportions, but on average they consist of ~70 vol% silica and ~30 vol.% K-feldspar (Fig. 4.3A) or in reverse, ~70 vol.% K-feldspar and ~30 vol.% silica (Fig. 4.3B) or it consists of K-feldspar with only minor silica (Fig. 4.3C).

The variations in the different spherulite composition suggest that during the formation of spherulites, there was both loss and gain of Si or K at different times depending on different physiochemical conditions.

Another evidence suggesting the existence of volcanic glass are remnants of shards and fragments now mostly composed of K-feldspar with small amount of silica (Fig. 4.3D, E). Dark lines at the center of these shards are always present. Juniper and

Fouquet (1988) suggested that these central lines are “filamentous” microbial structure that provides scaffolding for Fe-silica precipitation. For this study however, it may have been scaffolding for K precipitation. Another theory to explain the presence of these central dark lines may be that the replacement of glass shards started with the crystals nucleating from the margin instead of the core therefore leaving silica patches and a central line as it was happening.

K-feldspar also appears to pseudomorph amphiboles. In this case, there are crystals with hornblende crystal outline but with K-feldspar chemical composition (Fig. 4.3F).

Feldspars:

As mentioned, feldspars present in this sample are mostly hydrothermal K-feldspar compared to igneous K-feldspars and no analysed plagioclase. In comparison, feldspars from sample 840 (fresh ignimbrite) include mostly plagioclase of oligoclase-labradorite composition with only minor K-feldspar. This suggests that hydrothermal K-feldspar has also replaced the magmatic and detrital plagioclase crystals.

Clay minerals:

Clay minerals of hydrothermal origin also occur in this mineral assemblage. Illite has been seen intermixed with silica and contains small amounts of Cl and TiO_2, while kaolinite appears as direct deposition in vugs/amygdules. Kaolinite also replaces K-feldspar and biotite.

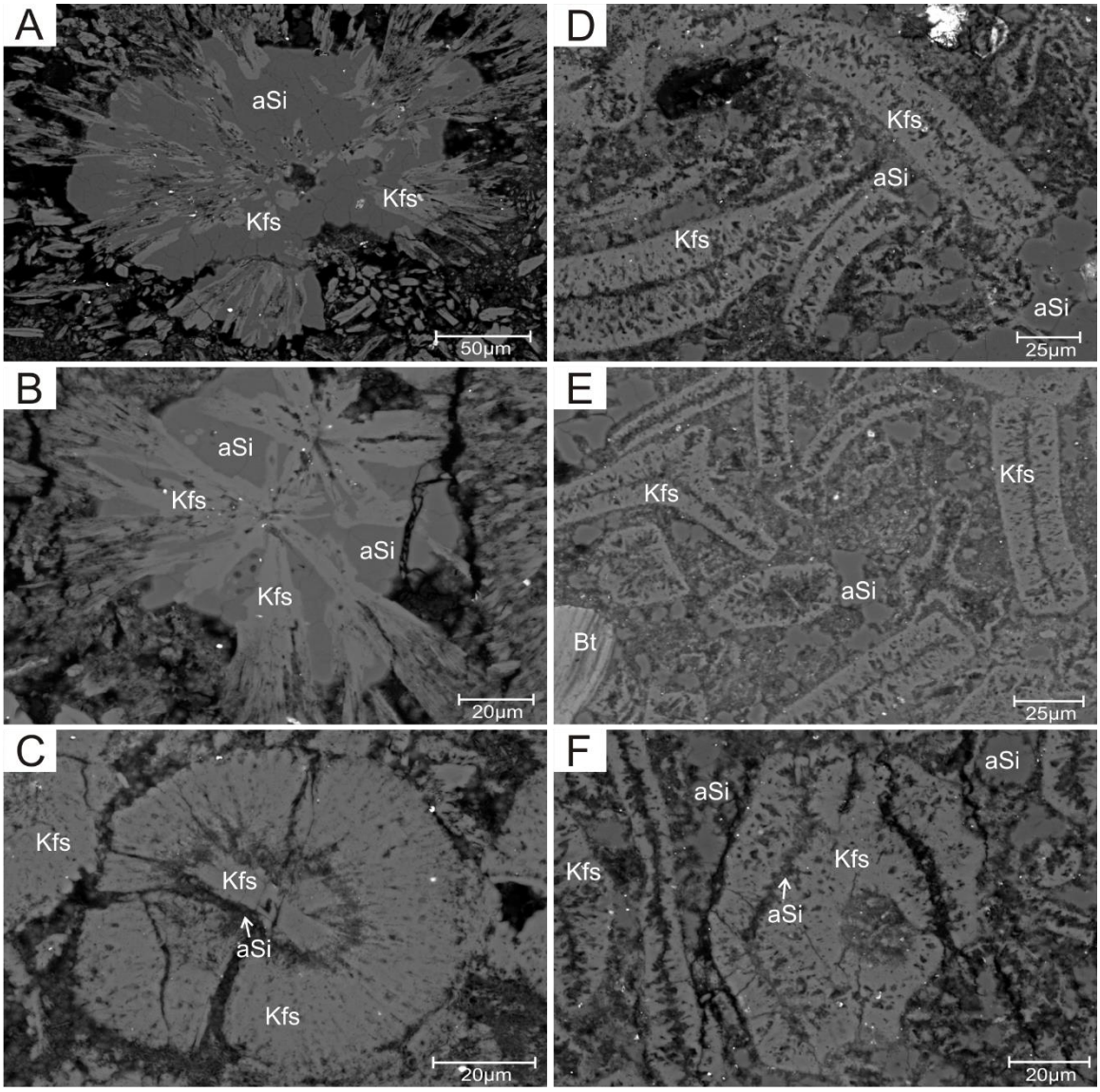

Figure 4.3. Representative BSE images of K-feldspar and amorphous silica textures and occurrences from the altered Jithra ignimbrite (sample 844a,b). (A) Spherulite consists of ~70% silica and ~30% K-feldspar. (B) Spherulite consists of ~70% K-feldspar and ~30% silica. (C) Spherulite consists mostly of K-feldspar and minor silica. (D-E) Glass shards now consists mostly of K-feldspar. (F) Mineral with hornblende crystal outline completely replaced by K-feldspar.

Biotite:

Biotite has been seen as both fresh and altered in the altered Jithra ignimbrite. Texturally, biotite was observed as: (a) ragged crystals surrounded by blocky mineral material glass vs K-feldspar (CS), (Fig. 4.4A); (b) crystals growing within vesicle (CV), (Fig. 4.4B); (c) magmatic fresh-looking crystals in ignimbrite (C), (Fig. 4.4C); ragged crystal in altered ignimbrite (CAI), (Fig. 4.4D). Chemically, biotite was classified into three types based on TiO_2 content: (i) very high value of TiO_2, ~9% (type CV); (ii) normal values of TiO_2, 5-6% (type C) and; low value of TiO_2, <1% (types CS, CAI). Table 4.1 shows biotite analyses from the altered ignimbrite. This sample shows evidence of TiO_2 loss in biotite during alteration.

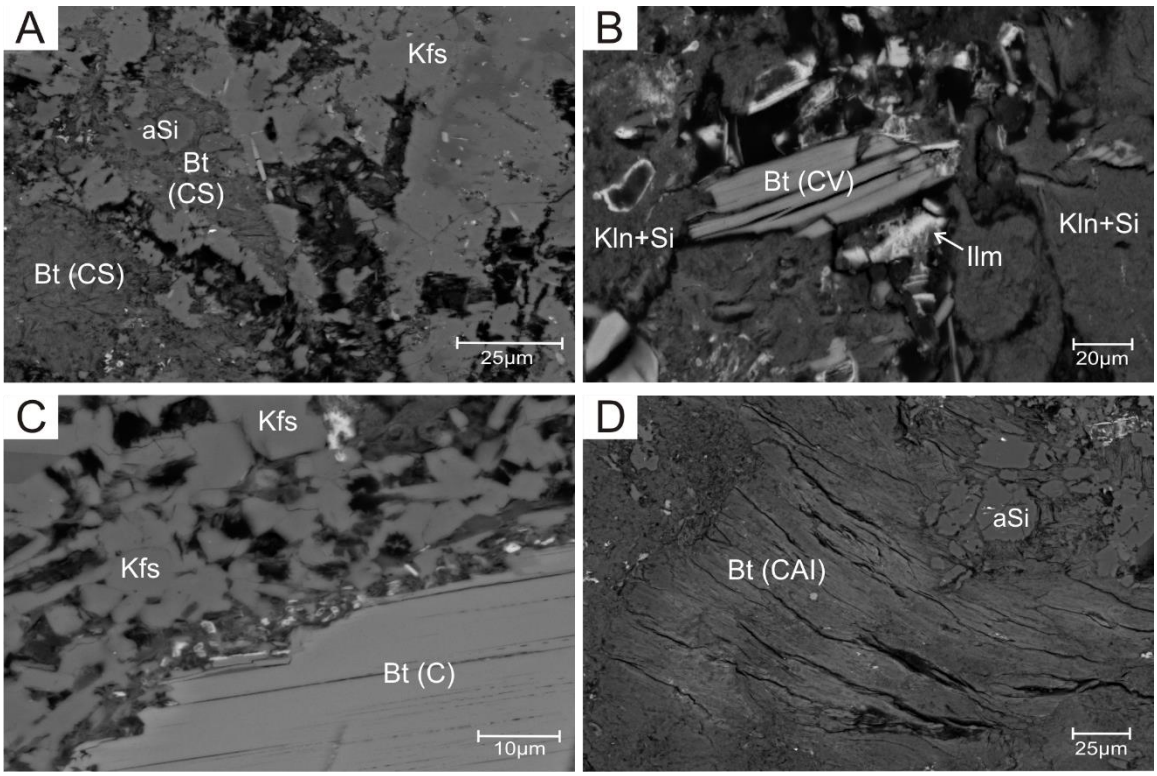

Figure 4.4. Representative BSE images of biotite and their textural relationship from the altered Jithra ignimbrite (sample 844a, b). (A) Altered biotite enclosed by a blockly mineral crystal. (B) A biotite crystal in a vesicle. (C) A fresh crystal of biotite in ignimbrite. (D) A ragged crystal in ignimbrite showing slight silicification.

Table 4.1. Representative EDS chemical analyses of selected biotite crystals in the altered Jithra ignimbrite (sample 844).

	Biotite (C)		Biotite (CAI)				Biotite (CS)			Biotite (CV)
SiO_2	40.39	43.15	44.54	46.59	45.2	44.93	57.94	45.05	47.87	41.94
TiO_2	7.36	5.67	0.32	-	0.28	-	0.95	0.58	0.45	9.29
Al_2O_3	14.95	14.64	15.2	17.49	15.83	14.64	14.45	16.65	18.84	14.46
FeO	9.32	11.08	3.94	3.82	4.14	3.68	7.27	3.68	3.76	7.49
MnO	-	-	-	-	-	-	-	-	-	-
MgO	18.06	16.55	19.34	17.39	18.56	19.5	12.65	17.82	16.1	17.89
CaO	-	-	0.52	-	-	0.42	0.88	0.34	-	-
Na_2O	0.82	0.72	0.45	0.39	0.43	0.52	0.58	0.41	0.41	0.57
K_2O	9.1	8.19	7.28	6.72	7.09	7.45	5.08	6.16	6.38	8.36
F	-	-	8.42	7.43	8.48	8.87	-	9.32	6.18	-
Cl	-	-	-	0.17	-	-	0.19	-	-	-
Total	100	100	100	100	100	100	100	100	100	100

Notes: C= fresh crystal in ignimbrite, CAI= altered crystal in ignimbrite, CS= altered crystal surrounded by K-feldspar and ?glass, and CV= crystal in vesicles.

4.1.3: "Hematite" veins in altered ignimbrite: Sample 846b

The Jarosite + hematite + amorphous silica is the second hydrothermal mineral assemblage observed in the Jithra ignimbrite. This mineral assemblage was seen in sample 846b. The minerals were found either as (a) direct deposition in vugs, (b) as replacement or (c) as direct deposition and replacement along fractures and cleavage planes.

As direct deposition (case a), jarosite fills vugs (Fig. 4.5A) or it occurs together with hematite and amorphous silica in vugs (Fig. 4.5B). In both occurrences, it shows crustiform-colloform textures. In addition, jarosite also fills fractures which are cut by hematite veins (Fig. 4.5C). In case of replacement (case b), jarosite invades and replaces kaolinite (Fig. 4.5D). As direct deposition and replacement (case c), jarosite may: i) replace hornblende, which is already replaced by amorphous silica, along its cleavage planes (Fig. 4.5E); ii) jarosite precipitates in fractures, but it also replaces oligoclase (Fig.

4.5F, 4.6A); iii) jarosite precipitates in fractures with gradual replacement of amorphous silica (Fig. 4.6B, Fig 4.6C).

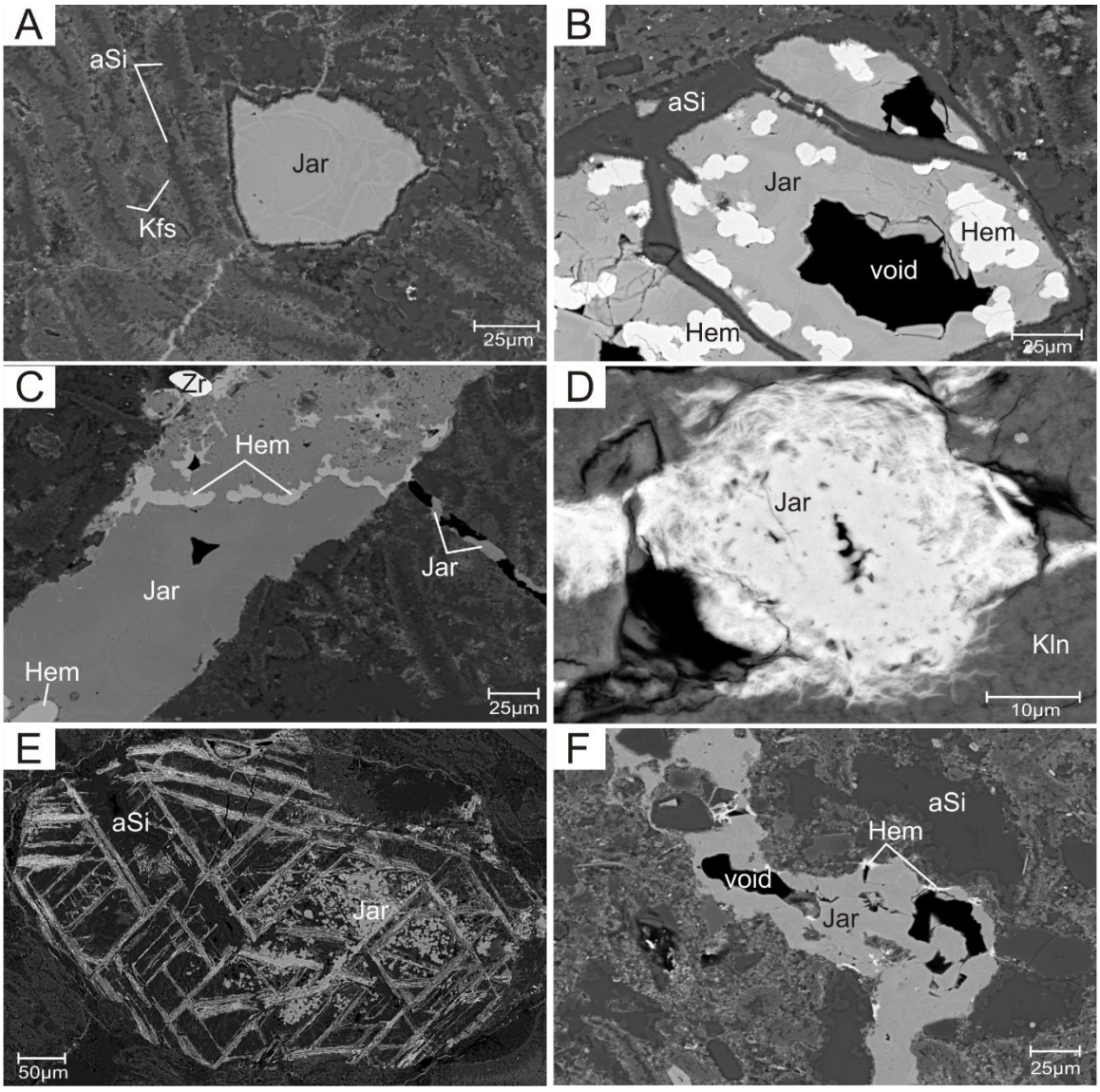

Figure 4.5. Representative BSE images of Jarosite occurrences and textures from the altered Jithra ignimbrite (sample 846b). (A) Jarosite fills a vug. (B) Jarosite + hematite + silica filling a vug. (C) Jarosite fills a fracture which is cut by hematite. (D) Jarosite invades kaolinite. (E) Jarosite replaces hornblende which has been previously replaced by silica. (F) Jarosite precipitates in fractures.

4.1.4: "Mn-oxide" vein in altered ignimbrite: Sample 846a

The third hydrothermal mineral assemblage observed in the Jithra ignimbrite is the occurrence of "Mn-oxide" observed in sample 846a. "Mn-oxide" occurs either as direct deposition in veins and vugs or as direct precipitation and ?replacement.

In case of direct deposition, "Mn-oxide" was seen as a vein filling fractures that cut kaolinite (Fig. 4.6D). "Mn-oxide" was also seen filling vugs that appeared to be banded (Fig. 4.6E). In higher magnification (Fig. 4.6F), such vugs have different zones where Fe-oxide/hydroxide is followed by "Mn-oxide" in several zones of different backscatter brightness with crustiform-colloform-banded textures. No amorphous silica rimming has been seen, instead often there is an empty zone that may be due to dissolution or volume reduction of the protolith after the precipitation of "Mn-oxide". The different zones also give the same "Mn-oxide" composition, but with very low totals suggesting empty spaces or high porosity (App.1, Table 1). Therefore the light and dark zones/bands that "Mn-oxide" formed in the vugs seem to be due to different sizes in mineral particles that resulted in different zones of porosity. An X-ray map of Fig. 4.6E (Fig. 4.7) also shows that the porous zones have the same "Mn-oxide" chemical composition throughout the different zones. The formation of these different zones in "Mn-oxide" may be related to different crystallization rate.

In the case of direct precipitation and replacement, Fig 4.6E shows kaolinite occupying the inner most zone of the cavity. Because of this, it can be argued that kaolinite was the last to form. However in Fig. 4.6D, "Mn-oxide" was seen to cut kaolinite. It may be that kaolinite is dissolving and is creating a cavity in which "Mn-oxide" precipitated.

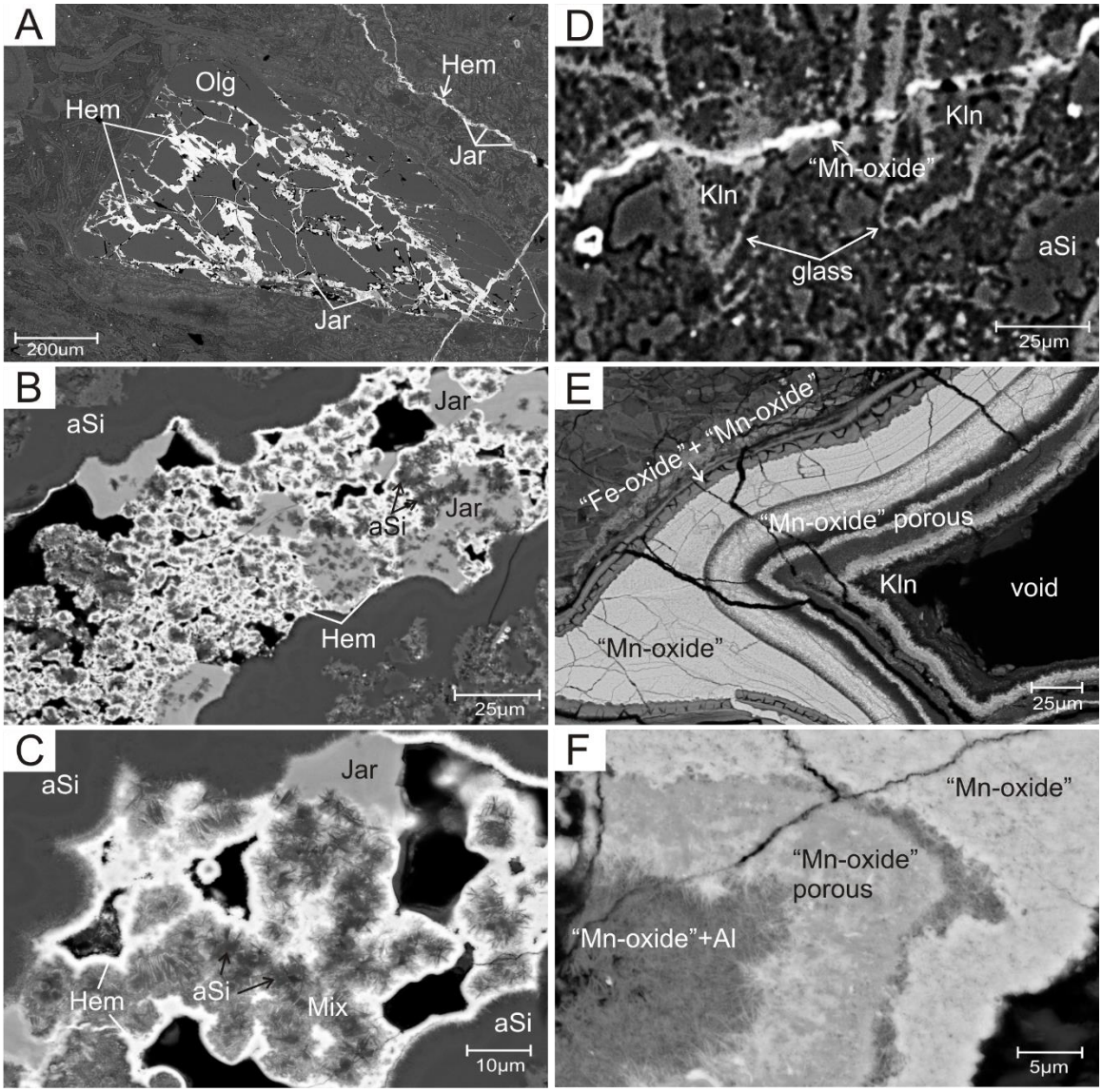

Figure 4.6. Representative BSE images of occurrences of Jarosite and "Mn-oxide" from the altered Jithra ignimbrite (samples 846b, a). BSE images of different occurrences of jarosite in sample 846b (A-C) and BSE images of "Mn-oxide" occurences in sample 846a (D-F). (A) Jarosite filling fractures in oligoclase. (B-C) Jarosite with hematite filling fractures with gradual replacement of silica. (D) "Mn-oxide" fills fracture that cut kaolinite and glass. (E) "Mn-oxide in vug showing zones of different backscatter brightness. (F) High magnification of "Mn-oxide" showing the different zones of porosity.

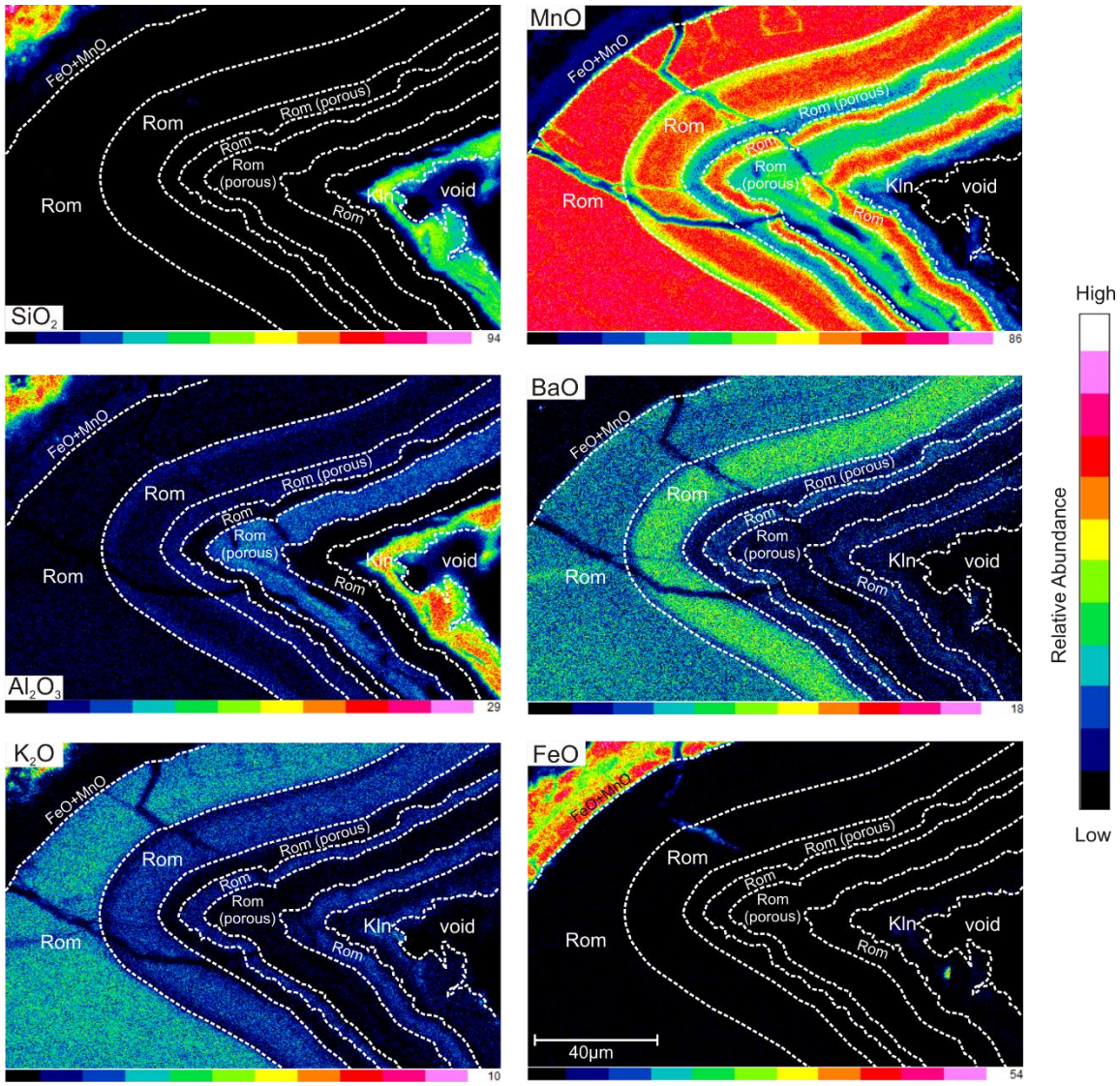

Figure 4.7. X-ray compositional map of "Mn-oxide" from the altered Jithra ignimbrite (sample 846b).

4.1.5: Summary: Jithra ignimbrite

The altered Jithra ignimbrite, compared to the fresh ignimbrite, exhibits extreme alteration that may have been the result of Fe_2O_3 to FeO reduction which is commonly associated with silification. It shows evidence of devitrification, where crystals grew more or less radially from randomly distributed spots, forming patches that resemble snowflakes or the development of spherulites. Devitrification of glass shards with crystals

nucleating from the margins of the shards was also observed. The main product of devitrification are K-feldspar and amorphous silica which forms abundant spherulites in the altered Jithra ignimbrite.

Feldspar and biotite are both present as igneous and hydrothermal minerals. Plagioclase feldspar which is only present in the fresh ignimbrite, is magmatic and varies from oligoclase to andesine in composition (App. 3). K-feldspar is usually an alteration product with contaminants of SiO_2 and FeO. SiO_2 and MgO contents increase whereas K_2O and FeO decrease with increasing alteration of biotite. The altered biotite also seems to have lost almost all of its TiO_2. Both K-feldspar and biotite are altered to kaolinite.

Kaolinite have elevated contents of one or more of the element/s: SiO_2, FeO, MgO and K_2O probably depending on what is replacing and what new minerals are forming. Overall the Jithra ignimbrite shows alteration by silicification (silica), potassic alteration (K-feldspar) and kaolinitization (kaolinite).

The “hematite” veins cutting across the altered Jithra ignimbrite appears to be not just hematite but an association of “Fe-oxide” (hematite) + jarosite + amorphous silica. Jarosite appears to be a hydrothermal mineral and not a low temperature alteration from pyrite. They are commonly seen in vugs and accessible pathways such as open fractures of rock and cleavage planes of mineral crystals. Based on the textural relationships observed, jarosite and hematite appear to precipitate simultaneously after silicification occurred.

The “Mn-oxide” vein was mostly seen as direct deposit in vugs and fractures. The vein appears to be texturally banded based on size particles and not chemically.

4.2: The fine-grained sediments underlying the Jithra ignimbrite

The fine-grained sediments underneath the Jithra ignimbrite appear to be stratified and can be separated into three layers based on their color: a white layer, a red layer, a grey layer and a black sediment layer (Fig. 4.8A). The white layer (sample 839) is made up of white clay with visible crystals of biotite and feldspar (Fig. 4.8B). The black layer (sample 842) is mostly made up of a black clay mineral with no noticeable crystals (Fig. 4.8C). The red layer (sample 843) is made up of red clay with tiny crystals of opaque minerals (Fig. 4.8D).

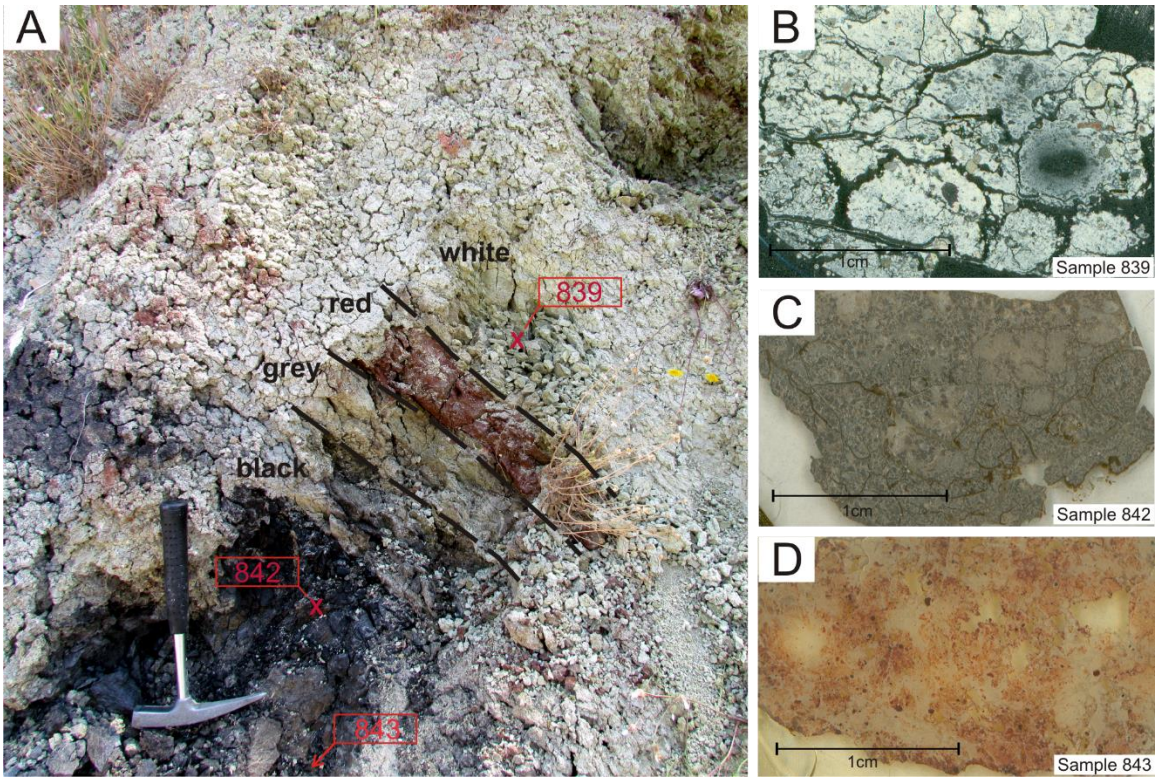

Figure 4.8. Field photograph and scanned thin section images of the layered fine grained sediments underlying the Jithra ignimbrite. (A) Field photograph of the clays underlying the Jithra ignimbrite showing three layers of colored sediment, white (sample 839), black (sample 842) and red (sample 843). (B) Scanned thin section of sample 839 showing the white clay layer. (C) Scanned thin section of sample 842 showing the black clay layer. (D) Scanned thin section of sample 843 showing the red clay layer.

4.2.1: White layer: Sample 839

The texture of sample 839 shows that it probably originates from a lithic-crystal tuff that has been altered to clay with some silica. The sediment is white in color and is mostly made up of detrital crystals of K-feldspar, plagioclase (oligoclase-andesine), apatite, zircon, ilmenite, rutile and quartz. Plagioclase and biotite crystals appear to alter to smectite (Fig. 4.9A). Two different lithic clasts were observed, andesite-dacite lava and a feldspathic crystal tuff (Fig. 4.10B).

Silica, monazite and TiO_2 minerals occur as alteration minerals together with smectite. This hydrothermal mineral assemblage in this sample occurs as a direct deposition of monazite along pathways of weakness, due to mineral weakness such as crystal boundaries and cleavage planes. It also occurs as replacement of various mineral grains by smectite in four different ways: (i) replacement of phenocrysts and microphenocrysts of plagioclase (Fig. 4.9B); (ii) replacement along cleavage planes of biotite (Fig. 4.9C); (iii) replacement of matrix in the protolith tuff/tuffite; and (iv) replacement of glass fragments (Fig. 4.9E). Similar to smectite, silica is seen as a replacement of plagioclase microphenocrysts in lithic clasts (Fig. 4.9D) and glass fragments (Fig. 4.9F) or silica is in the groundmass (Fig. 4.9C) intermixed with smectite which explains the high SiO_2 content of smectite analyses (App. 3, Table 3.3).

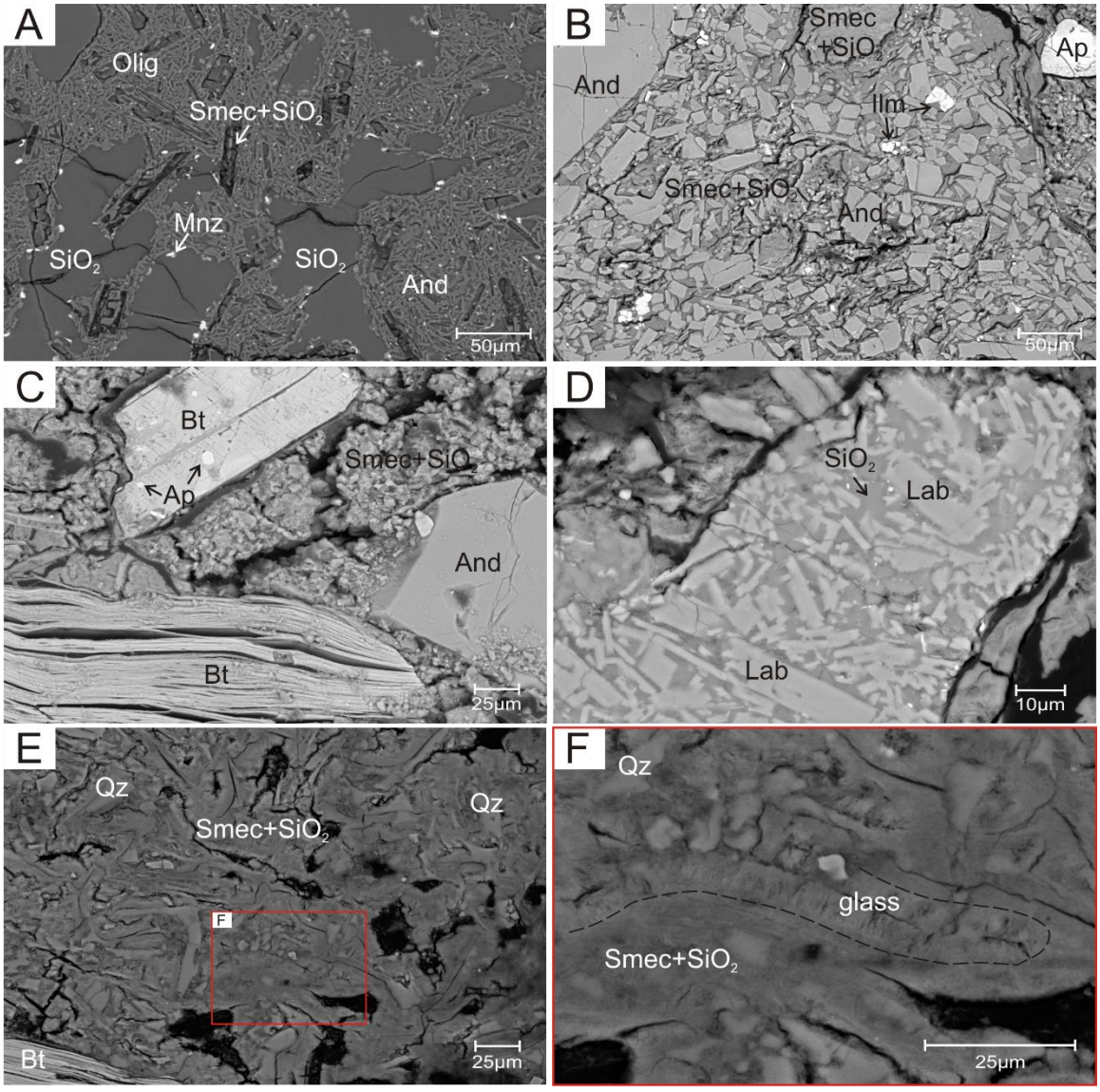

Figure 4.9. Representative BSE images of textures and minerals from the white layer of the fine grained sediments underlying the Jithra ignimbrite, sample 839. (A) Crystals of monazite precipitating along crystal boundary. (B) A feldsphatic crystal tuff showing smectite in the matrix. (C) Smectite present in the groundmass as well as along the cleavage planes of biotite. (D) Silica replacing phenocrysts and microphenocrysts of plagioclase. (E) Smectite replacing glass fragments with detrital crystals of quartz and biotite. (F) High magnification of Fig. E showing the replacement of glass fragments.

4.2.2: Black layer: Sample 842

Sample 842 is black and consists of predominantly smectite with tiny grains of silica (quartz) (Fig. 4.10A) and minor amount of relics of other detrital minerals that include K-feldspar, plagioclase, monazite, Ti-magnetite, biotite and ilmenite (Fig. 4.10B-C). It also contains fragments of organic carbon (phytodetritus) (Fig. 4.10D) and mesoscopic mottling on mm scale that suggests either pedogenesis or bioturbation. The >40 cm thick bed is most likely to be a swamp deposit receiving volcaniclastic or pyroclastic detritus.

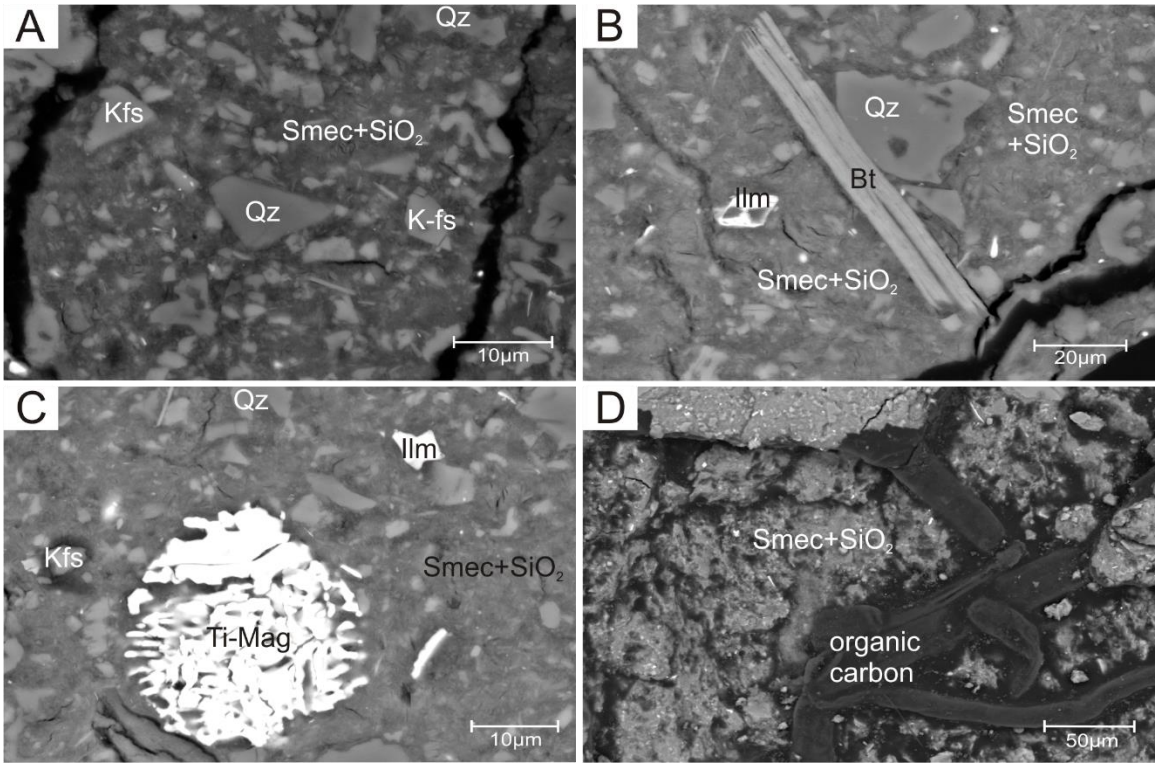

Figure 4.10. Representative BSE images of minerals from the black layer of the fine grained sediments underlying the Jithra ignimbrite, sample 843. (A) Smectite groundmass with tiny grains of detrital quartz and K-feldspar. (B) Smectite with crystals of quartz, biotite and ilmenite. (C) An altered Ti-Magnetite crystal in smectitic clay intermixed with tiny crystals of quartz and K-feldspars. (D) Organic carbon material in smectitic clay.

4.2.3: Red layer: Sample 843

Sample 843 is red in color and overlies 5m of mudflow deposits. Relics of detrital quartz, biotite, muscovite, ilmenite, and Ti-magnetite crystals are present (Fig. 4.11A). It is predominantly made up of clay with highly altered lithic clasts and crystals replaced by smectite and "Fe-oxide" (hematite) (Fig. 4.11B). Smectite appears to have partly altered ilmenite (Fig. 4.11C). Globules of hematite in smectite (Fig. 4.11D) look like an immiscible liquid.

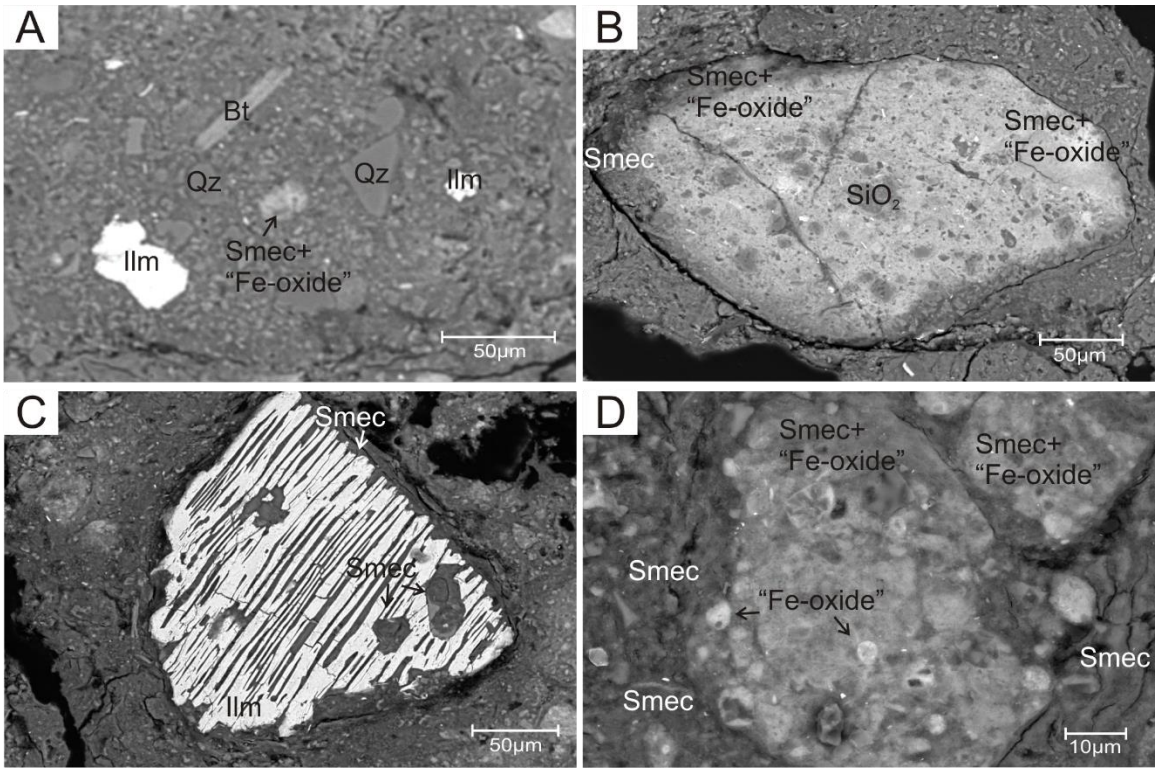

Figure 4.11. Representative BSE images of textures and minerals from the red layer of the fine grained sediments underlying the Jithra ignimbrite, sample 843. (A) Groundmass with relics of quartz, biotite and TiO_2 minerals with a globule of "Fe-oxide" (hematite) in the middle. (B) A clast altered and replaced by "Fe-oxide" and smectite. (C) A partly altered crystal of ilmenite. (D) Globules of "Fe-oxide" (hematite) in smectitic clay.

4.2.4: Summary: The fine-grained sediments underlying the Jithra ignimbrite

A similar mineral assemblage was observed from the three layers of the underlying sediments. *Smectite +silica +TiO_2 minerals* were all present in the three horizons. Smectite and silica are mostly products of alteration, replacing crystals of biotite, plagioclase, or matrix. Detrital silica (quartz) are often intermixed with smectite in the groundmass or matrix in the protolith fine-grained sediment. TiO_2 minerals are detrital and are found in the groundmass with quartz, feldspars and smectite. A slight difference in the mineralogical composition of the three layers is distinguishable with the occurrence of monazite along crystal boundaries in the white layer, the presence of organic carbon in the black layer, and the presence of hematite globules resembling immiscible liquid are present in the red layer.

All in all, the white layer appears to be originally a crystal-lithic tuff that has been altered to clay (smectite) and silica. The black layer appears to be a swamp deposit receiving transported volcanoclastic and pyroclastic rubble. While the red layer represents reworked materials from a mudflow deposit.

4.3: Yellow zoned nodule: Sample 800a

Sample 800a is a yellow nodule collected from a fault zone in a vitric-lithic tuff (Fig. 4.12A). The hand specimen shows three obvious zones. The outer zone is light colored, very pale yellow; the middle zone is yellowish green; while the inner zone is white/colorless (Fig. 4.12B).

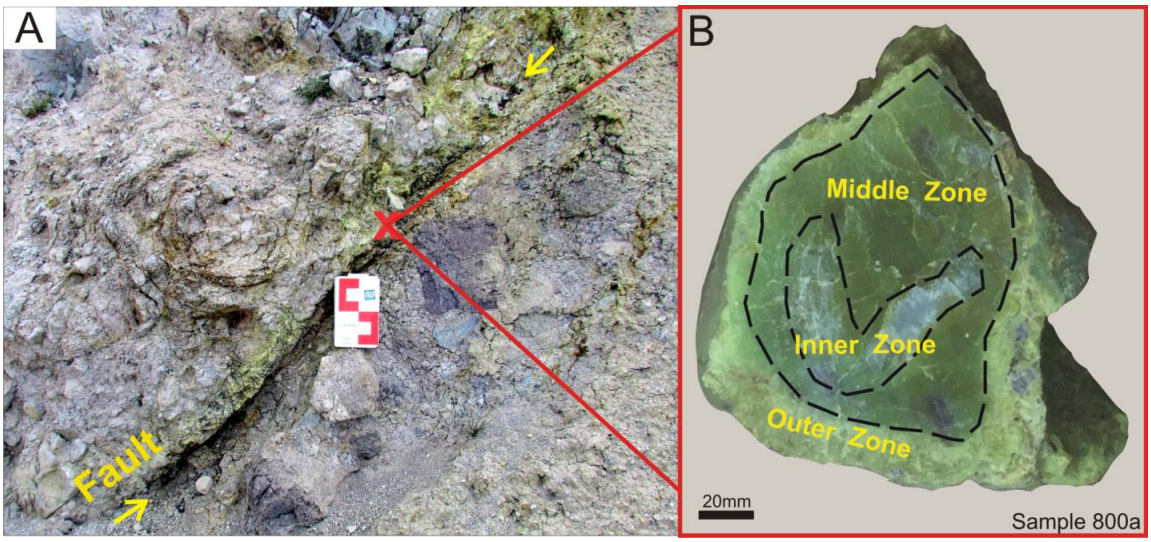

Figure 4.12. Field photograph of a yellow and brown mineralization along a fault zone in Sigri-Antissa road (West). (B) A nodule (sample 800a) collected along the fault zone in fig. A.

The zonation of the yellow zoned appears to be mineralogical. The inner zone is pure silica, occurring either as amorphous or microcrystalline quartz (Fig. 4.13A-C). The middle zone is predominantly made up of a gel-like mixture of mixture 2 (Si+Fe) with accretions of mixture 1 (Si + Mn ± Fe), veinlets of amorphous silica cutting through both mixture 2 (Si + Fe) and accretions of mixture 1 (Si + Mn ± Fe) were also seen (Fig. 4.13D-F). The outer zone shows crystallization of minerals, mostly of feldspar and iron-oxides (Fig. 4.13G-I). In this zone, Ti-magnetite with exsolution or patches of ilmenite

and ilmenite microphenocrysts, and apatite were also observed. Feldspar-rich patches altering to silica and “Fe-oxide” in tiny grains were abundant.

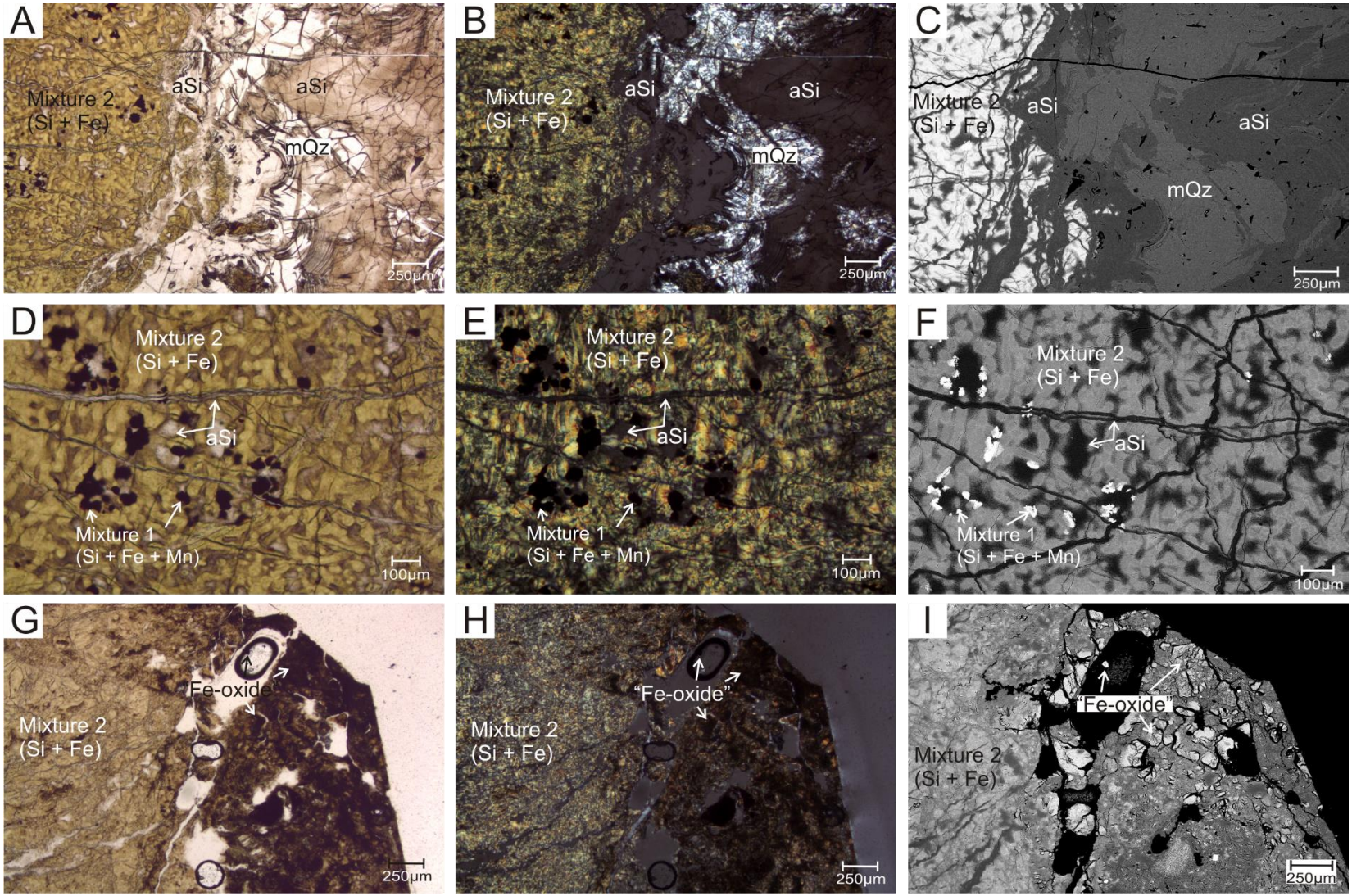
A
Mixture 2
(Si + Fe)
aSi
aSi
mQz
250µm
B
Mixture 2
(Si + Fe)
aSi
aSi
mQz
250µm
C
Mixture 2
(Si + Fe)
aSi
aSi
mQz
250µm
D
Mixture 2
(Si + Fe)
aSi
Mixture 1
(Si + Fe + Mn)
100µm
E
Mixture 2
(Si + Fe)
aSi
Mixture 1
(Si + Fe + Mn)
100µm
F
Mixture 2
(Si + Fe)
aSi
Mixture 1
(Si + Fe + Mn)
100µm
G
Fe-oxide
Mixture 2
(Si + Fe)
250µm
H
"Fe-oxide"
Mixture 2
(Si + Fe)
250µm
I
"Fe-oxide"
Mixture 2
(Si + Fe)
250µm

Figure 4.13. Representative microphotographs and BSE images of the hydrothermal yellow zoned nodule, sample 800a. (A) Microphotograph of amorphous and microcrystalline silica under PPL from the inner zone of the nodule. (B) Microphotograph of amorphous and microcrystalline silica under XPL from the inner zone of the nodule. (C) BSE image of amorphous and microcrystalline silica from the inner zone of the nodule. (D) Microphotograph of mixture 2 and aggregate crystals of "Mn-oxide" cut by numerous silica veinlets under PPL from the middle zone of the nodule. (E) Microphotograph of mixture 2 and aggregate crystals of "Mn-oxide" cut by numerous silica veinlets under XPL from the middle zone of the nodule. (F) BSE image of mixture 2 and aggregate crystals of "Mn-oxide" cut by numerous silica veinlets from the middle zone of the nodule. (G) Microphotograph of mixture 2 and tiny crystals of "Fe-oxide" under PPL from the outer zone of the nodule. (H) Microphotograph of mixture 2 and tiny crystals of "Fe-oxide" under XPL from the outer zone of the nodule. (I) BSE image of mixture 2 and tiny crystals of "Fe-oxide" from the outer zone of the nodule.

4.4: Yellow hydrothermal veins

The hydrothermal veins investigated in this study are yellow veins with or without brown patches. Similar to the yellow hydrothermal nodule, the veins cut vitric-lithic tuffs or lithic clasts. Figure 4.14A shows brown mineralization (sample 806) cutting across a pyroclastic rock with a possible paleosol on top in the Sigri area. The brown mineral vein appears to be an irregular vein cutting across a lithic clast (Fig. 4.14B). A yellow vein found outside Antissa cutting an ignimbrite (Fig. 4.14C) was also studied. The yellow vein in ignimbrite (sample 847) shows "Fe-oxide" mineralization on the top right corner of the sample (Fig. 4.14D). Another prominent yellow vein cutting across Sigri pyroclastic rocks was also studied (Fig. 4.14E). Similar to sample 847, the yellow vein also shows "Fe-oxide" mineralization as veinlets (Fig. 4.14F).

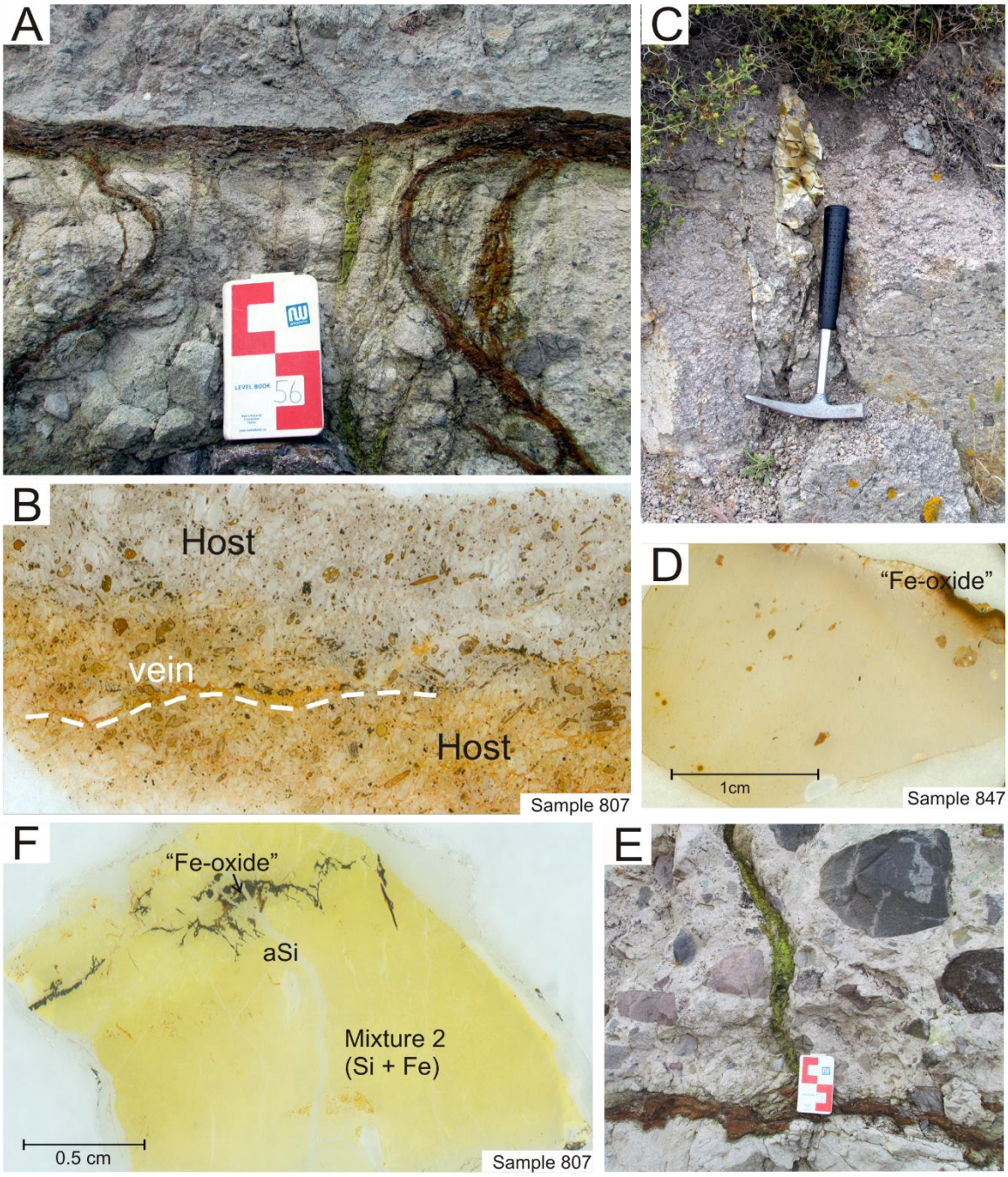

Figure 4.14. Field photographs and scanned thin section photographs of yellow and brown hydrothermal veins cutting pyroclastic rocks. (A) Field photograph of the brown, "hematite" vein (sample 806), cutting across Sigri pyroclastic rocks. (B) Scanned thin section of sample 806 showing an irregular brown vein cutting a lithic clast. (C) Field photograph of the yellow hydrothermal vein (sample 847) outside Antissa cutting an ignimbrite. (D) Scanned thin section of sample 847 showing "Fe-oxide" mineralization at the top right corner. (E) Field photograph of the yellow hydrothermal vein cutting Sigri pyroclastic rocks. (F) Scanned thin section of sample 807 showing "Fe-oxide" and amorphous silica veinlets cutting across the yellow hydrothermal vein.

4.4.1: Sample 806

Sample 806 is from a lithic clast cut by a brownish vein in a vitric-lithic tuff (Fig. 4.15A). The sample is made up of detrital crystals of K-feldspar, plagioclase (varying from oligoclase to andesine), quartz, diopside, Ti-magnetite and rare ilmenite. Two mineral assemblages were seen in this sample: (1) Mixture 1 (Si + Mn ± Fe) and (2) Mixture 2 (Si + Fe). The sample shows a complex vein system (Fig. 4.15B). The assemblages occur mainly as (a) direct deposition in veins, (b) replacement and (c) replacement and direct deposition.

In case of (a) direct deposition, mixture 2 is seen in veins in more than one generation. Silica and Fe-oxide various in proportions with rare occurrence of mixture 1. The first two veins are mixture 2 (Si + Fe) veins in different proportions (Fig. 4.15C). Vein III and vein II with FeO >60% SiO_2 <40%, and FeO <60% SiO_2 >40% respectively. While vein I is mixture 1 (Si + Mn ± Fe) with a feather-like morphology (Fig. 4.15D). In case of (b) deposition, outlines of hornblende were seen but they are often highly mineralized with “Fe-oxide” and silica.

As (c) replacement and direct deposition, the sample is highly brecciated or shattered, the mineralizing mixtures used these as pathways for the veins and veinlets (Fig. 4.15E). The hydrothermal fluid also follows crystal outline, crystal cleavage planes, and fractures as mineral pathways.

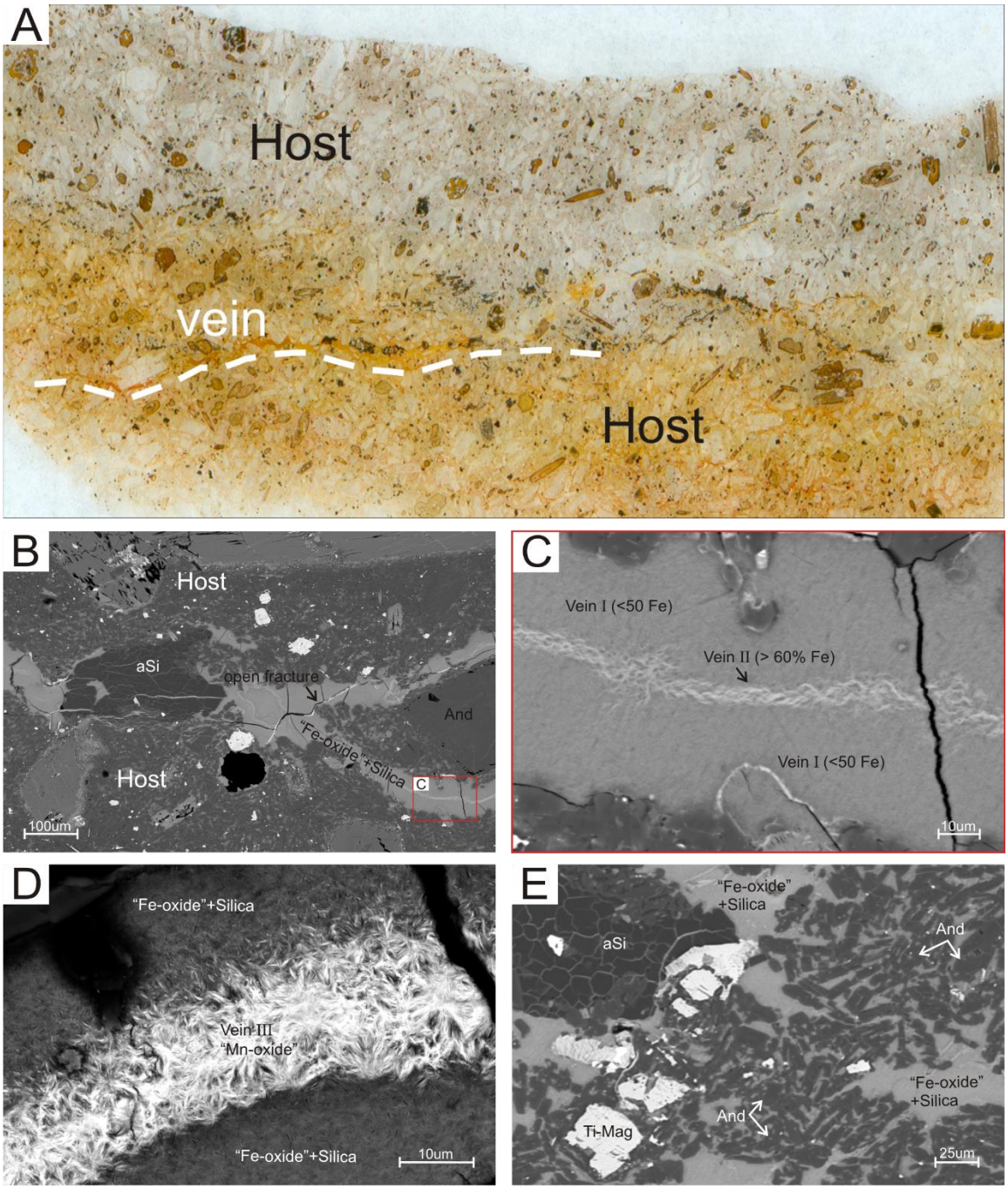

Figure 4.15. Scanned thin section photograph and representative BSE images of the brown hydrothermal vein cutting pyroclastic rocks. (A) Scanned thin section of sample 806 showing an irregular brown vein cutting a lithic clast. (B) Complex vein system. (C) Vein III and vein II with FeO >60% SiO_2 <40%, and FeO <60% SiO_2 >40%. (D) Vein I is mixture 1 (Si + Mn ± Fe) with a feather-like morphology. (E) Replacement and direct deposition, the sample is highly brecciated or shattered, the mineralizing mixtures used these as pathways for the veins and veinlets.

4.4.2: Sample 807

Sample 807 is a yellow vein with brownish patches in a lithic tuff. The sample is predominantly made up of mixture 2 (Si + Fe) and mixture 2 is best shown in this sample. Within this vein, several sets of smaller veins or veinlets were observed: (i) “Fe-oxide” or silica (Fig. 4.16A, E)

Different textures were created by the mineralizing solutions. (1) The globular form of mixture 2 and (2) evidence of early porosity in mixture 2 (Fig. 4.16B). The globular morphology suggests immiscible liquid separation from the hydrothermal solution. (3) Similar globular morphology of silica (Fig. 4.16C) may have led to more pronounced porosity that (4) later made way for “Fe-oxide” (Fig. 4.16D, F).

Based on the textures observed, paragenesis is:

Mixture 2 → Silica → mixture 1→ followed by more than one generation of silica veins → microporosity → and finally, “Fe-oxide” partly fills the microporosity.

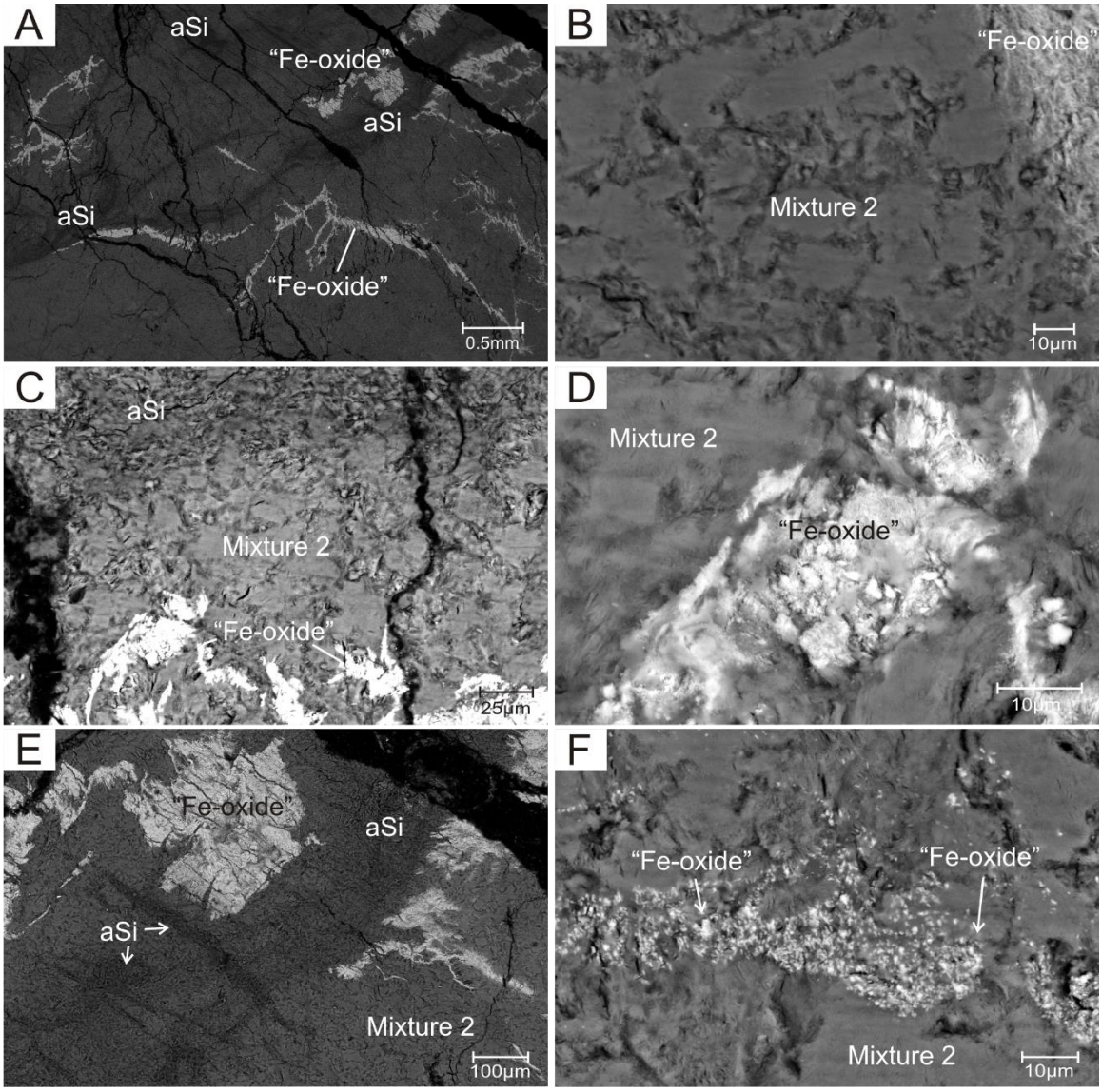

Figure 4.16. Representative BSE images of textures and minerals of a yellow hydrothermal vein cutting Sigri pyroclastic rocks, sample 807. (A) Intricate network of multiple silica and "Fe-oxide" veins cross-cutting each other. (B) Globular texture of mixture 2. (C) An amorphous silica vein and "Fe-oxide" vein cuts across mixture 2. (D) "Fe-oxide" precipitates along the porosity of mixture 2. (E) Veins and veinlets of silica cuts across an "Fe-oxide" vein. (F) Similar to Fig. 4.18D, "Fe-oxide" precipitates along the porosity of mixture 2.

4.4.3: Sample 847

Sample 847 is from a vein cutting across an ignimbrite, similar in color to sample 807. However sample 847 is mainly amorphous silica containing only <3% FeO. Close to the margin, the silica is in contact with glass and biotite crystals (Fig 4.17A). Mineralization/ crystallites of "Fe-oxide" (Fig. 4.17B) which form brown globules, irregular patches and elongate matches were present throughout the sample. Some of the irregular patches are zoned "Fe-oxide/hydroxide" patches that seems to have a clean core and patchy rim with mixture 2 (Si + Fe) margins (Fig. 4.17C). The yellow amorphous silica displays a globular texture as seen in Fig. 4.17D.

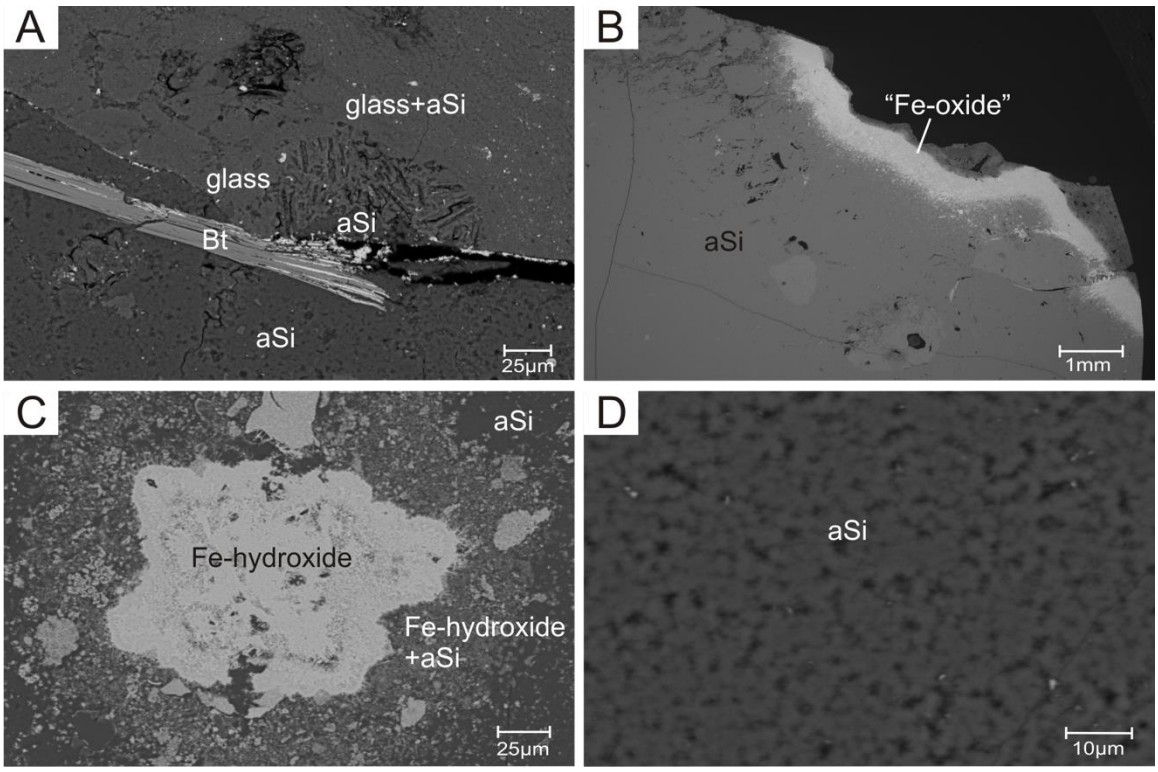

Figure 4.17. Representative BSE images of textures and minerals from a yellow hydrothermal vein in Antissa-Jithra ignimbrite, sample 847. (A) BSE image of sample 847 showing silica in contact with glass and biotite. (B) "Fe-oxide" mineralization or "Fe-oxide" crystallites. (C) An irregular patch of "Fe-oxide/hydroxide" showing a clean core and patchy rim. (D) Globular texture of the amorphous silica.

4.5: Wood samples from the Petrified Forest

As mentioned above, the fossilized trees (Fig 4.18A) in the Petrified Forest are silicified remnants of a sub-tropical forest that existed on the north-west part of the island about 20 Ma ago. The petrification of the forest is directly related to the intense volcanic activity in Lesbos Island during late Oligocene to middle Miocene. The volcanic eruptions during this time produced lavas, pyroclastic materials and volcanic ash, which covered the vegetation of the area. The rapid covering of tree trunks, branches, and leaves led to isolation from atmospheric conditions. Along with the volcanic activity, solutions of SiO_2 penetrated and impregnated the volcanic materials that covered the tree trunks.

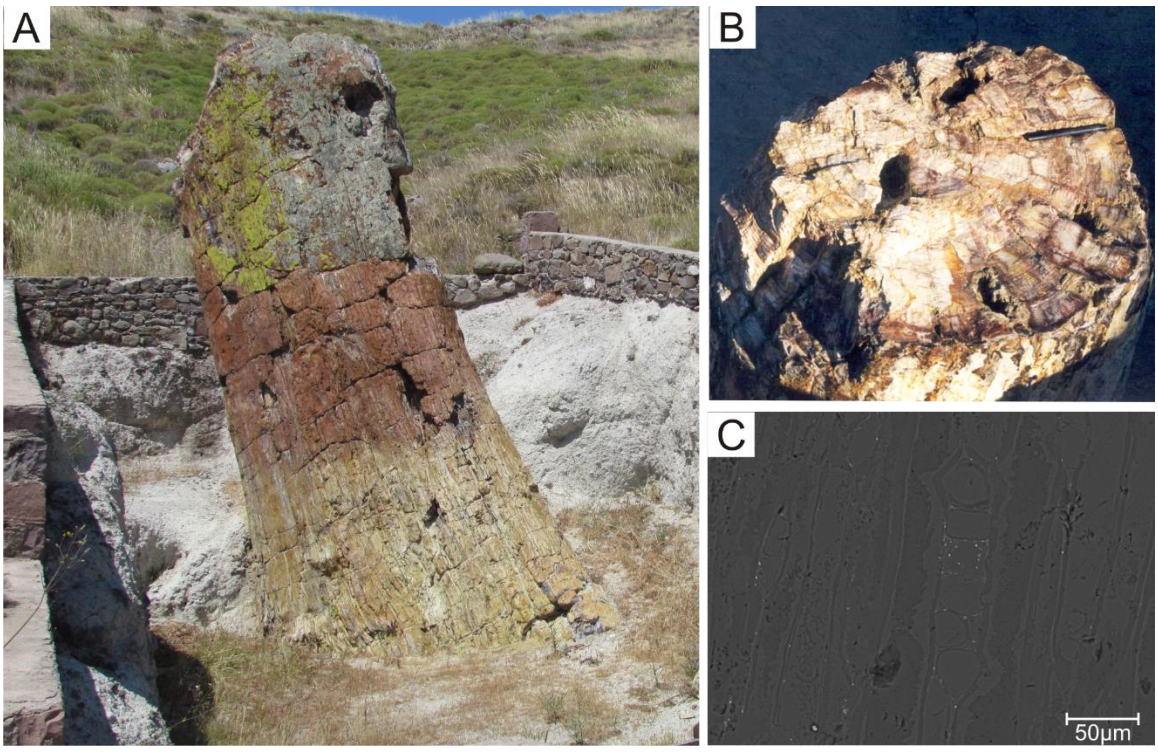

Figure 4.18. Field photographs and BSE image of a petrified wood from the Petrified Forest of Lesbos. (A) Field photograph of an upright tree buried in tuff. (B) A petrified tree showing delicate growth rings preserved in silica. (C) BSE image of a petrified wood showing internal structure replaced by silica.

Fossilization process in Lesbos was ideal due to the intensity of volcanic activity, the rate of volcanic ash fall and the composition of erupted lava. As a result morphological characteristics of the tree trunks, such as annual rings (Fig. 4.18B) and internal structure of the wood are all well preserved (Fig. 4.18C).

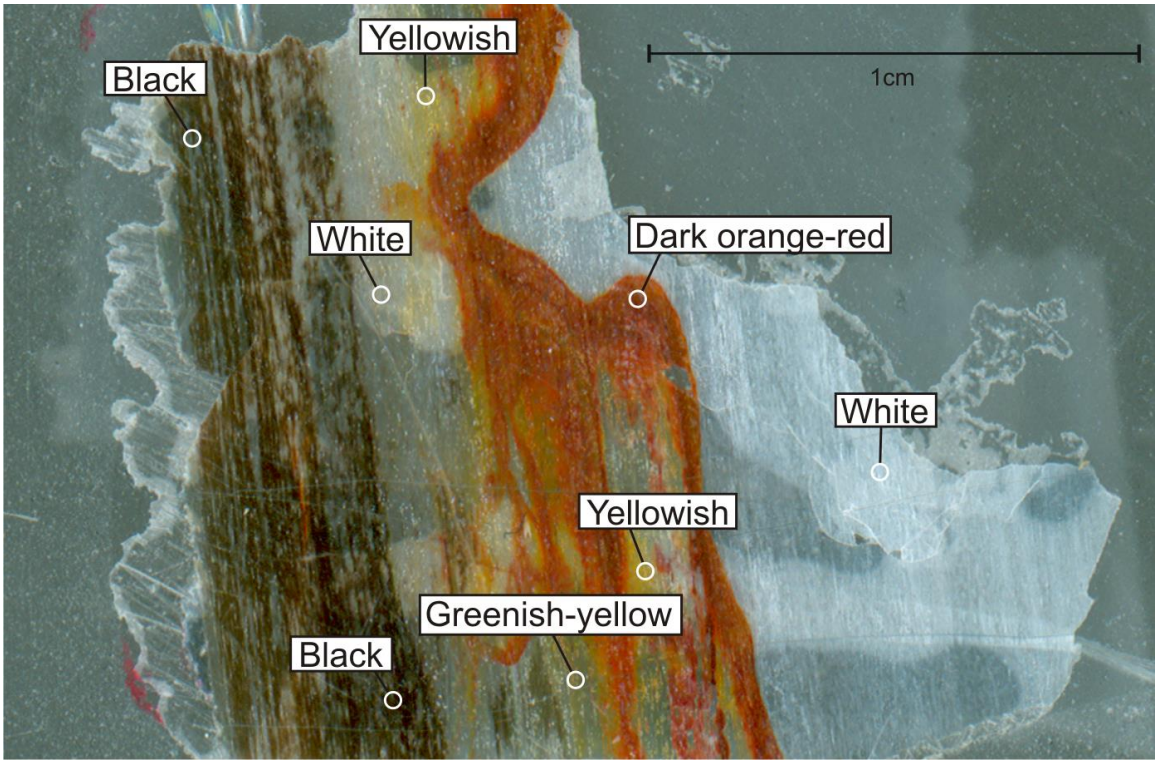

Figure 4.19. Scanned thin section photograph of a petrified wood (sample 856-1) showing different colours of silica petrification.

Samples 856-1 and 856-2 were taken from a petrified wood. The sample shows tree structures preserved by silicification, either by mineral replacement and/or permineralization. Sample 856-1 shows the different layers of colors (Fig. 4.19) of petrification. EMP chemical analyses showing the variations in chemical composition of the different colors of silica petrification is summarized in Appendix 2. The various colors observed are:

(1) **Black** – this layer is predominantly made up of SiO_2, organic matter and tiny amount of zinc (Fig. 4.20A).

(2) **Greenish-yellow** – this layer is made up of SiO_2 with small amount of FeO. Zinc is still present (Fig. 4.20B)

(3) **Yellowish** – this layer has SiO_2 with higher amounts of FeO than the Greenish-yellow layer. Occasional As is also present. (Fig. 4.20C)

(4) **Dark orange-red** – this layer is mostly a mixture of FeO and SiO_2 inside wood vessels either mostly or completely filled with pure SiO_2 on the edges. Traces of As, V are sometimes present.

(5) **Yellow-orange** – similar to the dark orange-red layer however this layer appears to have more SiO2 than FeO in proportion. Occasional Zn is present.

(6) **White** – this layer is mostly just SiO_2 (Fig. 4.21E)

The sample shows there was background silicification of most of the wood structure. Any residual plant vessels are pathways for later hydrothermal fluids and precipitation of amorphous silica, "Fe-oxide", hematite crystallites and barite. In other words, the silicification of the wood probably involved three stages:

1) Silicification

2) Filling of voids with amorphous mixture 2 SiO_2 + FeO (Si+Fe)

3) Precipitation of "Fe-oxide" crystallites

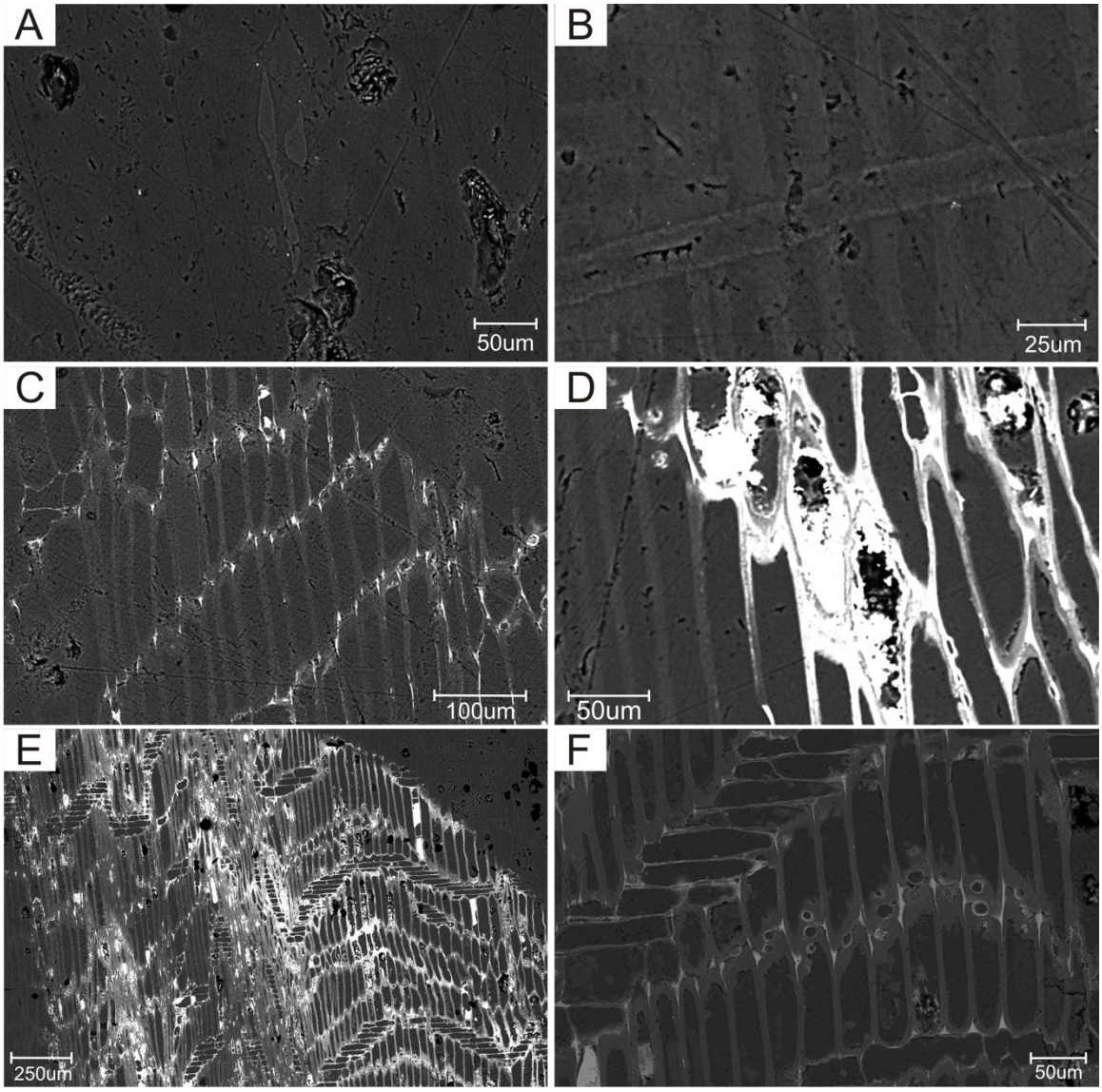

Figure 4.21. Representative BSE images of textures and minerals from the petrified wood (sample 856-1). (A) Black layer: SiO_2 +small amount of Fe, Ca and Zn. (B) Wood vessels cut by silica vein. (C) Wood vessels filled with SiO_2 +Fe-oxide mixture. (D) Yellowish-red layer with complex pattern of wood structure. (E) Dark-orange-red layer. (F) Weakness pathways defined by wood structure of vessels.

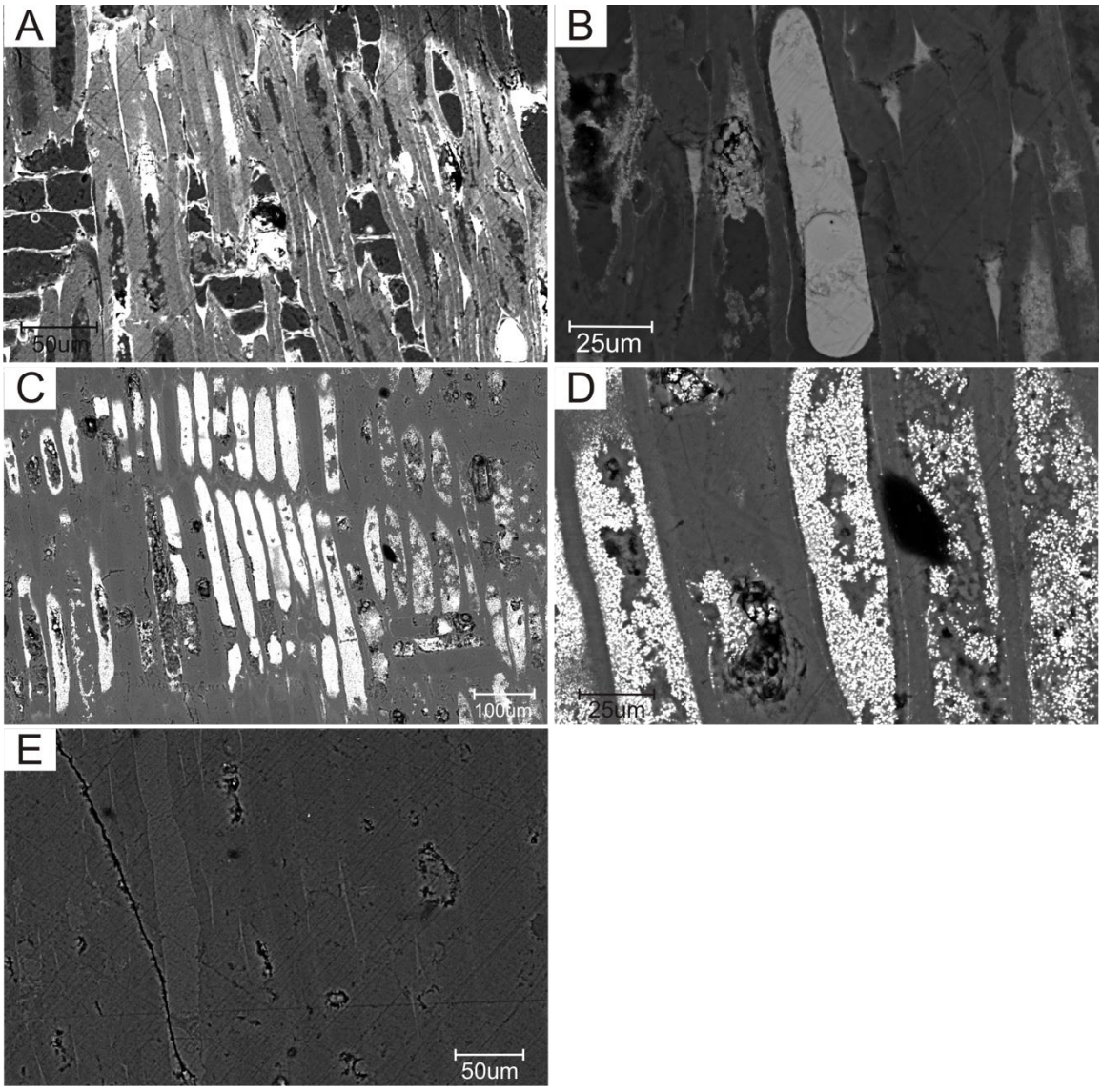

Figure 4.21. Representative BSE images of textures and minerals from the petrified wood (sample 856-1). (A) SiO_2 +Fe-oxide fill wood vessels walls and cross-cuts vessels. (B) Large vessel completely filled with SiO_2 +Fe-oxide. (C) Vessels mostly or completely filled with mixture of SiO_2 +Fe-oxide. (D) Vessels partly filled with Fe-oxide aggregates. (E) White layer: Silicified wood.

4.6: X-ray powder diffraction (XRD)

10 samples were studied using acquired diffractograms from quantitative X-ray diffraction analyses. Although X-ray diffraction was mainly used to identify clay minerals present in the sediments underlying the Jithra ignimbrite, samples containing yellow hydrothermal veins and "Mn-oxide" were also analysed using this method for more precise mineral identification of the Fe and Mn-rich minerals/mixtures. Mineral assemblages identified from diffractograms closely resembles mineral assemblages identified using SEM.

The principal minerals were identified from their characteristic d-spacing using criteria summarized by Brown and Brindley (1980) and available data from webmineral. A table summarizing the d-spacing of the expected minerals present can be found in the Methods, Table 3.5.

4.6.1: Clay minerals in sediments: samples 839, 842, 843

The layered sediments underlying the Jithra ignimbrite are mostly made up of clay which has replaced volcaniclastic detritus. The black layer (sample 842) and red layer (sample 843) show very similar X-ray diffractograms (Fig. 4.22). Identified primary minerals are kaolinite, quartz, α-cristobalite (low temperature cristobalite) and andesine (feldspar). All identified mineral appears to be present in both samples. Smectites are probably present, but have not yet been confirmed by glycolation.

Kaolinite:

Kaolinite is the only clay mineral convincingly identified in the sediments and appears to be present in both samples. Its peak occurs at its diagnostic position at 7.1 Å. Clear kaolinite peaks at 4.45 Å and 3.58 Å were also observed.

Quartz:

Quartz is present in both samples, showing characteristic peaks at 4.26 and 3.35 Å. The peak at 3.35 Å overlaps with the clay mineral illite, and the 10 Å illite peak is obscured by possible smectite so that illite was not conclusively identified in the rocks.

α-cristobalite:

α-cristobalite produces diffraction peaks at 4.05 and 2.50 Å. α-cristobalite is present in both samples 842 and 843.

Andesine:

Andesine occurs at d-spacings of 2.85 and 3.7 Å. Andesine is present in both the black (sample 842) and red (sample 843) layer of the sediments.

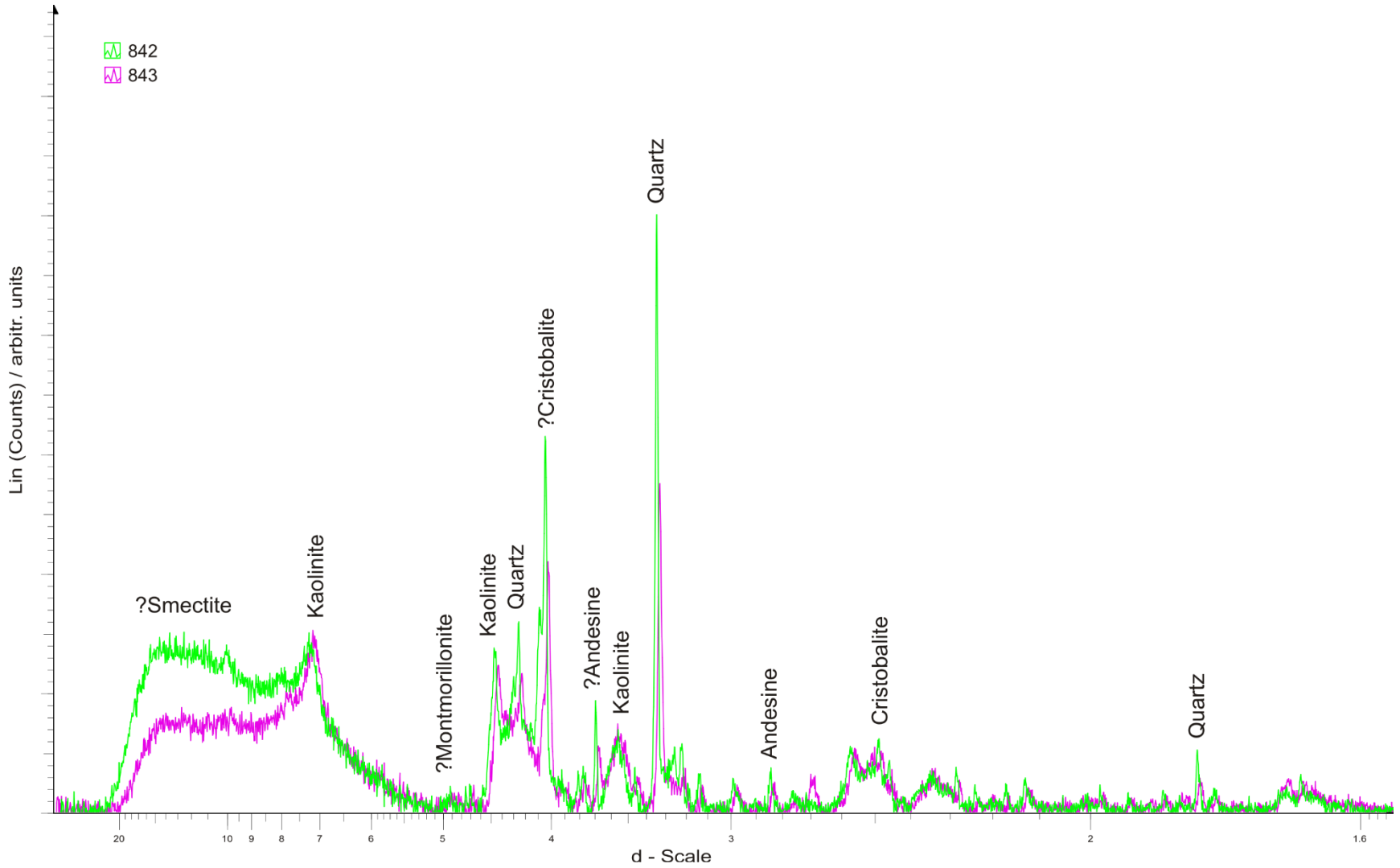

Figure 4.22. X-ray diffractogram of the fine grained sediments underlying the Jithra ignimbrite, samples 842 and 843.

4.6.2: Hydrothermal veins: samples 806, 807, 819, 847

Hydrothermal veins from different localities were analysed for X-ray diffraction. Samples 806 (brown) and 807 (yellow) are hydrothermal veins cutting across Sigri pyroclastic rocks. Sample 847 is a yellow hydrothermal vein cutting an ignimbrite outside Antissa. Sample 819 is a yellow cement in sandstone collected on the Antissa-Sigri road. For comparison, a silicified top of a paleosol, sample 815, collected in the island of Nissiopi was also analysed.

X-ray diffractograms from sample 806 and sample 847 both shows silica as the principal mineral. Tridymite and α-cristobalite (polymorphs of quartz) are present in sample 847 (Fig. 4.23). While sample 807 shows α-cristobalite plus an unknown mineral to be its main mineral (Fig. 4.23).

Diffractogram of the yellow cement in sandstones (sample 819) collected near the Jithra ignimbrite shows similar diffractogram to a sample 815, a silicified top of a paleosol collected in the island of Nissiopi (Fig. 4.24). They both show αcristobalite and feldspar as principal minerals present in the rocks. Prominent peaks at 8.3 Å and 15.2 Å in sample 819 will need further identification after glycolation.

Tridymite:

Tridymite is present in sample 847 showing peaks at 4.35 and 4.08 Å. However tridymite overlaps cristobalite at peak 4.08 Å.

α-cristobalite:

α-cristobalite shows diagnostic peaks at 4.05 Å and 2.50 Å. It is also observed at 4.75, 3.13 Å and overlaps an anorthoclase peak at 4.5 Å. α-cristobalite is present in all samples.

?Smectite/Montmorillonite:

Smectite/montmorillonite is present in samples 807 and 819. It occurs at d-spacing of approximately 15 Å and a less intense peak at 5 Å.

Feldspar:

Feldspar is present in sample 819 and 815. K-feldspar peaks occur at 3.75 Å, 3.25, 3.0 and 2.92 Å.

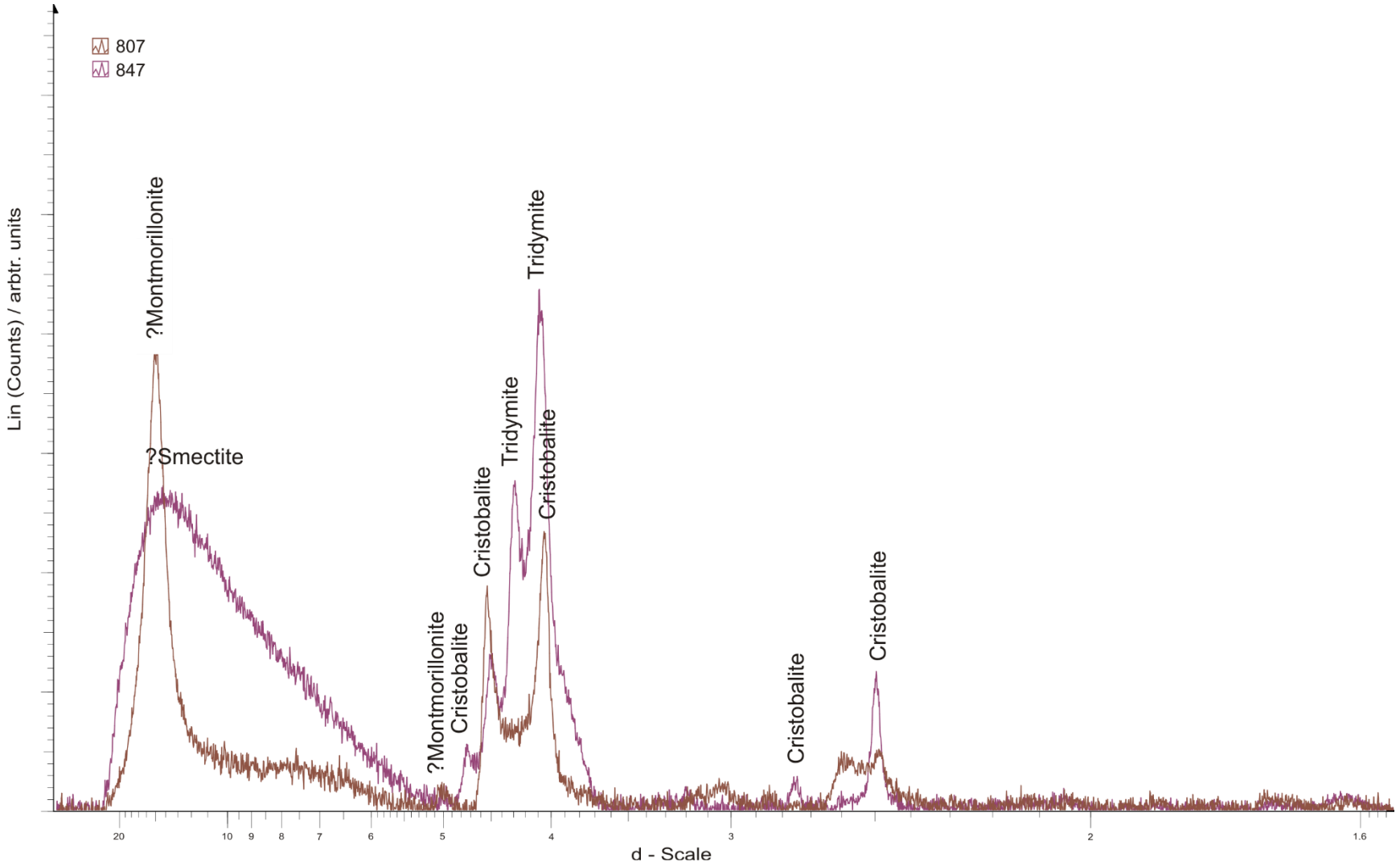

Figure 4.23. X-ray diffractogram of yellow hydrothermal veins cross cutting pyroclastic rocks, samples 807 and 847.

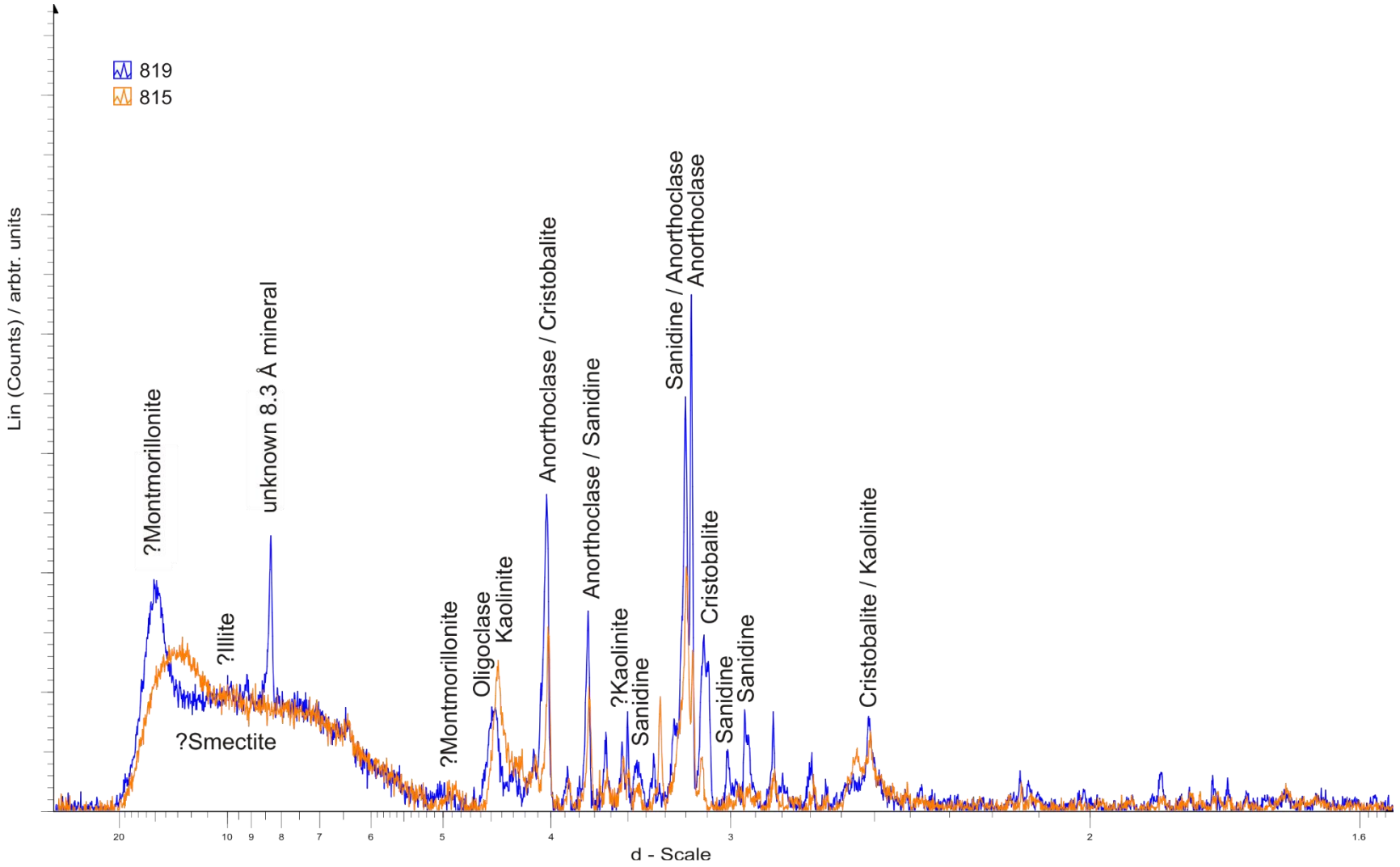

Figure 4.24. X-ray diffractogram of yellow cement in sandstone (sample 819) and a silicified top of a paleosol (sample 815).

4.6.3: Altered Jithra ignimbrite: samples 844, 846a

The altered white ignimbrite (sample 844) and a dark "Mn-oxide" vein (sample 846a) were analysed using X-ray powder diffraction. Diffractogram of the altered ignimbrite shows kaolinite, illite, feldspar and cristobalite as principal minerals, while the dark "Mn-oxide" vein shows a very similar diffractogram (Fig. 4.25). A manganese mineral, Todorokite shows plausible peaks that can be matched to the dark mineral vein diffractogram (Fig. 4.36), however significant peak overlapping with other minerals prevents a definite conclusion for the identity of the "Mn-oxide" mineral.

Kaolinite:

Characteristic peak of kaolinite at 7.1 Å was observed. It also shows peak at d-spacing of 3.51, 2.55 and 2.48 Å.

Illite:

Illite produces diffraction peaks at 4.49, 2.99, and 2.55 Å. Illite overlaps with feldspar at peak 2.99 Å and overlaps kaolinite at 2.55 Å.

Feldspar:

K-feldspar (sanidine) peaks occurs at 6.48, 5.7, 4.15, 3.92, 3.75, 3.25, 3.0, and 2.92 Å. Sanidine overlaps with illite at 2.92 Å. An orthoclase peak at 6.5 Å was also present.

Cristobalite:

Cristobalite produces diffraction peaks at 4.05 Å and 2.50 Å. Cristobalite overlaps kaolinite at 2.48 Å.

Todorokite:

Todorokite's most intense peak occurs at 9.65 Å with less intense peaks at 3.32, 3.25 and 3.2 Å.

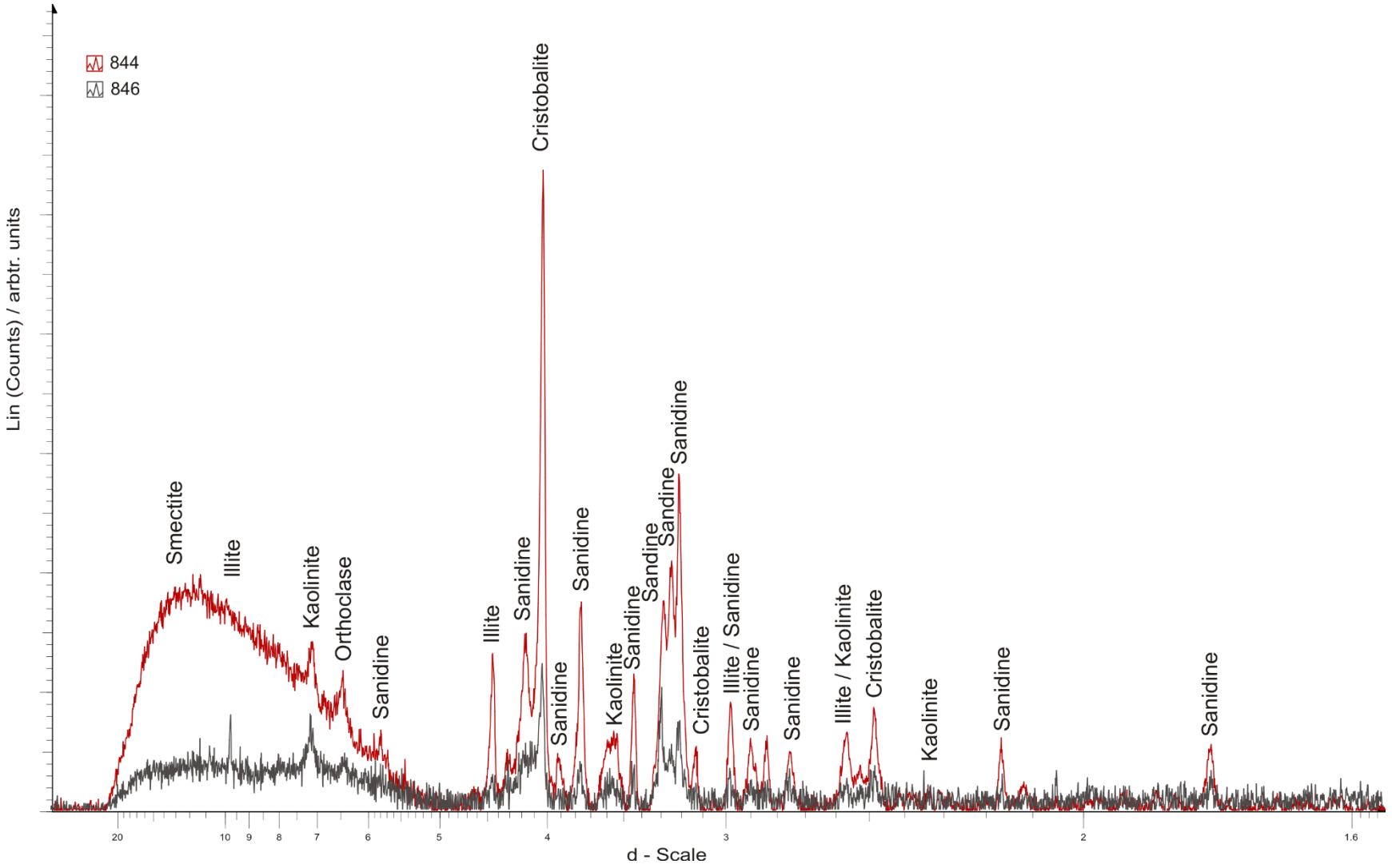

Figure 4.25. X-ray diffractogram of the altered Jithra ignimbrite (sample 844) and its dark mineralized vein, "Mn-oxide" vein (sample 846a).

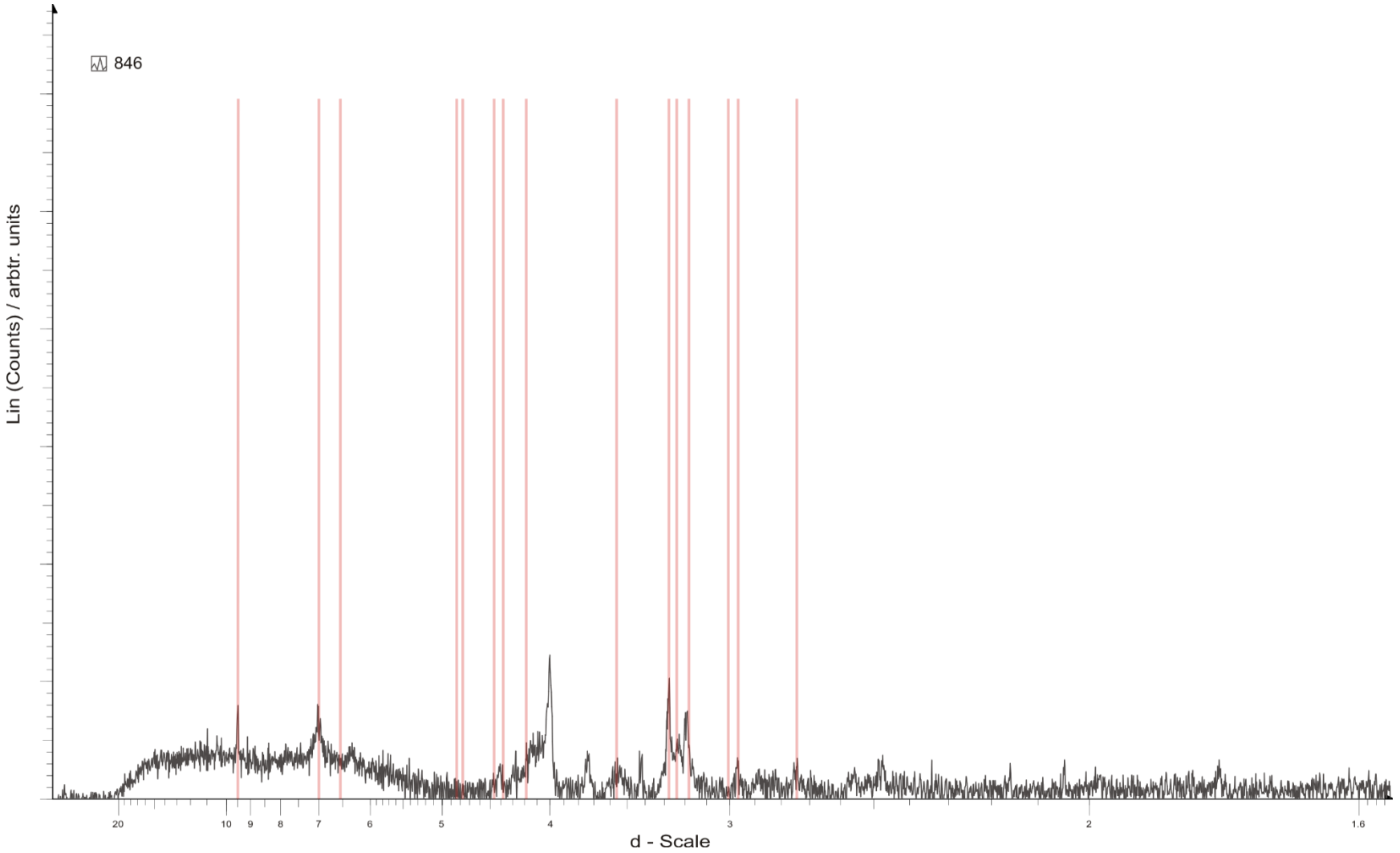

Figure 4.26. X-ray diffractogram of the dark mineralized, "Mn-oxide" vein (sample 846a) from the altered ignimbrite showing Todorokite (manganese mineral) reference peaks (red lines).

4.7: Laser Raman Microspectroscopy (LRM)

Selected silica analyses from the zoned nodule, (sample 800a), the altered Jithra ignimbrite (sample 844a) and the petrified wood (sample 856-1) were analysed using Raman Laser spectroscopy to better understand the silica found in the rocks. In the literature, silica has six common polymorphs:

(1) α-quartz or low quartz: typically known as the "ordinary" quartz. α-quartz is a stable polymorph of silica at low temperature

(2) β-quartz or high quartz: β-quartz is a high temperature polymorph of silica.

(3) Moganite: a meta-stable silica polymorph. Moganite is typically intergrown with cryptocrystalline quartz to form chalcedony (Florke et al., 1976).

(4) Opal: micro to non-crystalline forms of hydrated silica with high degree of structural disorder (Ilieva et al., 2007).

Opal is usually not considered a mineral because it is amorphous and varies considerably in composition, but because it has some degree of homogeneity, it is called a mineraloid. Opal forms from silica rich watery solutions and is very similar to chalcedony watery silica gels. In volcanic rocks it may form on rock walls from silica transported with steam water (Florke, 1973). Opals differ considerably in their microstructure and composition, their common denominator is their overall non-crystalline structure and their water content. Florke, (1991) classified opals as:

(4.1) Opal-C: microcrystalline opals made up of cristobalite

(4.2) Opal-CT: microcrystalline opals made up of intergrowns of cristobalite and tridymite

(4.3) Opal-AG: Amorphous opals with gel-like structure

(4.4) Opal-A: Amorphous opals with a network –like structure (hyalite, glass opal)

(5) Cristobalite: is a constituent of many opals, but it is quite rare as an individual mineral. Cristobalite is a rock-forming mineral, and occurs as a transitional silica polymorph in the form of Opal-C.

(6) Tridymite: like cristobalite, tridymite is more common as a component of opal (in particular opal-CT) than as an individual mineral.

Using Laser Raman spectroscopy, four different silica polymorphs were detected from the studied samples: (a) α-quartz; (b) moganite; (c) opal-C and/or α-cristobalite and; (d) opal-CT. For this study, it is unsure if α-cristobalite is an individual mineral or a component of opal C. Therefore opal-C and α-cristobalite are treated as one.

Moganite and α-quartz were seen as the microcrystalline silica in the inner zone of the yellow nodule (sample 800a). Raman spectra from Kingman and Hemley (Fig. 4.27) was used to differentiate α-quartz from moganite. Characteristic spectra of α-quartz shows a strong peak at 465 cm^{-1} while moganite represents the intense peak at 501 cm^{-1}.

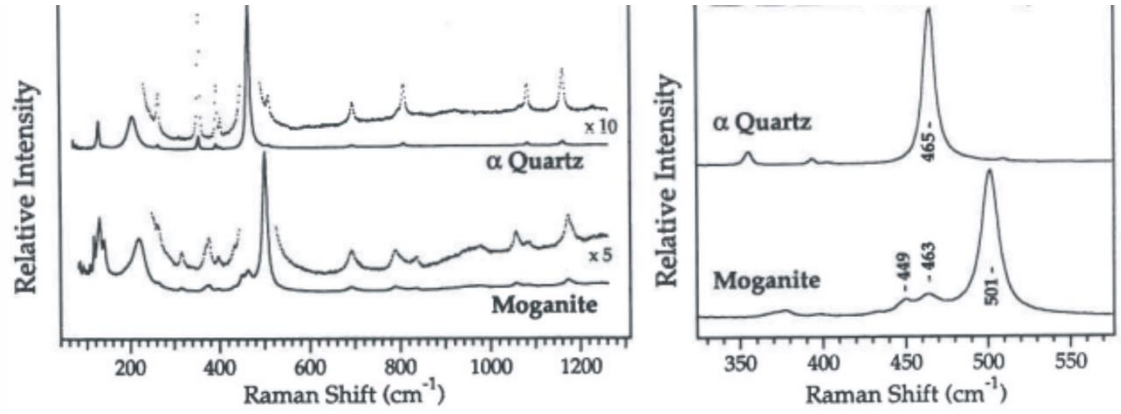

Figure 4.27. Raman spectra of α-quartz and Moganite (adapted from Kingman and Hemley, 1994).

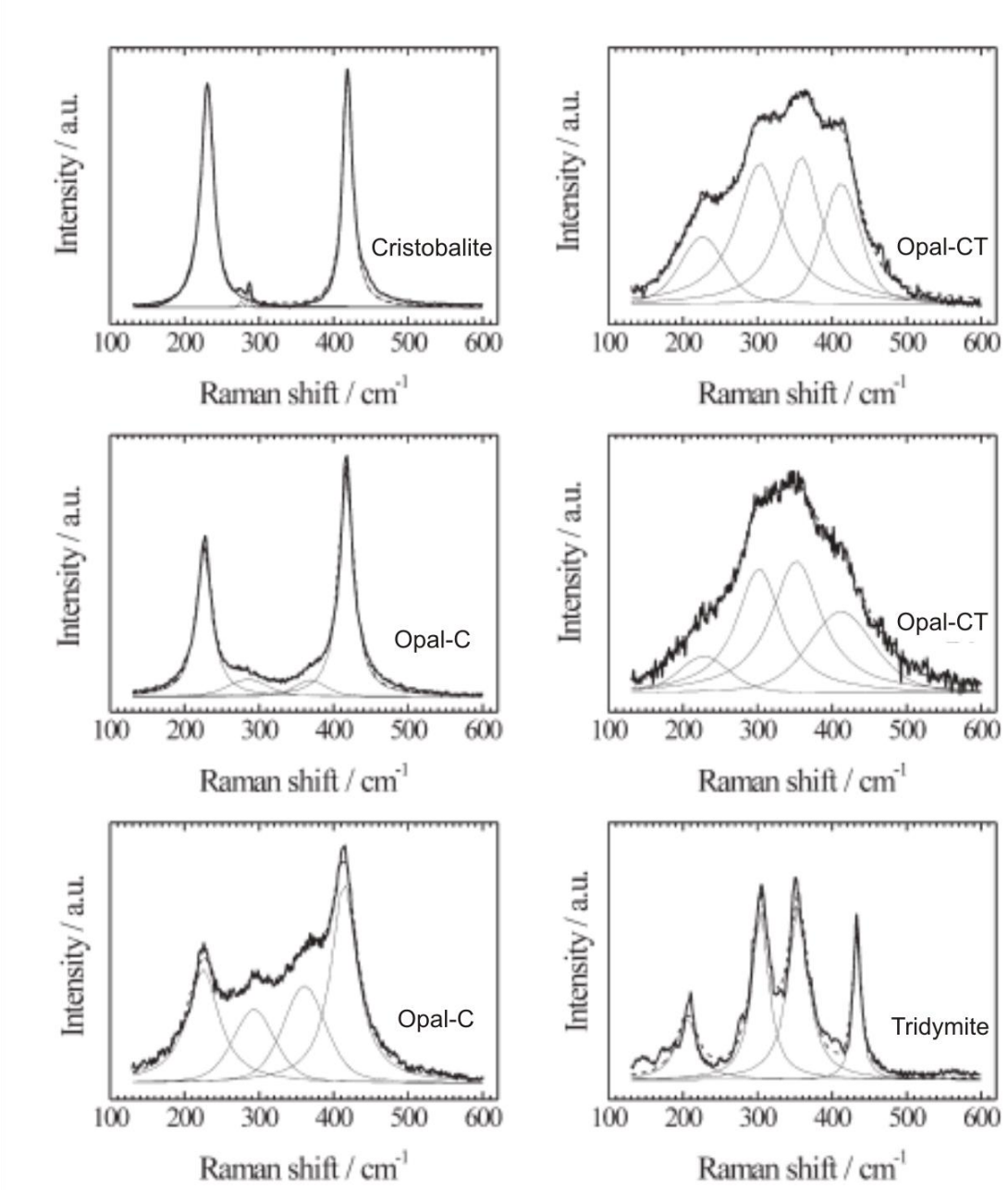

Figure 4.28. Raman spectra of cristobalite, opal-C, opal-CT and tridymite (adapted from Ilieva et al., 2007).

Opal-C (α-cristobalite) and opal-CT were seen in both the yellow nodule (sample 800) and the altered Jithra ignimbrite (sample 844a). Opal C (cristobalite) displays intense peaks at 230 and 415 cm^{-1}, while broad scattering between the two peak are also

possible (Fig. 4.28). Opal-CT however does not indicate any intense specific peak but a broad Raman scattering from 200 to 600 cm^{-1} are always present (Fig. 4.28).

The petrified wood sample (sample 856-1) detected α-quartz spectra with indications of non-silica broad peaks.

4.7.1: Yellow zoned nodule: sample 800a

Silica from the inner, middle and outer zones of the yellow nodule were analysed under Raman spectroscopy. Spectra acquired seem to suggest four silica polymorphs present in the sample (Fig. 4.29). A combination of α-quartz and Moganite appears to be the microcrystalline silica observed in the inner zone.

Analysis spot b and c demonstrate intense Raman peaks centered at 462, and 209 cm^{-1} with less intense peaks found from 250-380 cm^{-1} which indicates an α-quartz spectrum while an intense peak at 501 cm^{-1} was also observed which is characteristic of Moganite. The concentration of α-quartz and Moganite can be estimated using the relative intensities of α-quartz (462 cm^{-1}) and Moganite (501 cm^{-1}) peaks. *Spectrum b* and *c* from Fig. XA suggests a higher α-quartz concentration in the inner zone of the nodule than Moganite.

The dark amorphous silica in the inner zone and the middle zone observed in backscattered images of SEM appears to be opal-CT. Raman spectra of opal-CT is highly variable, opals classified as opal-CT by Ilieva et al., 2007 (Fig. X) exhibited broad and intense Raman scattering from 200 to 600 cm^{-1}, with peaking at ~335 cm^{-1}. Spectra observed in all zones of this sample show a very broad but intense scattering from 200-550 cm^{-1}, with most peaks at ~300-350 cm^{-1}. *Spectrum a* from the middle zone best demonstrate the opal-CT spectrum from this sample (Fig. XB).

Cristobalite was seen in the outer zone. Spectrum c from Fig. XC shows Raman peaks a 227 and 413 cm^{-1}. These peaks are diagnostic of Cristobalite.

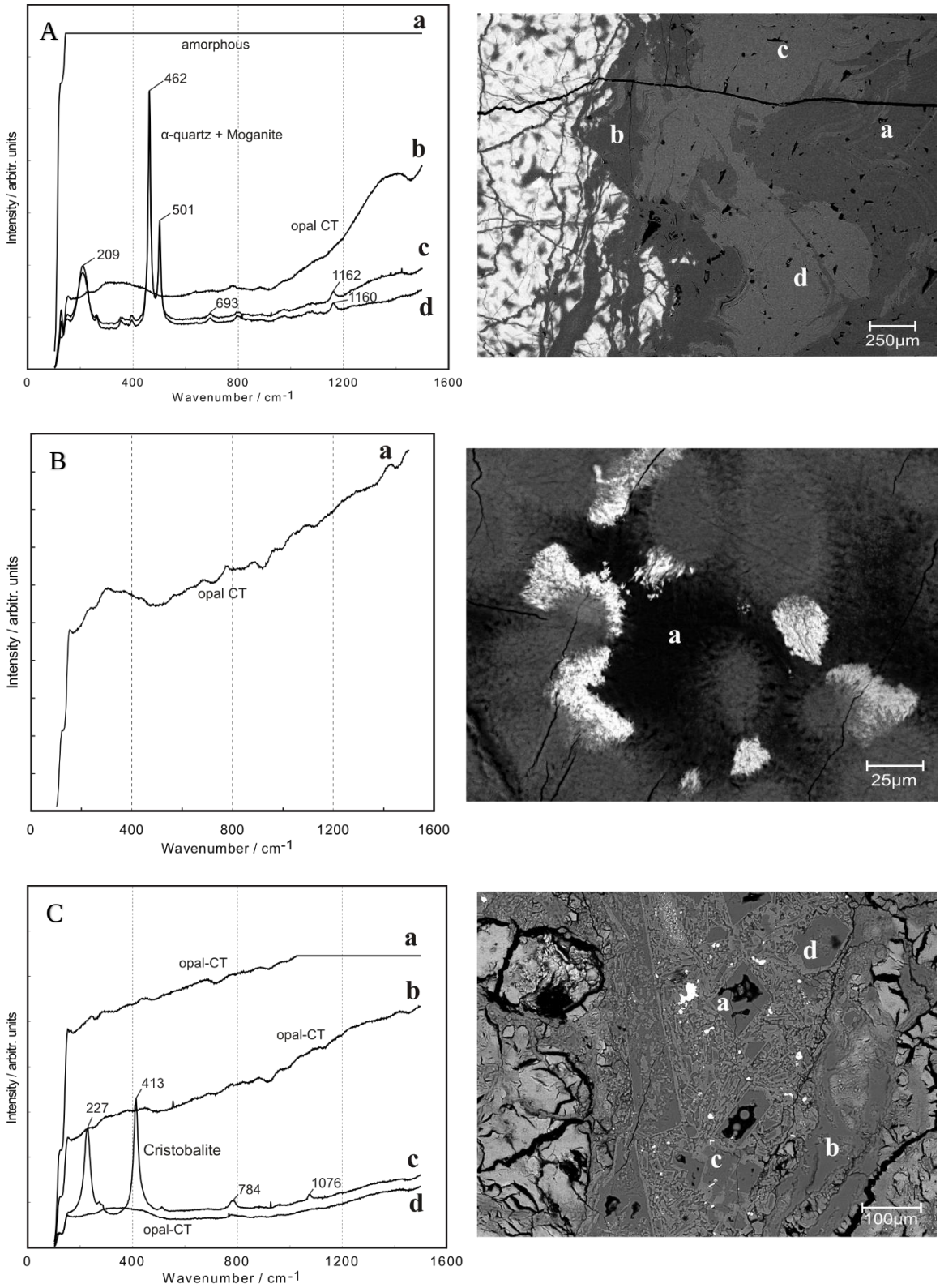

Figure 4.29. Raman spectra of silica polymorphs in the yellow zoned nodule (sample 800a). (A) Raman spectra of silica in the inner zone. (B) Raman spectra of silica in the middle zone. (C) Raman spectra of silica in the outer zone.

4.7.2: Altered Jithra ignimbite: sample 846a

The glass shards of the altered ignimbrite were mostly replaced by hydrothermal K-feldspar and silica. Cristobalite appears to be the silica polymorph that replaces the glass shards. Spectrum a, b, and c from Fig. 4.30B shows peaks at 227 and 413, 229 and 416, and 229 and 416 cm^{-1} respectively. Silica from an altered megacryst or xenocryst appears to be probably opal-CT with broad peaking ~200-600 cm^{-1}. Background noise was not removed so identification of spectrum b is inconclusive (Fig. 4.30A).

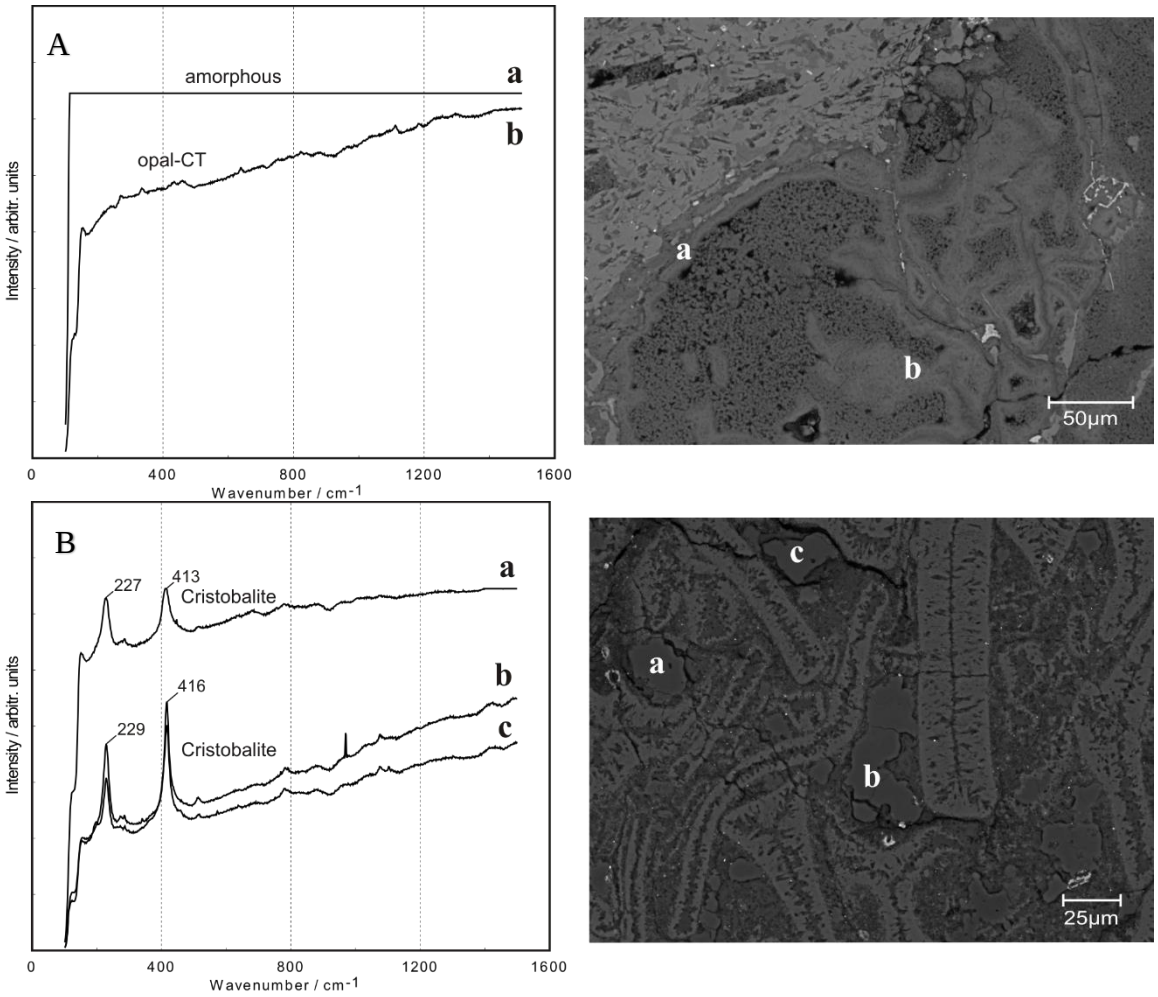

Figure X. Raman spectra of silica polymorphs in the altered Jithra ignimbrite (sample 846a). (A) Raman spectra of silica in an altered megacryst or xenocryst. (B) Raman spectra of silica replacing glass shards.

CHAPTER 5: DISCUSSION

5.1: Geological setting analogue

Western Lesbos is predominantly made up of thick Miocene volcanic rocks. Fig. 5.1 shows a cross section diagram of western Lesbos from Vatoussa (caldera) to Nissiopi (an island out west) based on field work (Pe-Piper and Piper, pers. comm.). The pyroclastic rocks are mostly unwelded pyroclastic flows with minor air tuff. In the study area, welded pyroclastic rocks are more abundant than ignimbrite. An isolated ignimbrite in Antissa may be related to the Polychintos ignimbrite on the eastern side of the island. Lava flows are also rare but increases closer to the caldera. The pyroclastics are interbedded with stream flow deposit originating from the caldera. There is no direct evidence of when silicification occurred. No silicified tree material has been seen re-worked into stream deposits and no silicified wood seen as clasts in conglomerate.

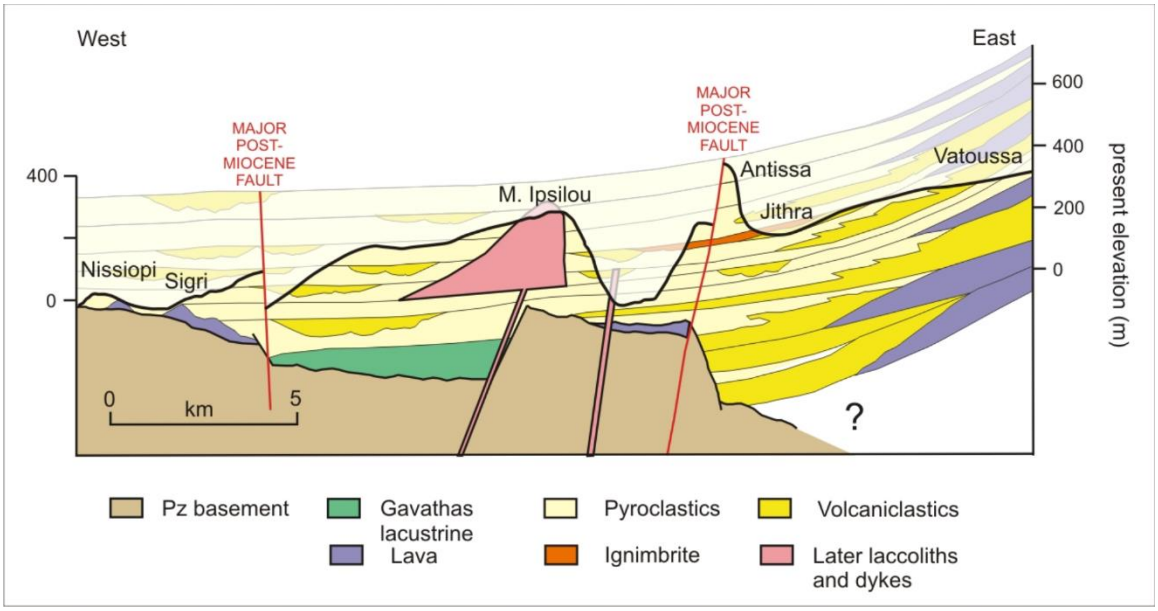

Figure 5.1. Cross section diagram of western Lesbos from Vatoussa (caldera) to the island of Nisiopi, based on fieldwork by G. Pe-Piper and D.J.W. Piper (pers. comm.).

Among possible analogues in the literature, the Taupo volcanic zone in New Zealand has some similarities to the setting of the Sigri Pyroclastic rocks. In the Taupo volcanic zone, three types of circulating groundwater are recognized (Simmons and Browne 2000, Rowland and Simmons 2012) and the chemical and physical properties assigned to these three types of water may be applicable to the Sigri Pyroclastics:

i. The deep parent water is almost neutral (pH) and is rich in CO_2 (about 26000 ppm), Cl (about 1000 ppm). These waters are probably the result of interaction between magma, host rock and groundwater. These fluids would enter open fractures (about 2 km depth) and start "boiling" due to loss of volatiles, notably H_2O and CO_2. This would then lead to the production of Cl-rich liquids.

ii. The acid-sulfate stream heated water forms in the vadose zone or the unsaturated zone. The vadose zone is thin and may only be a few metres thick.

iii. The steam rich in CO_2 condenses against cooler groundwater and produces H_2O with up to 13000 ppm of CO_2, but no Cl.

The preservation of alteration produced by these three water types greatly depends on hydrology, level of erosion, shifts in fluid flow over time. In the study area we have managed to find examples of all these types of alteration. Using the Taupo volcanic zone as an analogue for the Sigri Pyroclastics, the main features of the hydrothermal system can be summarized to:

1. The hydrothermal system in the region is epithermal

2. The distribution of hydrothermal minerals and mineral assemblages suggest variable distribution of the main thermal water types that have been found in the Taupo volcanic zone:
   (a) Deeply derived “chloride” containing waters. Such waters are probably responsible for the hydrothermal minerals quartz and K-feldspar we see in the studied rocks
   (b) Surficial acid-sulfate stream-heated waters responsible for the identified kaolinite
   (c) Peripheral CO_2-rich steam-heated waters responsible for the presence of smectite minerals

The heat from the emplacement of the Moni Ipsilou laccolith around 18 Ma ago may have driven the circulation of hydrothermal fluids. Figure 5.2 shows a schematic interpretation of the circulation of the three water types.

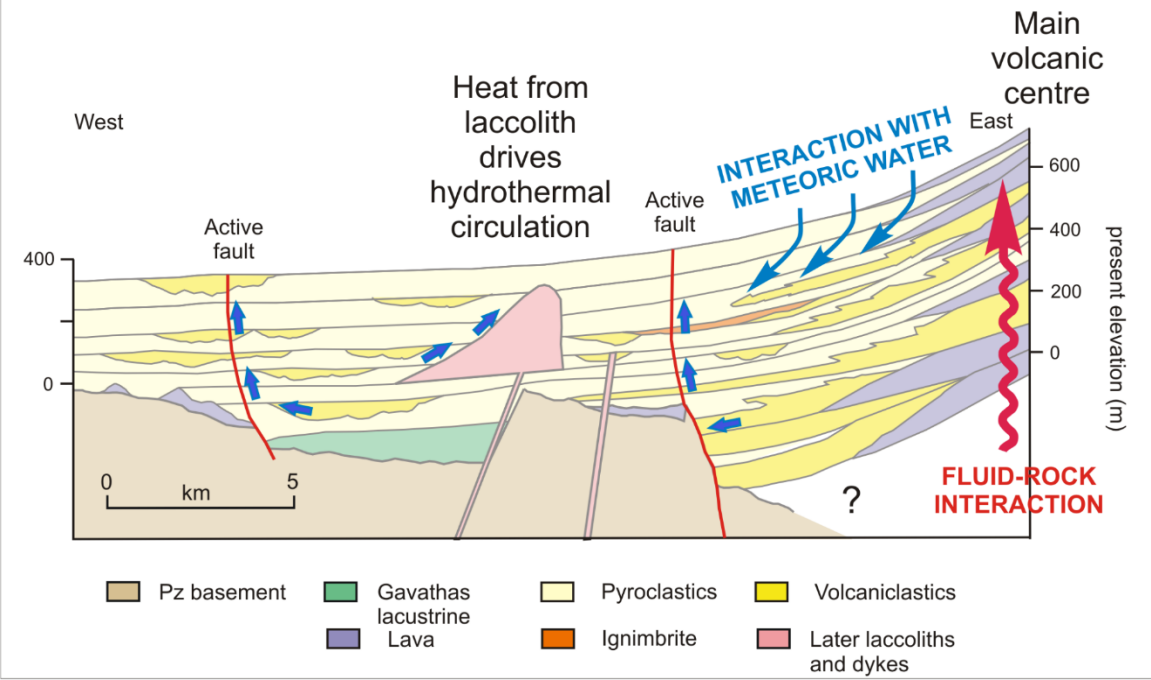

Figure 5.2. Cross section of western Lesbos from Figure 5.1 showing possible hydrothermal circulation pathways based on analogy with the Taupo volcanic zone (Rowland and Simmons, 2012).

5.2: "Mn-oxide" in the studied rocks

Possible Mn-minerals considered to be "Mn-oxide" in the studied rocks are hollandite/ ferrihollandite, romanechite, todorokite, ramsdellite and nsutite. These Mn-minerals are very similar with only slight variations chemically and structurally. Table 5.1 shows the chemical analyses from manganese minerals considered to be the "Mn-oxide" mineral. Detailed SEM-EDS analyses, EMP chemical analyses (App. 1, Tables 1&2) and X-ray powder diffraction was used to determine the "Mn-oxide" mineral present in the studied rocks.

Table 5.1. Chemical analyses from the literature of possible Mn-oxide mineral that might be present in the studied rocks (analyses are from the Handbook of Mineralogy).

	Romanechite		Hollandite/ Ferrihollandite			Todorokite		Nsutite		Ramsdellite	
WO_3		0.89									
As_2O_5	1.50										
SiO_2	0.40	0.52		0.58	0.70	0.45	0.24	1.17	0.46	0.36	0.42
MnO_2	**66.87**	**66.62**	**65.63**	**65.63**	**62.17**	**65.89**	**72.15**	**90.57**	**93.27**	**95.02**	**97.14**
Al_2O_3			0.94	1.45	1.20	0.28	0.14	0.22	0.50	0.72	0.48
Fe_2O_3	**1.45**	**0.15**	**10.56**	**12.63**	**12.17**	**0.20**	**0.06**	**1.07**	**0.49**	**0.22**	**0.34**
Mn_2O_3				**4.57**							
MnO	**8.23**	**7.09**	**5.12**		**4.16**		**8.87**	**2.60**	**1.76**		
NiO								0.14			
ZnO										0.25	n.d.
MgO								0.12	0.22		0.12
PbO				4.45	5.23						
CoO		0.90					0.02				
CuO	0.10	0.48									
MgO	0.20	0.15				1.01	3.51				
CaO	0.40	0.19				3.28	3.28	0.08	0.72	1.12	
SrO							0.24				
BaO	**16.20**	**17.46**	**17.59**	**13.81**	**14.38**	**2.05**	**2.05**				
Na_2O				0.58	0.36	0.21	1.23	0.06	<0.05	n.d.	0.31
K_2O	**0.10**			**0.23**		**0.54**	**0.48**	**0.22**	**0.19**	**n.d.**	**0.41**
H_2O^+		4.38				9.72		2.64	2.10	1.39	
H_2O^-		0.48				1.56		0.33	0.57	0.05	
H_2O	4.65						10.61				1.24
C								0.03			
CO_2						trace					
Pb_2O_5						0.42					
SO_3						0.28					
insol.						1.28					
Total	100.1	99.68	99.84	101.21	100.38	99.24	99.27	99.25	100.28	99.13	100.46

Chemically using SEM-EDS analyses, “Mn-oxide” shows the most resemblance to ferrihollandite and romanechite. In literature, the main difference between the two is the presence of Fe. Hollandite/ferrihollandite is an Fe-rich manganese mineral, while romanechite has little to no Fe. Most EDS analyses of “Mn-oxide” are mixtures of manganese + silica + iron, often having > 10% FeO and 3-20% BaO (App. 1, Table 1-1). Chemically todorokite, nsutite and ramsdellite do not contain Ba and therefore they cannot be the “Mn-oxide” mineral present in the studied rocks. The analysed “Mn-oxide” minerals are: 1) mixtures of hollandite/ferrihollandite with SiO_2 impurities; 2) mostly romanechite that has been analysed together with mixture 2 (Fe + Si) and; 3) mixture of both romanechite and hollandite with SiO_2 impurities. According to Post (1999), it has been shown that romenechite and hollandite often occur together on a very fine scale and that romanechite alters to hollandite during high temperatures. However, some analyses from sample 846 show little to no FeO (App. 1, Table 1-1) which suggests that romanechite is present in the rocks.

In addition, “Mn-oxide” minerals, presumed to be homogeneous, were analysed using the microprobe for more accurate chemical analyses. Most WDS chemical analyses from the microprobe of our “Mn-oxide” shows little, often < 1%, Fe, Al and Si (App. 1, Table 1-2). This further supports romanechite as the “Mn-oxide” mineral.

However no signs of romanechite or hollandite/ferrihollandite wre detected using X-ray diffraction analysis. Todorokite, ramsdellite and nsutite have diffraction peaks that match our “Mn-oxide” diffractogram of sample 846a. It is not known how reliable are the X-ray data for these minerals, or if all three co-exist. Furthermore chemically these

manganese minerals do not match the studied “Mn-oxide” minerals. However the presence of an amorphous manganese mineral of romanechite chemical composition should not be ruled out. It is also in the literature (Post, 1999) that Mn-oxide minerals often are very fine-grained with poor crystalline structures. Therefore chemically and structurally an amorphous manganese mineral with a chemical composition of romanechite is the most plausible “Mn-oxide” mineral present in the studied rocks. Samples with lower BaO content may have some better crystalline grains of todorokite, ramsdellite and/or nsutite in addition to romanechite.

5.3: Abundance of concentrated Mn-oxides in Lesbos

The volcano slopes in Lesbos were forested with multiple tree horizons (Vasileiadou and Zouros, 2012) creating multiple soil horizons. Therefore bacterial decay of organic matter would have been very important in the creation of local reducing conditions. The mobility of manganese may be related to this decay of organic matter because of the variable oxidation states of Mn.

In the ocean, during bacterial decay of organic matter, it is easier to reduce Mn rather than Fe, and thus easier to produce manganous compounds than ferrous compounds (Canfield and Thamdrup, 2009).

Mn-oxide precipitation appears to be microbially mediated (Kilias et al., 2007; Polgari et al., 2012) and may also result in enrichment in bioessential elements including Fe, S, Mg, As, Ba, Sr, P, Co and Ce. Most examples in the literature are from marine exhalative systems, but there appears to be no theoretical barrier to similar processes taking place in terrestrial systems. There are no evidence for marine conditions in Lesbos before the Tortonian (ca. 12 Ma).

5.4: Fe-rich silica (mixture 2) and its deposit analogue

The structure of the yellow zoned nodule (sample 800a) appears to indicate a gradual formation shown in Fig. 5.3. Being formed in a fault zone it was on the pathway of the hydrothermal solutions. It appears to have started with the alteration of the country rock (outer zone). The outer zone consists of altered crystals of feldspars, ilmenite and Ti-magnetite, evidence of fluid interaction with the country rock (F.R.I) which are the Sigri Pyroclastic rocks. An Fe-rich silica (mixture 2) (stippled yellow zone in Fig. 5.3) later filled the void followed by the formation of "Mn-oxide" crystallites/aggregates (purple pebbles in Fig. 5.3). The nodule suffered fracturing before pure silica finally clogged the whole void. This is depicted by pure silica veins cross-cutting mixture 2 and the "Mn-oxide" aggregates in the middle zone.

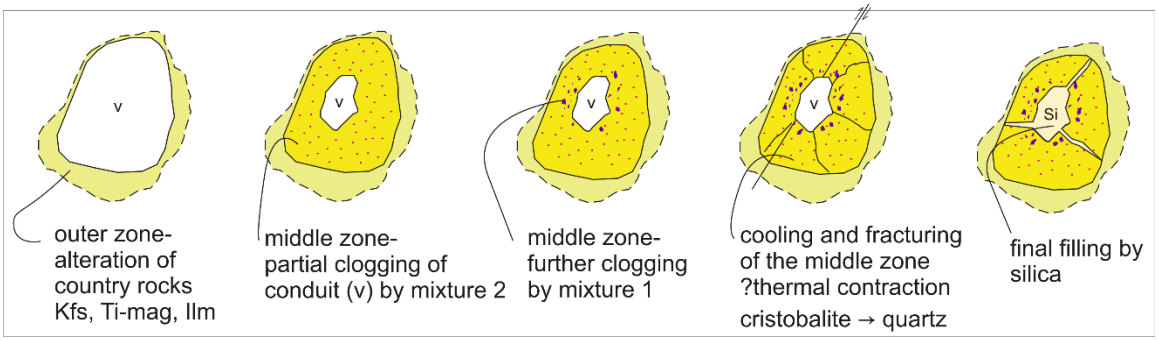

Figure 5.2. The stages of how the yellow nodule (sample 800a) possibly got filled. The stippled yellow middle zone is mixture 2 (Si + Fe). The purple tiny pebbles are mixture 1 (Si + Fe + Mn).

A possible rock type analogue for what we see in the yellow zoned nodules and the yellow or yellow brown veins are the Fe-silica mixtures (jaspers) found in exhalative marine systems and their sub-surface fluid pathways (e.g. Bathurst in New Brunswick Canada, and Ireland). Table 5.5.1 shows how mixture 2 (Si + Fe) compares to jasper

described by Hollis. Such rocks appears to be chemically and mineralogically similar with mixture 2, based on chemical compositions reported by Hollis et al (2015).

Table 5.2. Average chemical analyses of Fe-silica, mixture 2 (Si + Fe), from the studied rocks and whole rock analyses of sea floor jasper and hematitic slate from Hollis et al., 2005.

Sample	800a	807	Hollis et al. (WRA)		
Type	Nodule	Vein	Layer	Clast	Slate
SiO_2	**66.89**	**74.65**	**69.30**	**81.20**	**59.20**
TiO_2	0.06	0.00	0.08	0.03	0.43
Al_2O_3	2.54	0.54	1.50	0.59	7.40
FeO	**26.11**	**21.17**	**21.92**	**13.88**	**18.10**
MnO	0.06	0.06	0.12	0.05	0.13
MgO	2.59	2.07	1.10	0.05	6.30
CaO	1.26	1.15	1.80	1.10	2.20
Na_2O	0.23		0.11	0.09	0.07
K_2O	0.20	0.33	0.34	0.06	<0.01
P_2O_5	0.02		<0.05	0.06	0.16
SO3	0.04				
Cl		0.01			
BaO	0.01	0.02			
CO_2			1.00	0.78	0.03
H_2O^+			1.30	0.76	4.00
H_2O^-			0.13	0.02	0.39
Total	100.00	100.00			
Actual Total	104.07	85.68	100.38	100.19	99.71
No. of analyses	98	86	1	1	1

5.5: Different colours of (silica) petrification

The colours of petrification investigated through chemical analyses acquired using energy dispersive spectroscopy and wavelength dispersive spectroscopy, or SEM and EMP respectively shows that the different hues of colours are related to availability of carbon/ organic material and iron. The various colors observed from the petrified wood (sample 856-1) range from black to yellow to greenish green to dark orange-red to white. Analysed silica from the petrified wood shows Fe as a major element and various trace elements that could be potentially the source of the different hints of colours observed.

The black color can be associated with the presence of carbon or organic matter when silicification occurred. Chemically the black areas are mostly pure silica. In literature, petrification produces a black colour when pyrite is present however no pyrite was detected both using SEM and EMP analysis. EMP chemical analyses from the black areas however show traces of bio-essential trace elements of Zn, V, Sr and S that could be responsible for the dark/ colour of silica.

The various hints of either yellow, green, orange or red colours may have been influenced by the presence of Fe. SEM-EDS analyses of the petrified wood shows an abundant Fe content in the yellow to dark orange-red areas suggesting the presence of Fe-oxide in silica may be responsible for those colours. The intensity of the colour seems to increases with the amount of Fe-oxide present. Analyses from the yellow area shows “Fe-oxide” + silica mixtures with few crystallites of “Fe-oxide”. Analyses from the yellow orange and orange areas shows “Fe-oxide” + silica mixtures with precipitates of “Fe-oxide” in wood vessels. Analyses from the dark orange area shows “Fe-oxide” precipitates completely or mostly filling wood vessels. Using these observations, it can be

concluded that the colour range of yellow to dark orange-red are influenced by the amount of Fe present in the wood. Microprobe analyses from the same areas coincide with this hypothesis (App. 2, Table 2). Chemical analyses with higher Fe content shows a darker shade of the orange colour. While less Fe content gives off a faint or pale yellow hint of colour.

The white colour observed chemically are mostly pure silica.

CHAPTER 6: CONCLUSIONS

1) The epithermal system of the Taupo volcanic zone in New Zealand has a very similar geological setting to the Sigri Pyroclastics. The types of alteration produced by different circulating waters were also observed in the study area.

2) The distinctive amorphous silica + Fe-oxide are chemically and mineralogically comparable with “jaspers” found in marine exhalative systems. Faulting and complex hydrothermal mineralization may have been related to the emplacement of laccoliths around 18 Ma, the silicification of the petrified wood was probably earlier.

3) The various colours observed from the petrified wood is related to the abundance and availability of carbon and/or organic matter and iron in the area. The black color is produced by carbon while the variety of yellow-red colours are produced by iron. The intensity of the yellow-red color is proportionate to the quantity of iron present in the petrified wood.

REFERENCES

Ballhaus, C., Gee, C.T., Bockrath, C., Greef, K., Manfeldt, T., and Rhede, D., 2012. The silicification of trees in volcanic ash – An experimental study. Geochimica et Cosmochimica Acta, v. 84, pp. 62-74.

Brindley, G.W., and Brown, G., 1980. Crystal Structures of Clay Minerals and Their X-Ray Identification. Mineralogical Society, p. 495.

Canfield, D.E., and Thamdrup, B., 2009. Towards a consistent classification scheme for geochemical environments, or, why we wish the term 'suboxic' would go away. Geobiology, v. 7, no. 4, pp. 385-392.

Dekov, V.M., Lalonde, S.V., Kamenov, G.D., Bayon, G., Shanks III, W.C., Fortin, D., Fouquet, Y., and Moscati, R.J., 2015. Geochemistry and mineralogy of a silica chimney from an inactive seafloor hydrothermal field (East Pacific Rise, 18°S). Chemical Geology, v. 415, pp. 126-140.

Florke, O.W., Hollman, R., von Rad, U., Rosch, H, 1976. Intergrowth and twinning in opal-CT lepispheres. Contributions to Mineralogy and Petrology, v.58, pp. 235-242.

Florke, O.W., Jones, J.B., and Segnit, E.R., 1973. Opal CT crystals. Neues Jahrbuch fuer Mineralogie: Monatshefte, v. 8, pp. 369-377.

Florke, O.W., Graetsch, H., Martin, B., Roller K. and Wirth, R., 1991. Nomenclature of micro- and non-crystal- line silica minerals, based on structure and micro structure. Neues Jahrbuch Mineralogie Abhandlungen, v. 163, pp. 19-42.

Hecht, J. Geological map of Greece, 1:50,000, 1972-1976

Hollis, S.P., Cooper, M.R., Herrington, R.J., Roberts, S., Earls, G., Verbeeten, A., Piercey, S.J., Archibald, S.M., 2015. Distribution, mineralogy and geochemistry of silica-iron exhalites and related rocks from the Tyrone Igneous Complex: Implications for VMS mineralization in Northern Ireland. Journal of Geochemical Exploration, v. 159, pp. 148-168.

Ilieva, A., Mihailova, B., Tsintsov, Z., and Petrov, O., 2007. Structural state of microcrystalline opals: A Raman spectroscopic study. American Mineralogist, v. 92, pp. 1325-1333.

Juniper, S.K., and Fouquet, Y., 1988. Filamentous iron-silica deposits from modern and ancient hydrothermal sites. Canadian Mineralogist, v. 26, pp. 859-869.

Kilias, S.P., 2012. Microbial mat–related structures in the Quaternary Cape Vani manganese-oxide (-barite) deposit, NW Milos island, Greece. Microbial Mats in

Siliciclastic Depositional Systems Through Time, SEPM (Society for Sedimentary Geology) Special Publication, 101, pp.97-100.

Kingman, K.J., and Hemley, R.J., 1994. Raman spectroscopic study of microcrystalline silica. American Mineralogist, v. 79, pp. 269-273.

Pe-Piper, G., Piper, D.J.W. and Reynolds, P.H., 1983. Paleomagnetic stratigraphy and radiometric dating of the Pliocene volcanic rocks of Aegina, Greece. Bull. Volc., v. 46, pp. 1-7.

Pe-Piper, G., and Piper, D.J.W., 1992. Geochemical variation with time in the Cenozoic high-K volcanic rocks of the island of Lesbos, Greece: significance for shoshonite petrogenesis. Journal of Volcanology and Geothermal Research, v. 53, pp. 371-387.

Pe-Piper, G., Matarangas, D., Reynolds, P.H., and Chatterjee, A.K., 2003. Shoshonites from Agios Nectarios, Lesbos, Greece: origin by mixing of felsic and mafic magma. Eur. J. Mineral, v. 15, pp. 117-125.

Pe-Piper, G., 1980. Geochemistry of Miocene Shoshonites, Lesbos, Greece. Contrib. Mineral. Petrol., v. 72, pp. 387-396.

Polgári, M., Hein, J.R., Vigh, T., Szabó-Drubina, M., Fórizs, I., Bíró, L., Müller, A. and Tóth, A.L., 2012. Microbial processes and the origin of the Úrkút manganese deposit, Hungary. Ore Geology Reviews, 47, pp.87-109.

Post, J.E., 1999. Manganese oxide minerals: Crystal structures and economic and environmental significance. The National Academy of Sciences, v. 96, no. 7, pp. 3447-3454.

Rodgers., K.A., and Hampton, W.A., 2003. Laser Raman identification of silica phases comprising microtextural components of sinters. Mineralogist Magazine, v. 67(1), pp. 1-13.

Rowland, J.V. and Simmons, S.F., 2012. Hydrologic, magmatic, and tectonic controls on hydrothermal flow, Taupo Volcanic Zone, New Zealand: Implications for the formation of epithermal vein deposits. Economic Geology, 107(3), pp.427-457.

Sener, M., and Gevrek, A.I., 2000. Distribution and significance of hydrothermal alteration minerals in the Tuzla hydrothermal system, Canakkale, Turkey. Journal of volcanology and geothermal research, v. 96, pp. 215-228.

Simmons, S.F., and Browne, P.R.L., 2000, Hydrothermal minerals and precious metals in the Broadlands-Ohaaki geothermal system: Implications for understanding low sulfidation epithermal environments. Economic Geology, v. 95, p. 971−999.

Vasileiadou, K. and Zouros, N., 2012. Early Miocene micromammals from the Lesvos Petrified Forest (Greece): preliminary results. Palaeobiodiversity and Palaeoenvironments, 92(2), pp.249-264.

Voudouris, P., Velitzelos D., Velitzelos, E., and Thewald, U., 2007. Petrified wood occurrences in western Thrace and Limnos Island: Mineralogy, Geochemistry and depositional environment. Bulletin of the Geological Society of Greece, v. 40.

Appendix 1: SEM-BSE images, energy dispersive spectroscopy (EDS) mineral analyses, and electron microprobe (EMP) chemical analyses of “Mn-oxide” minerals for samples 806 and 846a

Appendix 1-1: SEM-BSE images and energy dispersive spectroscopy (EDS) mineral analyses of “Mn-oxide” minerals for samples 806, 846a

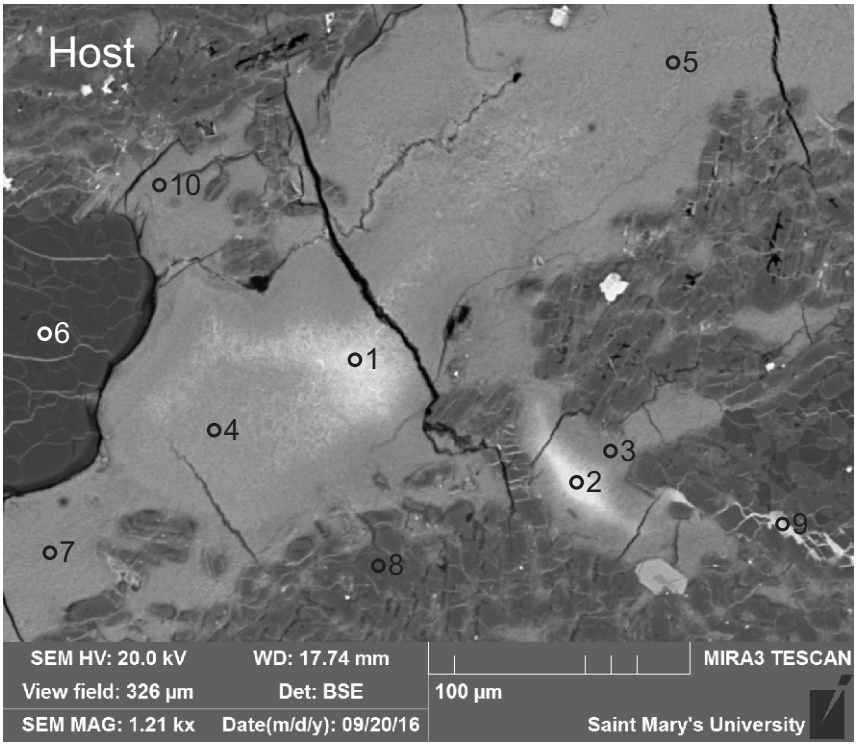

1:"Mn-oxide"
2:"Mn-oxide"
3:Mn+Silica+ "Fe-oxide"
4:Mn+Silica+ "Fe-oxide"
5:Mn+Silica+ "Fe-oxide"
6:Silica
7:Mix
8:Andesine
9:"Mn-oxide"
10:Mix

Figure 1-1.1: Sample 806 site 1 (SEM) (Table 1-3.1). A site showing a vein made up of Mn+silica+"Fe-oxide" mixture (3-5) with "Mn-oxide" crystallites (1,2) growing in the middle.

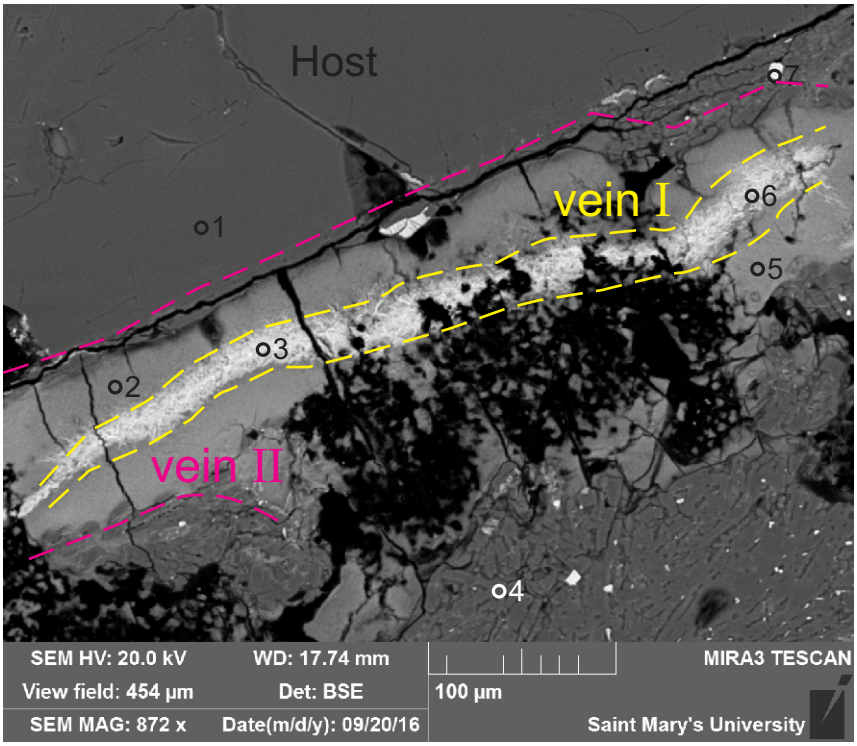

1:Andesine
2:Mix
3:"Mn-oxide"
4:Sanidine
5:"Fe-oxide"+Silica
6:"Mn-oxide"
7:Ti-Magnetite

Figure 1-1.2: Sample 806 site 2 (SEM) (Table 1-3.1). A site showing vein I (mixture of Mn+silica+"Fe-oxide") and vein II (mixture of "Fe-oxide" and silica cut the host tuff. Vein I posdates vein II.

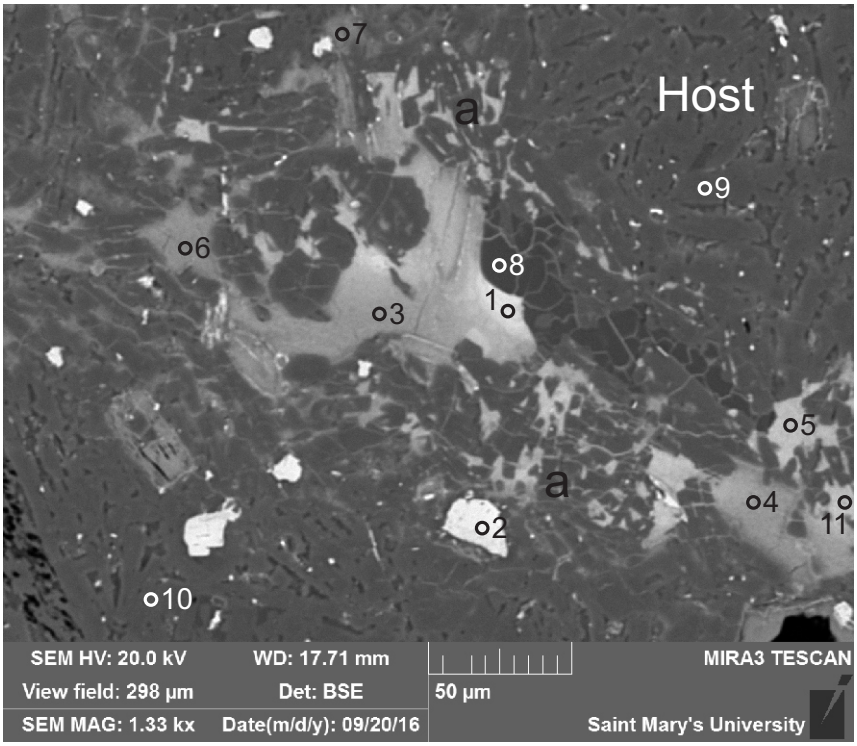

1:"Mn-oxide"
2:Ti-Magnetite
3:Mix
4:Mix
5:"Mn-oxide"
6:Mix
7:Mix
8:Silica
9:Andesine
10:K-feldspar
11:"Mn-oxide"

Figure 1-1.3: Sample 806 site 3 (SEM) (Table 1-3.1). A highly brecciated silica (8) cut by a diffuse vein, a mixture of Mn+silica+"Fe-oxide" (romanechite, 1). It appears that the same vein mixture later filled in the spaces in between the silica fragments (position a).

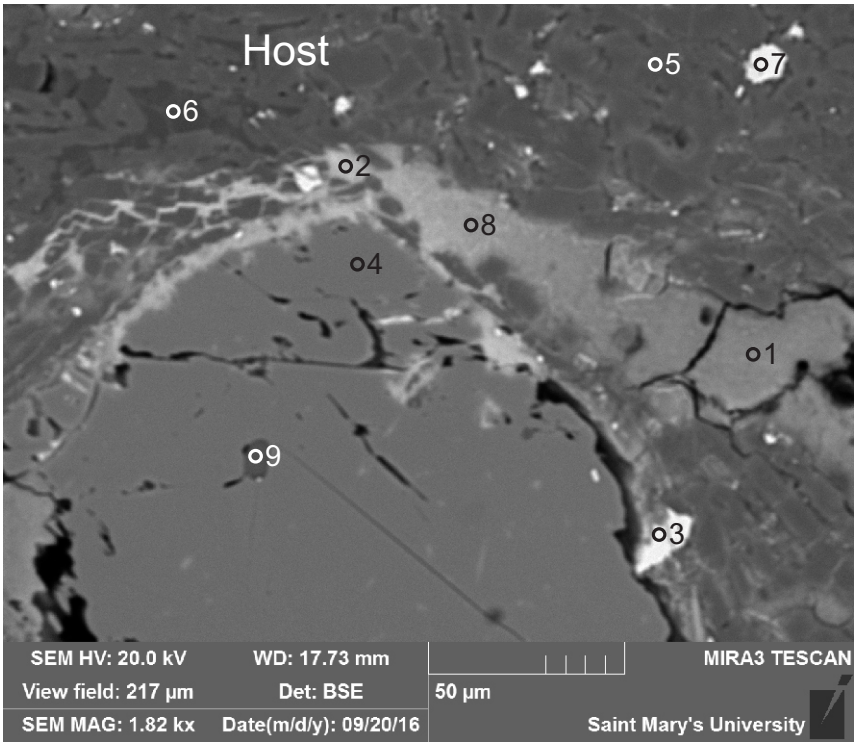

1:Mix
2:"Mn-oxide"+Silica
3:Ti-Magnetite
4:Diopside
5:Andesine
6:Silica
7:Ti-Magnetite
8:"Mn-oxide"
9:Andesine

Figure 1-1.4: Sample 806 site 4 (SEM) (Table 1-.3.1). A site showing the "Mn-oxide"+silica vein (1,2) rimming a diopside (4) crystal with andesine inclusions (9).

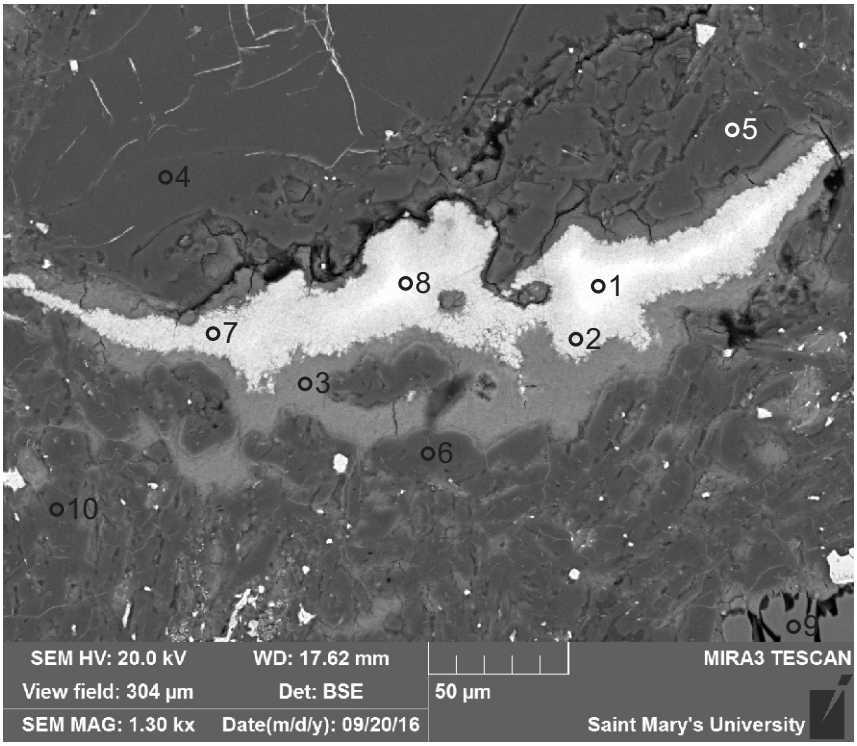

1:"Mn-oxide"
2:"Mn-oxide"
3:"Fe-oxide"+Silica
4:Andesine
5:Andesine
6:K-feldspar
7:"Mn-oxide"
8:"Mn-oxide"
9:Diopside
10:Andesine

Figure 1-1.5: Sample 806 site 5 (SEM) (Table 1-3.1). In this site, it appears that "Mn-oxide"(?to be finalized) (1,2,7,8) is replacing the "Fe-oxide" + silica mixture (3).

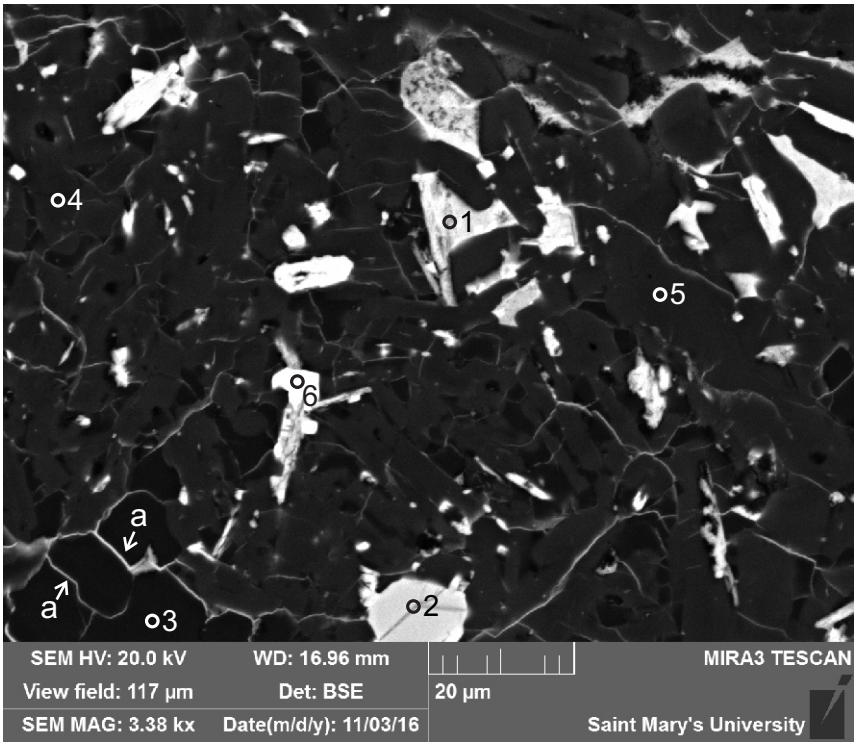

1:"Mn-oxide"+Silica
+"Fe-oxide"
2:Ilmenite
3:Silica+
4:Oligoclase
5:Oligoclase
6:Zirconolite?

Figure 1-1.6: Sample 806 site 6 (SEM) (Table 1-3.2). It appears that the oligoclase crystals (4,5) are often rimmed by silica (3). Silica is then cross-cut by "Mn-oxide"+Silica+"Fe-oxide" mixture (1) or rimmed by it (positions a).

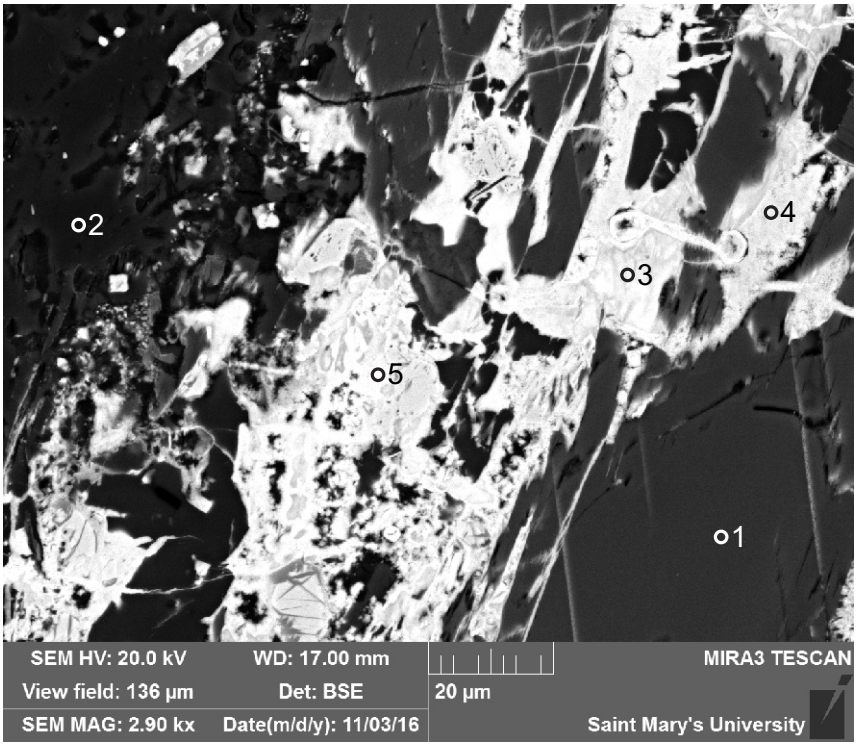

1:Hornblende
2:Andesine
3:"Mn-oxide"+Silica +"Fe-oxide"
4:"Mn-oxide"+Silica +"Fe-oxide"
5:"Mn-oxide"+Silica +"Fe-oxide"

Figure 1-1.7: Sample 806 site 7 (SEM) (Table 1-.3.2). It appears that silica first invaded hornblende along it's cleavage planes and fractures (positions a) and is later followed by the "Mn-oxide"+Silica+"Fe-oxide" mixture (3,4,5 and position a in Fig. 1-3.23)

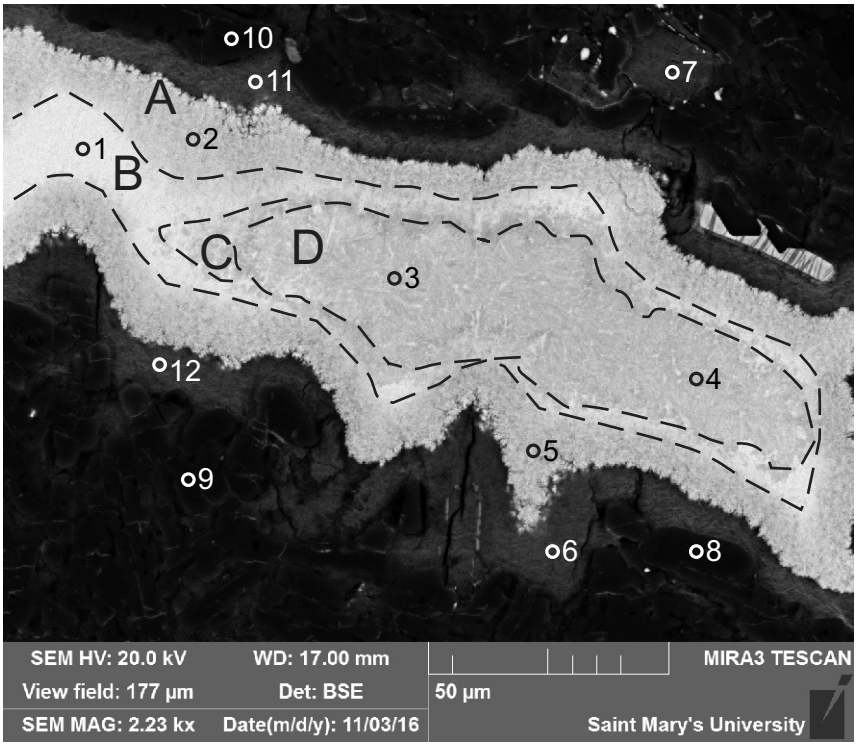

1:"Mn-oxide"+Silica
2:"Mn-oxide"+Silica+ "Fe-oxide"
3:"Mn-oxide"
4:"Mn-oxide"+Silica
5:"Mn-oxide"+Silica+ "Fe-oxide"
6:"Fe-oxide"+Silica
7:"Fe-oxide"+Silica
8:Andesine
9:Andesine
10:Andesine
11:"Fe-oxide"+Silica
12:"Fe-oxide"+Silica

Figure 1-1.8: Sample 806 site 8 (SEM) (Table 1-3.2). A site showing a mineral zonation in the "Mn-oxide"+silica+"Fe-oxide" vein. Zone D appears to have high Mn analyses and lower Ba and Fe analyses. In contrast, Zone B has a higher Ba analyses. Zone A has the highest SiO_2 contents.

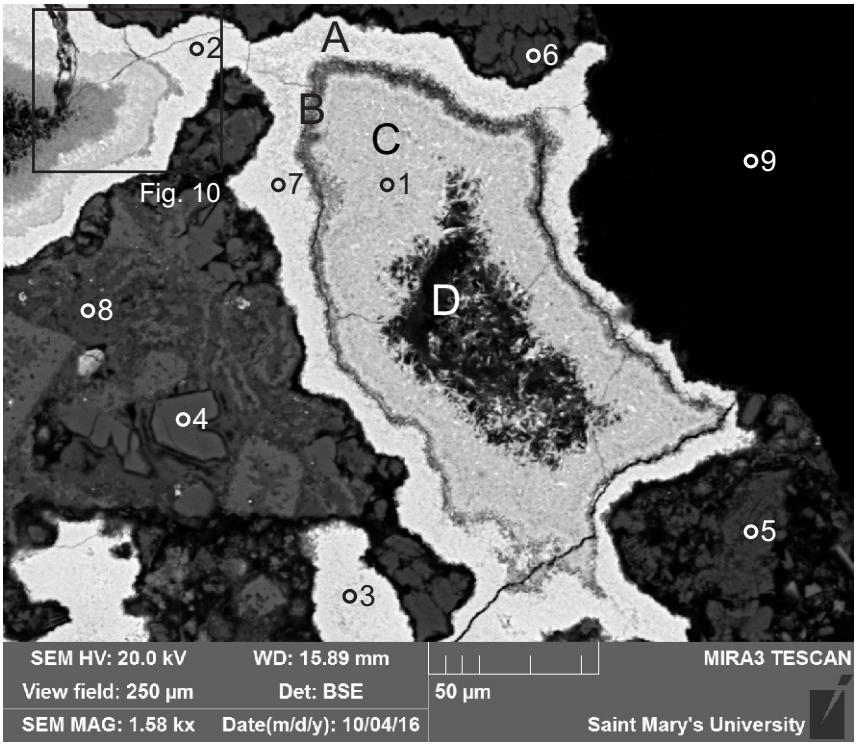

1:"Mn-oxide"
2:"Mn-oxide"
3:"Mn-oxide"
4:Silica
5:Kaolinite
6:Kaolinite+
"Fe/ Mn-oxide"
7:"Mn-oxide"
8:Silica+Glass
9:Void

Figure 1-1.9: Sample 846a site 9 (SEM) (Table 1-11.1). A cavity filled in by "Mn-oxide" (7) in zone A, a different looking "Mn-oxide" (1) in zone C and partly filled in zone D.

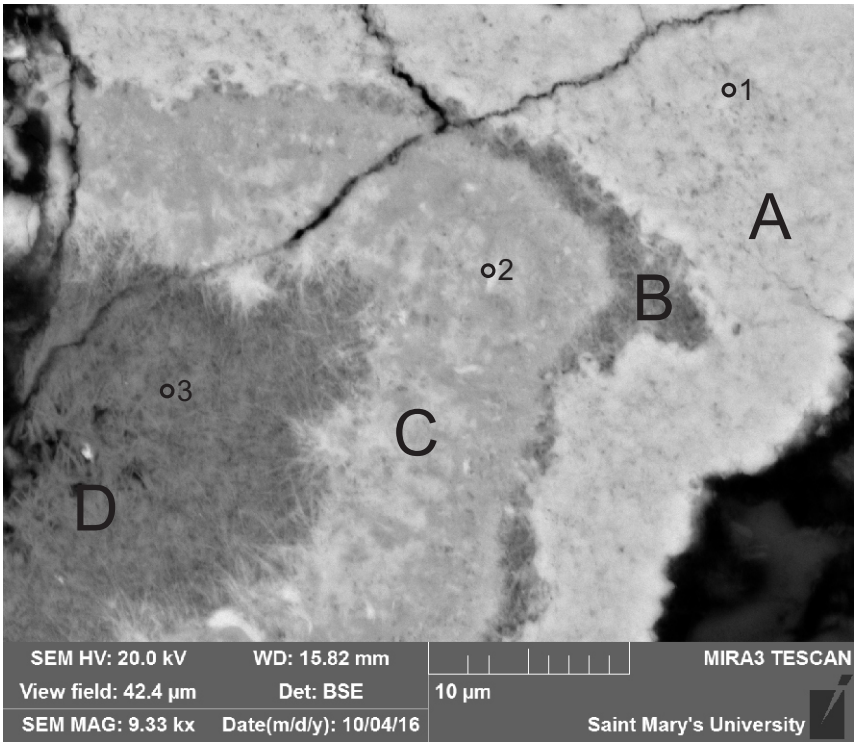

1:"Mn-oxide"
2:"Mn-oxide"
3:

Figure 1-1.10: Sample 846a site 10 (SEM) (Table 1-11.1). A site showing the zonation of the Mn-vein. Zone A represent "Mn-oxide" with high Ba (1), Zone B was not analysed, Zone C represent low Ba (2) "Mn-oxide", while Zone D is an Al-Mn-mineral.

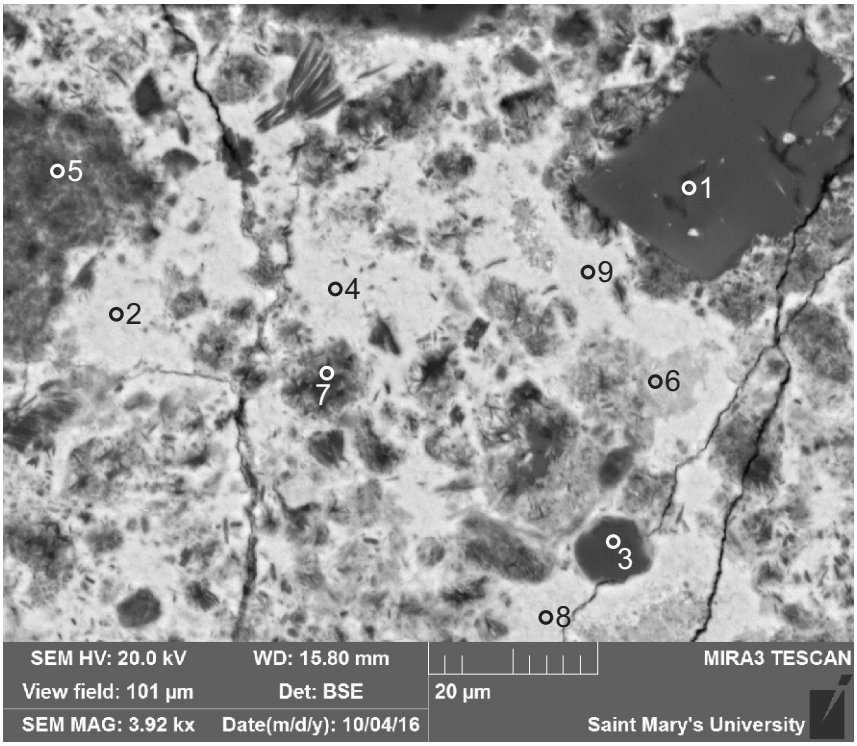

1:K-feldspar
2:"Mn-oxide"
3:Silica
4:"Mn-oxide"
5:Kaolinite+
"Mn-oxide"
6:"Mn-oxide"
7:Kaolinite+
"Mn-oxide"
8:"Mn-oxide"
9:"Mn-oxide"

Figure 1-1.11: Sample 846a site 11 (SEM) (Table 1-11.1). A highly brecciated site. "Mn-oxide" (2,4,6,8,9) later filled in the cracks?

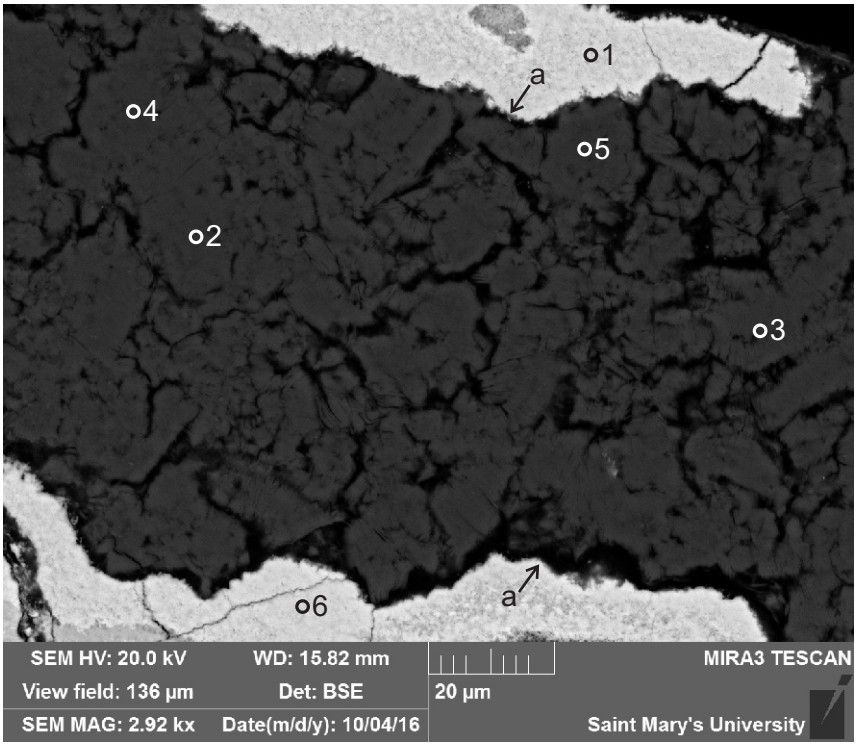

1:"Mn-oxide"
2:Kaolinite
3:Kaolinite
4:Kaolinite
5:Kaolinite
6:"Mn-oxide"

Figure 1-1.12: Sample 846a site 12 (SEM) (Table 1-11.1). Feldpar or glass has been altered to kaolinite (2-5). It appears that there was variable volume reduction after "Mn-oxide" precipitation (positions a).

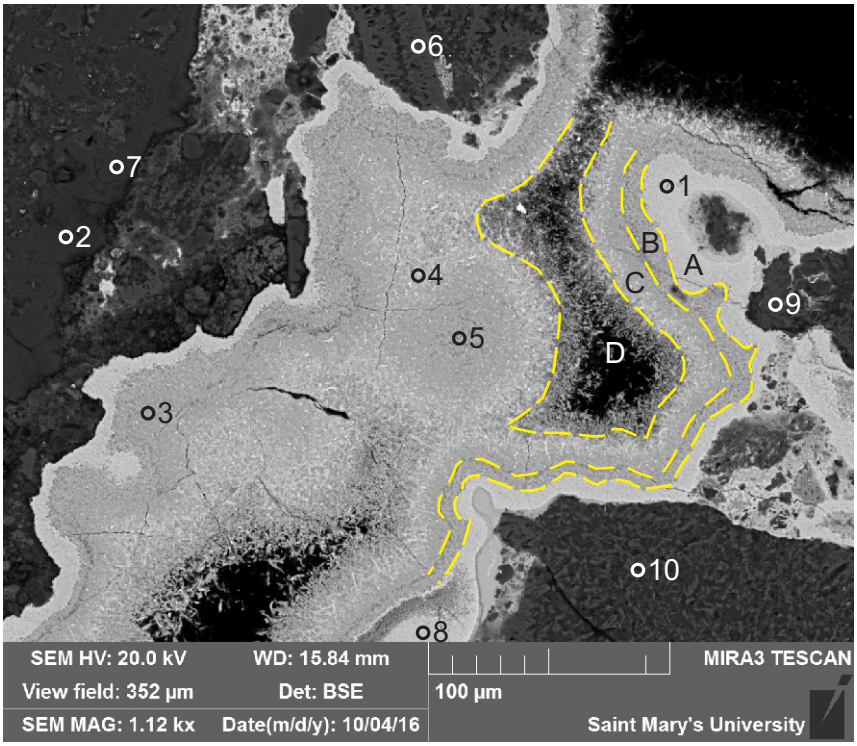

1:"Mn-oxide"
2:Silica
3:"Mn-oxide"
4:"Mn-oxide"
5:"Mn-oxide"
6:K-feldspar
7:Silica
8:"Mn-oxide"
9:Glass
10:Silica+Glass

Figure 1-1.13: Sample 846a site 13 (SEM) (Table 1-11.1). "Mn-oxide" appears to grow in bands of different brightness (A,B,C and D) that reflect increase in MnO as the brightness goes from light (1) to dark (5).

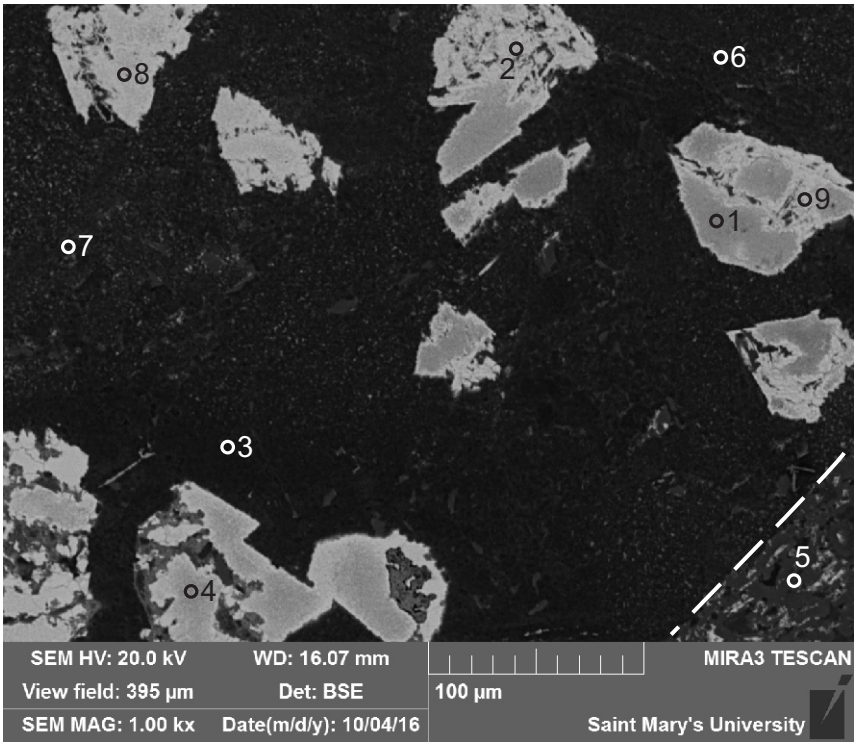

1:"Mn-oxide"
2:"Mn-oxide"
3:Kaolinite
4:"Mn-oxide"
5:K-feldspar
6:Kaolinite+
"Mn-oxide"
7:Kaolinite+
"Mn-oxide"
8:"Mn-oxide"
9:"Mn-oxide"

Figure 1-1.14: Sample 846a site 14 (SEM) (Table 1-11.1). A site showing "Mn-oxide" (1,2,4,8,9) growing in glass (5).

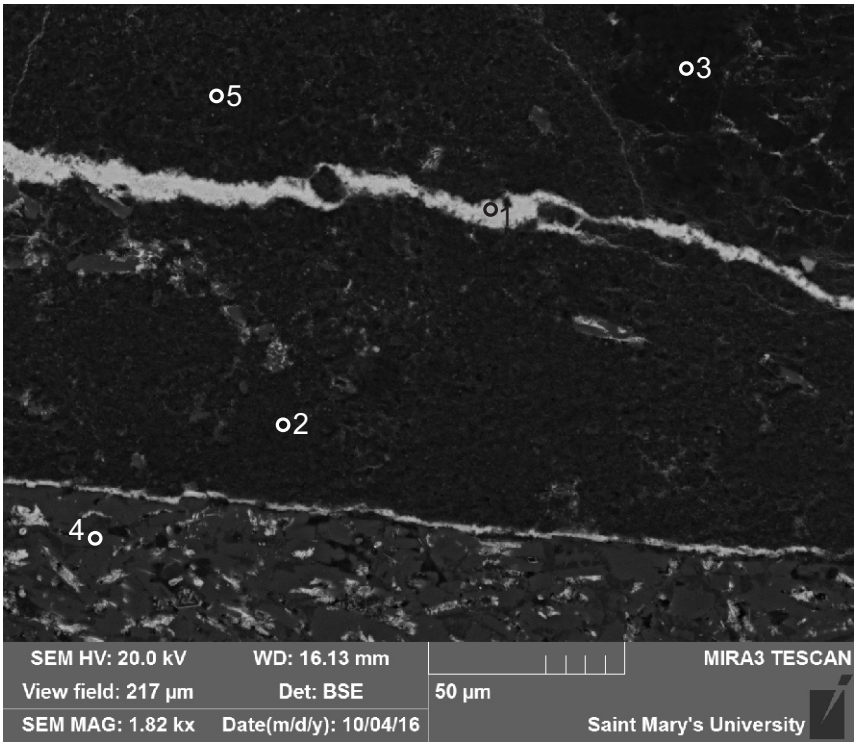

1:"Mn-oxide"
2:Kaolinite+Mn
3:Kaolinite
4:Glass
5:Kaolinite

Figure 1-1.15: Sample 846a site 15 (SEM) (Table 1-11.1). A vein of "Mn-oxide" (1) cutting across kaolinite.

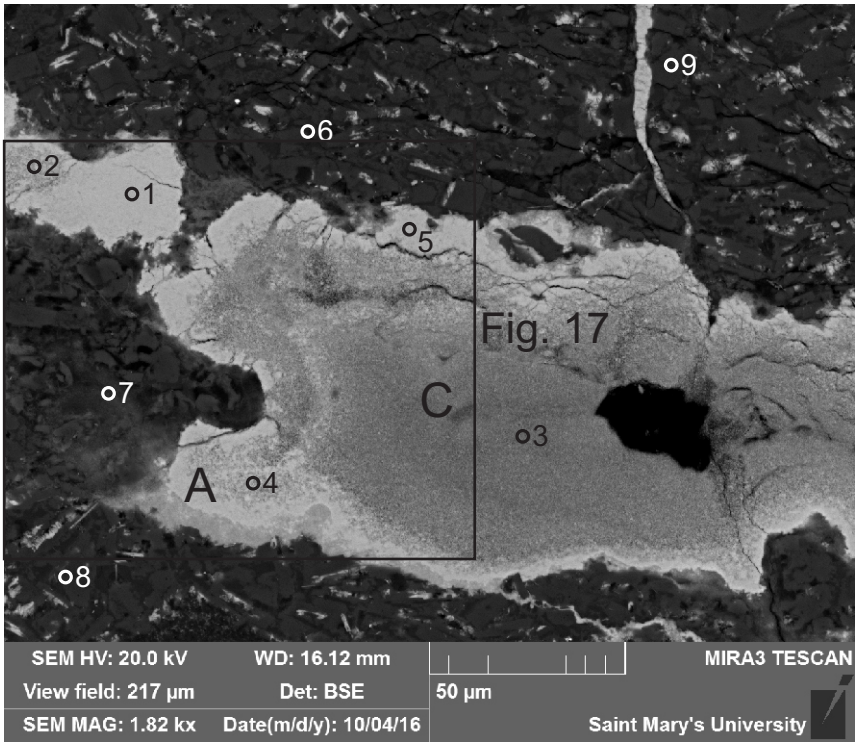

1:"Mn-oxide"
2:"Mn-oxide"
3:"Mn-oxide"
4:"Mn-oxide"
5:"Mn-oxide"
6:Glass+Silica
7:Mix
8:Glass+Silica
9:K-feldspar

Figure 1-1.16: Sample 846a site 16 (SEM) (Table 1-11.1). Another site showing the "Mn-oxide" vein zoning in partly silicified glass. Zone A has higher Ba while Zone C has a lower Ba content (6,8). K-feldspar (9) are also present(9).

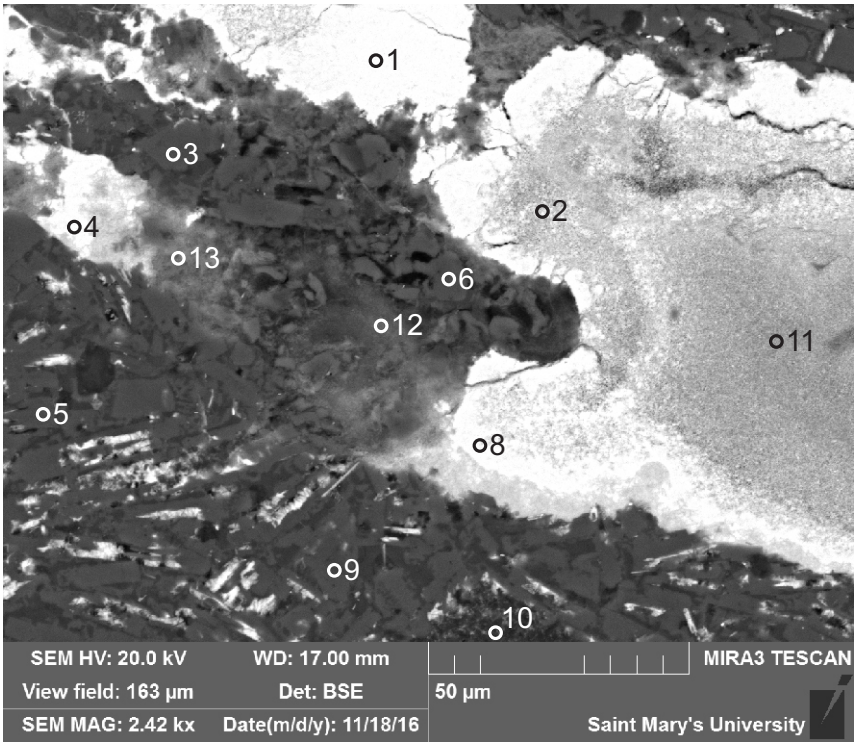

1:"Mn-oxide"
2:"Mn-oxide"
3:K-feldspar
4:"Mn-oxide"
5:K-feldspar
6:K-feldspar
7:"Mn-oxide"
8:"Mn-oxide"
9:K-feldspar
10:Kaolinite
11:"Mn-oxide"+
12:"Mn-oxide"+
"Fe-oxide"
13:"Mn-oxide"+
"Fe-oxide"

Figure 1-1.17: Sample 846a site 17 (SEM) (Table 1-11.2). A site showing what appears to be a K-feldspar-rich rock (3,5,6,9) with some kaolinite (10) and is cut by the Mn-vein system.

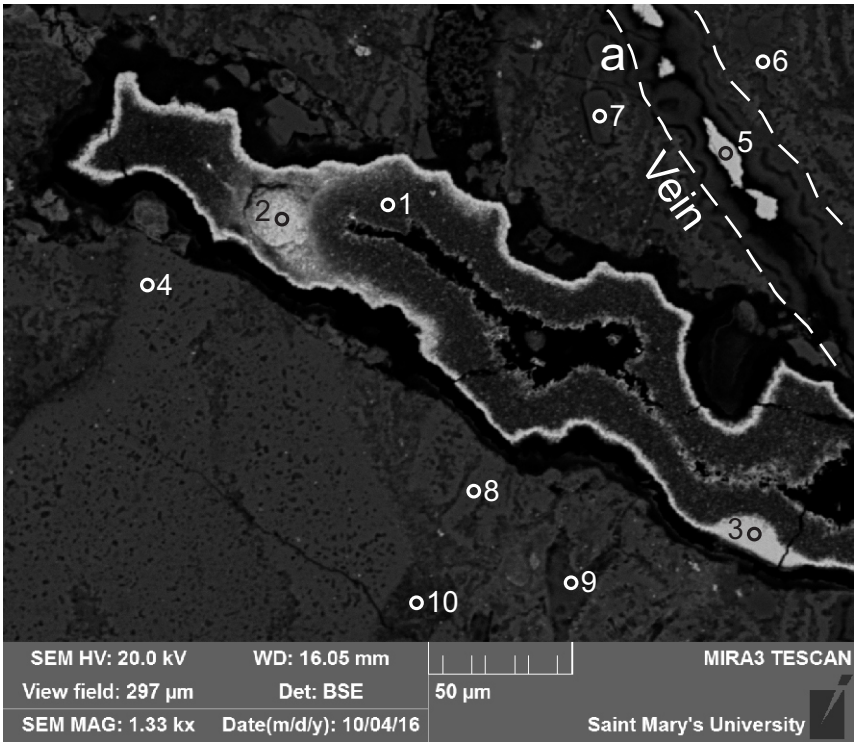

1:"Mn-oxide" (porous)
2:"Mn-oxide"
3:"Mn-oxide"
4:K-feldspar
5:"Mn-oxide"
6:Silica
7:Silica
8:Glass
9:Silica
10:Silica+Glass

Figure 1-1.18: Sample 846a site 18 (SEM) (Table 1-11.1). An open fracture is partly filled with "Mn-oxide" (1-3,5). A smaller "Mn-oxide" vein (5) rimmed with silica (position a) is also present.

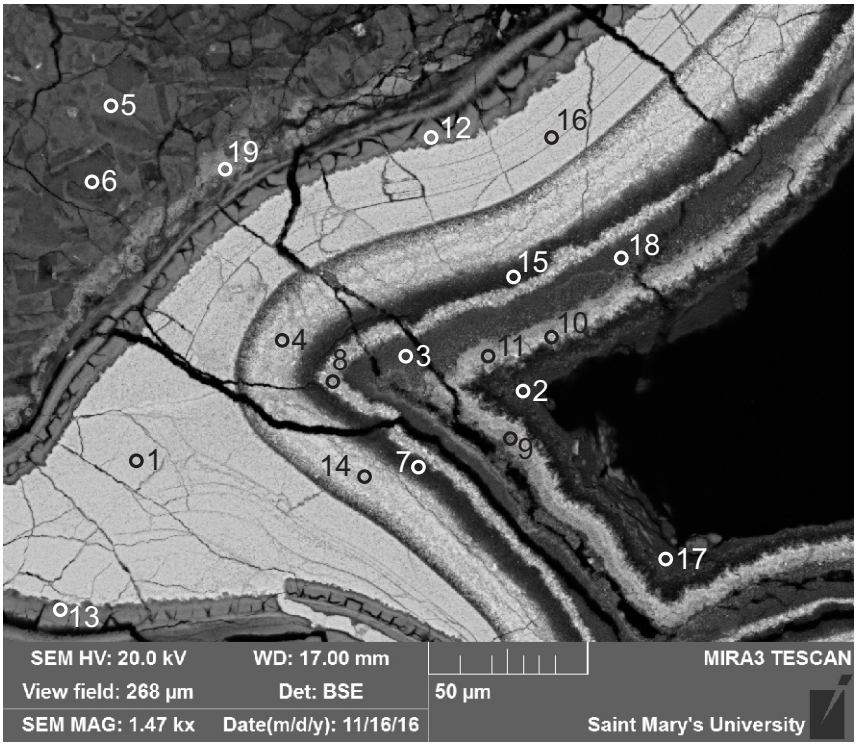

1:"Mn-oxide"
2:Kaolinite
3:"Mn-oxide" (porous)
4:"Mn-oxide"
5:Glass
6:Silica (Am)
7:"Mn-oxide"
8:"Mn-oxide"
9:"Mn-oxide"
10:"Mn-oxide"
11:"Mn-oxide"
12:"Fe-oxide"+ "Mn-oxide"
13:"Fe-oxide"+ "Mn-oxide"
14:"Mn-oxide"
15:"Mn-oxide"
16:"Mn-oxide"
17:Kaolinite
18:"Mn-oxide"
19:"Fe-oxide"+ K-feldspar

Figure 1-1.19: Sample 846a site 19 (SEM) (Table 1-11.2). A site showing the possible hydrothermal mineral precipitation sequence: "Fe-oxide" - "Mn-oxide" - kaolinite - mixture.

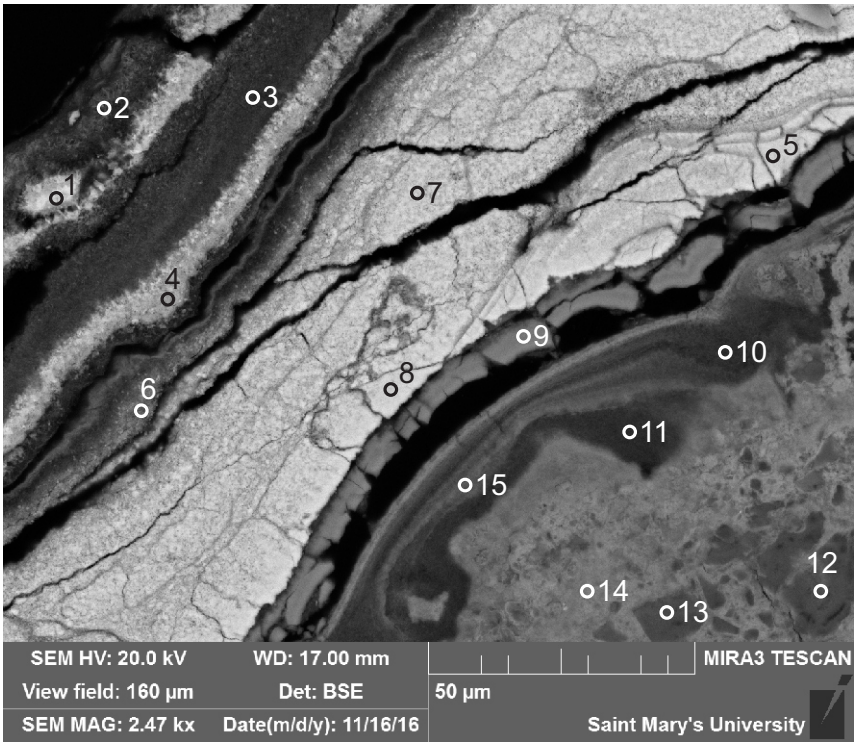

1:"Mn-oxide"
2:"Mn-oxide"+Kln
3:"Mn-oxide"+Kln
4:"Mn-oxide"
5:"Mn-oxide"
6:"Mn-oxide"
7:"Mn-oxide"
8:"Mn-oxide"
9:"Fe-oxide"+ Mn-oxide+other
10:"Fe-oxide"+ Mn-oxide+other
11:"Fe-oxide"+ Mn-oxide+other
12:Silica+
13:Silica
14:"Fe-oxide"+ Mn-oxide+other
15:"Fe-oxide"+ Mn-oxide+other

Figure 1-1.20: Sample 846a site 20 (SEM) (Table 1-11.2).

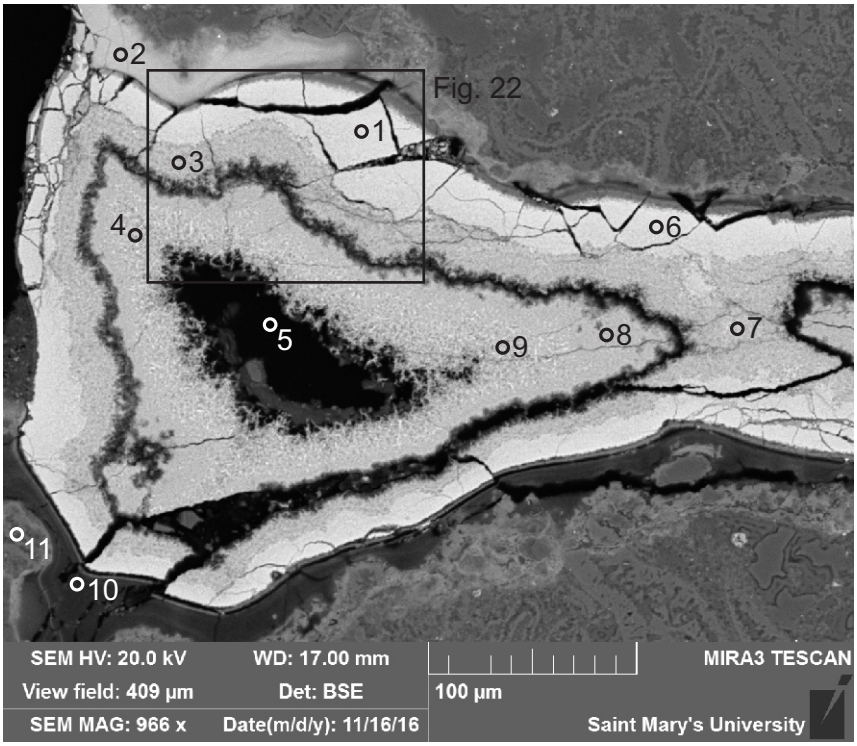

1:"Mn-oxide"
2:"Mn-oxide"
3:"Mn-oxide"
4:"Mn-oxide"
5:Void
6:"Mn-oxide"
7:"Mn-oxide"
8:"Mn-oxide"
9:"Mn-oxide"
10:"Fe-oxide"+
Mn-oxide+other
11:Mix

Figure 1-1.21: Sample 846a site 21 (SEM) (Table 1-11.2). Similar to site 3. A cavity with a zoned "Mn-oxide" precipitation.

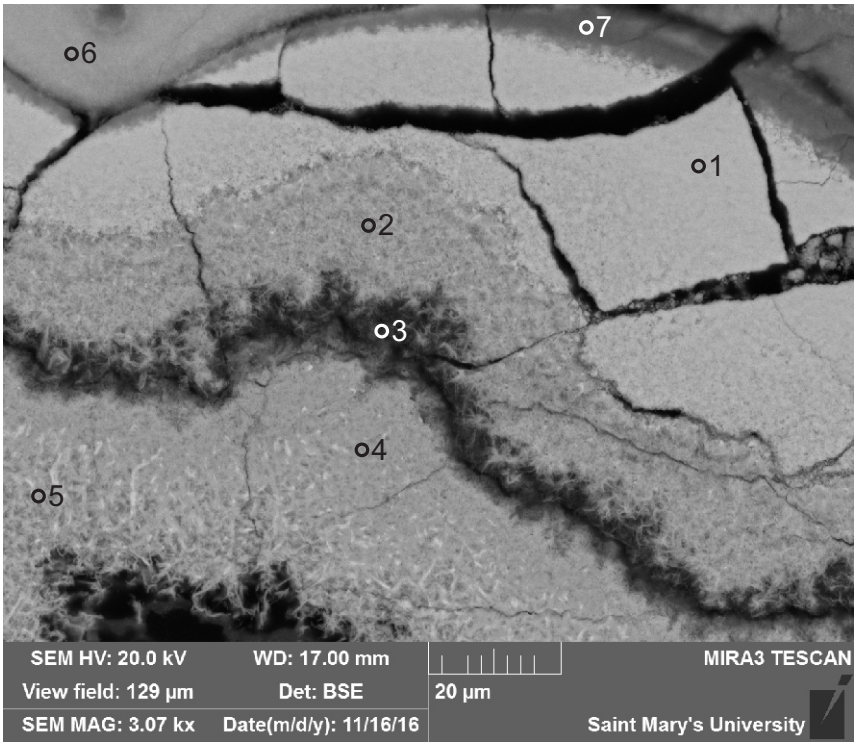

1:"Mn-oxide"
2:"Mn-oxide"
3:"Mn-oxide"
4:"Mn-oxide"
5:"Mn-oxide"
6:"Mn-oxide"+
"Fe-oxide"
7:"Mn-oxide"+
"Fe-oxide"

Figure 1-1.22: Sample 846a site 22 (SEM) (Table 1-11.2). A zoomed inimage of Fig. 24 showing a thin porous layer of "Mn-oxide".

Table 1-1: EDS chemical analyses of "Mn-oxide" in samples 806 and 846a.

Sample	Site	Position	Mineral	Silica	TiO2	Al2O3	FeO	MnO	MgO	CaO	Na2O	K2O	P2O5	F	Cl	CoO	CuO	NiO	ZnO	BaO	Ce2O3	Total	Actual Total
806	1	1	"Mn-oxide"+	21.2		0.81	19.3	44.4	1.18	1.04	0.65	0.9		0						10.6		100	77
806	1	2	"Mn-oxide"+	16.4		0.9	17.2	50.3	1.27	0.98	0.52	0.7								11.8		100	76
806	1	3	"Mn-oxide"+Silica+"Fe-oxide"	49	0.6	4.4	30.1	9.18	3.17	1.26	1.11	1.2										100	84
806	1	4	"Mn-oxide"+Silica+"Fe-oxide"	47.2		1.27	35.6	9.41	2.58	0.87	1.09	2										100	82
806	1	5	"Mn-oxide"+Silica+"Fe-oxide"	49.5		2.33	40.7	0.61	3.56	1.02	0.85	1.4										100	82
806	1	9	"Mn-oxide"+	23.5		4.81	16.5	41.4	1.23	1.31	0.76	0.9								9.71		100	77
806	2	3	"Mn-oxide"+	22.7		0.99	15.3	45.8	1.5	0.9	0.56	0.9								11.3		100	77
806	2	6	"Mn-oxide"+	24		1.08	17.3	42.8	1.62	0.93	0.64	0.9								10.7		100	77
806	3	1	"Mn-oxide"+	16.9		3.72	18.1	45.5	1.03	1.43	0.58	0.5		1.4						10.8		100	76
806	3	5	"Mn-oxide"+	30.1		3.75	17.4	35.9	2.27	1.48	0.64	1								7.47		100	80
806	3	11	"Mn-oxide"+	29.3		4.15	16	37.4	2.27	1.32	0.67	1								7.88		100	80
806	4	2	"Mn-oxide"+Silica+"Fe-oxide"	30		4.04	18.8	35.6	2.06	1.64	0.64	0.9								6.37		100	77
806	4	8	"Mn-oxide"+	42.5		3.19	24.7	20.6	2.86	1.47	1.1	1.2								2.33		100	82
806	5	1	"Mn-oxide"+	7.47			8.83	64.6	0.79	0.9		0.4								17		100	73
806	5	2	"Mn-oxide"+	19.8		0.98	13	50.4	1.68	0.8		0.9								12.4		100	78
806	5	7	"Mn-oxide"+	20.3		0.87	12.9	49.9	1.61	0.71	0.5	0.9								12.3		100	78
806	5	8	"Mn-oxide"+	8.25			9.92	63.3	0.75	0.91		0.5								16.5		100	73
806	6	1	"Mn-oxide"+Silica	24.65		5.75	8.68	43.85	1.08	1.21	0.88	1.69								12.19		100	100
806	7	3	"Mn-oxide"+Silica+"Fe-oxide"	3.67			5.64	67.61	0.9	1.78	1.25					1.36	0.61			17.16		100	91
806	7	4	"Mn-oxide"+Silica+"Fe-oxide"	13.48		2.53	10.4	54.65	1.33	1	0.65	0.57								15.39		100	97
806	7	5	"Mn-oxide"+Silica+"Fe-oxide"	8.03	1.6	2.13	9.93	59.11	0.89	0.86	0.61	0.35								16.49		100	97
806	8	1	"Mn-oxide"+Silica	1.78			3.64	74.22		0.77										19.59		100	90
806	8	2	"Mn-oxide"+Silica+"Fe-oxide"	12.44		0.79	10.51	58.55	1.42	0.82		0.46								15		100	97
806	8	4	"Mn-oxide"+Silica	1.35			1.34	79.43	2.68	0.95		0.34								13.91		100	87
806	8	5	"Mn-oxide"+Silica+"Fe-oxide"	14.94		0.8	11.17	55.69	1.56	0.89		0.68								14.28		100	99
846a	9	1	"Mn-oxide"			0.91		90.6		0.7		1.8				1.1			1.1	3.88		100	94
846a	9	2	"Mn-oxide"			1.89		83.5		0.74		2.5	0.87						0.5	9.98		100	100
846a	9	3	"Mn-oxide"			1.44		85.6		0.45	0.75	2.5								9.27		100	101
846a	9	7	"Mn-oxide"			1.9		83.5		0.66	0.89	2.4	0.78			0.5				9.38		100	100
846a	10	1	"Mn-oxide"			2.32		83.1		0.73	0.83	2.6	1.02							9.43		100	101
846a	10	2	"Mn-oxide"			2.01		87.2		0.81		2	0.81						0.8	6.45		100	97
846a	10	3	"Mn-oxide"+Al	1.5		30.53		61.5								2.1	0.6	2.1	1.7			100	97
846a	11	2	"Mn-oxide"			1.05		85.1		0.33	0.5	3							0.6	9.46		100	102
846a	11	4	"Mn-oxide"			1.18		85		0.43	0.63	2.6								10.2		100	101
846a	11	6	"Mn-oxide"	1.65		5.18	5.46	73.9		1.21		0.9	1.84			1.2				8.67		100	99
846a	11	8	"Mn-oxide"	0.68		1.31	1.21	82.8		0.67	0.62	1.9	0.78							10		100	101
846a	11	9	"Mn-oxide"	0.65		1.09		84.6		0.52	0.86	2.6				0.5				9.19		100	102
846a	12	1	"Mn-oxide"			2.23		83		0.81	0.66	2.6	0.92			0.5				9.27		100	100
846a	12	6	"Mn-oxide"			1.84		82.9		0.79	0.49	2.2	0.91						0.7	10.1		100	101
846a	13	1	"Mn-oxide"	0.67		2.77		81.9		0.82		1.5	1			0.5				10.8		100	99
846a	13	3	"Mn-oxide"					93.8		0.61		1.1							1.1	3.34		100	92
846a	13	4	"Mn-oxide"			2.54		84.7		0.79		1.2	0.95							9.87		100	99

Table 1-1: EDS chemical analyses of "Mn-oxide" in samples 806 and 846a.

Sample	Site	Position	Mineral	Silica	TiO2	Al2O3	FeO	MnO	MgO	CaO	Na2O	K2O	P2O5	F	Cl	CoO	CuO	NiO	ZnO	BaO	Ce2O3	Total	Actual Total
846a	13	5	"Mn-oxide"					92.8		0.68		1.2				0.6			1.3	3.47		100	94
846a	13	8	"Mn-oxide"			2.06		83.2		0.41	0.81	2.7	0.84							9.92		100	104
846a	14	1	"Mn-oxide"	1.03		6		78.5		0.41		1.9	1.04			0.5		0.5	0.7	9.39		100	86
846a	14	2	"Mn-oxide"	0.79		1.32		83.9		0.58	1.02	2.2								10.2		100	95
846a	14	4	"Mn-oxide"	0.85		3.04		82.4		0.51		2.5	1.04							9.65		100	89
846a	14	8	"Mn-oxide"	0.72		2.79		82.8		0.45	0.89	2.5								9.87		100	95
846a	14	9	"Mn-oxide"			1.47		84		0.52	0.98	2.4								10.6		100	96
846a	17	1	"Mn-oxide"			1.01		84.3		0.58		3.3							0.3	10.5		100	82
846a	17	2	"Mn-oxide"	0.64		3.92		80.6		0.5	0.44	2.8	1.05							10.1		100	77
846a	17	4	"Mn-oxide"			0.76		83.1		0.67	0.41	2.3				0.4	0.5		0.6	11.2		100	82
846a	17	7	"Mn-oxide"			0.86		85		0.55		2.9								10.7		100	82
846a	17	8	"Mn-oxide"	0.64		1.01		83.6		0.51	0.61	2.6					0.5			10.5		100	83
846a	17	11	"Mn-oxide"+	0.82		9.01		75.3		0.51		2.1	1.24			1.1	0.6	0.9	0.8	7.59		100	69
846a	17	12	"Mn-oxide"+"Fe-oxide"	2.95		6.55	51.5	29.9		0.41			5.54		0.4					2.8		100	59
846a	17	13	"Mn-oxide"+"Fe-oxide"	29.4	5.27	9.58	24	23.7		0.44	0.85	3.2	2.49								1.04	100	86
846a	18	1	"Mn-oxide"	0.71		1.18		83.8		0.47	0.66	2.2				0.4				10.6		100	96
846a	18	1	"Mn-oxide"			1.08		85			0.7	2.6								10.6		100	96
846a	18	1	"Mn-oxide" (porous)	1.45		14.42		72.6		0.48		0.9		0	0.4	1.4	1	1.6	2	3.81		100	50
846a	18	2	"Mn-oxide"	0.95		2.7		83.5		0.54		2.1								10.2		100	92
846a	18	2	"Mn-oxide"			1.12		84.3		0.54	0.76	2.2							0.6	10.4		100	99
846a	18	3	"Mn-oxide"	0.78		9.14		76		0.5		1.8	1.32			1.2		0.9	0.8	7.59		100	82
846a	18	3	"Mn-oxide"	0.79		1.42		81.7		0.67	0.63	1.7					0.7		0.7	11.8		100	100
846a	18	4	"Mn-oxide"	0.73		3.12		81.4		0.51	0.63	2.3	1.13							10.2		100	97
846a	18	5	"Mn-oxide"	0.68		0.72		84.4		0.59	0.63	2								11		100	94
846a	18	5	"Mn-oxide"	1.23		0.66		84.8		0.54		2.1								10.7		100	97
846a	19	1	"Mn-oxide"			2.81		85.2		0.51	0.49	3.8				0.5			0.6	6.08		100	80
846a	19	3	"Mn-oxide" (porous)	1.12		16.13		66.4		1.14		0.7		2.7	2.5	1.6	0.7	1.7	1.5	3.85		100	42
846a	19	4	"Mn-oxide"	0.8		3.32		81.5		0.76		2.3	0.92			0.5			0.6	9.31		100	75
846a	19	7	"Mn-oxide"			9.69		73.1		1.13	1.34	1.3			4.1	1.7		1.5		6.31		100	32
846a	19	8	"Mn-oxide"			1.14		89.2		0.64		1.8				1.3	0.6		1.4	3.88		100	67
846a	19	9	"Mn-oxide"			0.85		90.4		0.98		2.3				1			1.3	3.12		100	64
846a	19	10	"Mn-oxide"			1.15		90.2		0.93		2.5				0.8			1.2	3.24		100	69
846a	19	11	"Mn-oxide"			2.16		87.9		0.87		1.7			0.3	1	0.9	0.6	1.9	2.86		100	65
846a	19	14	"Mn-oxide"			2.99		82.2		0.81	0.86	2.3	0.94			0.5				9.39		100	78
846a	19	15	"Mn-oxide"			7.44		75.9		1.11		1.6	1.21		2.4	1		0.8	1	7.61		100	41
846a	19	16	"Mn-oxide"	0.79		2.02		85.6		0.61	0.77	3.2				0.7				6.47		100	79
846a	19	18	"Mn-oxide"	1.06		14.76		72.8		0.89		0.9			0.6	1.7		1.7	1.1	4.44		100	41
846a	20	1	"Mn-oxide"			1.61		84.9		1.35	0.75	2.9				0.7	0.6		0.9	6.33		100	73
846a	20	2	"Mn-oxide"+Kln	18.1		11.34		55.1	0.81	1.69	0.6	1.3	1.19	3.4	1.8	0.6			0.9	3.2		100	50
846a	20	3	"Mn-oxide"+Kln	1.06		13.92		66.1		1.2		0.8		7.2	0.8	1.4	0.9	1.9	1.9	2.85		100	34
846a	20	4	"Mn-oxide"			1.03		88.5		1.01		1.9				1.2	0.8		1.7	3.88		100	68
846a	20	5	"Mn-oxide"			1.33	1.36	82.8		0.75		2.1				0.8	0.6		0.5	9.79		100	78

Table 1-1: EDS chemical analyses of "Mn-oxide" in samples 806 and 846a.

Sample	Site	Position	Mineral	Silica	TiO2	Al2O3	FeO	MnO	MgO	CaO	Na2O	K2O	P2O5	F	Cl	CoO	CuO	NiO	ZnO	BaO	Ce2O3	Total	Actual Total
846a	20	6	"Mn-oxide"	1.17		4.46		76.1		1.17		1.7	1.44	3.7	0.7	1.1			0.9	7.58		100	53
846a	20	7	"Mn-oxide"			2.19		84.9		0.58		2.8							0.4	9.16		100	78
846a	20	8	"Mn-oxide"			1.1		84.7		0.74		2.2				0.6			0.5	10.1		100	77
846a	21	1	"Mn-oxide"			0.86		85.8		0.61		2.2				0.5				10.1		100	79
846a	21	2	"Mn-oxide"	1.14		4.83	6.82	73.3	0.66	1.64		0.5	1.96			1.5				7.7		100	77
846a	21	3	"Mn-oxide"	0.69				90		0.83	0.63	1.7				1.6			1.2	3.51		100	75
846a	21	4	"Mn-oxide"			1.63		90		0.81		1.4				0.5			0.9	4.87		100	74
846a	21	6	"Mn-oxide"			1.13		85		0.54		2.2				0.5			0.5	10.1		100	79
846a	21	7	"Mn-oxide"			0.91		90.2		0.69	0.71	1.8				0.9			1.1	3.71		100	77
846a	21	8	"Mn-oxide"			0.74		93		0.84		1.2							1.2	2.98		100	74
846a	21	9	"Mn-oxide"	0.6		1.38		89.2		0.97		1.3				0.6			1	4.87		100	75
846a	22	1	"Mn-oxide"			0.77		85.3		0.58		2							0.5	10.9		100	78
846a	22	2	"Mn-oxide"			0.7		91.5		0.77		1.5				1.2			1	3.32		100	73
846a	22	3	"Mn-oxide"			1.03		86.1		0.76		1.1		5.9	0.5				1.6	3.05		100	42
846a	22	4	"Mn-oxide"			0.8		92.6		0.76		1.6							1.1	3.14		100	74
846a	22	5	"Mn-oxide"			1.1		90.8		0.77	0.48	1.2				0.5			1.1	4.11		100	74
846a	22	6	"Mn-oxide"+"Fe-oxide"	1.45		5.54	15.6	64.3		1.06		0.5	2.86			1.2				7.53		100	76
846a	22	7	"Mn-oxide"+"Fe-oxide"	3.16		5.33	33.2	46.8		0.82		0.5	4.32							5.95		100	59

Appendix 1-2: SEM-BSE images and electron microprobe (EMP) chemical analyses of “Mn-oxide” minerals for samples 806 and 846a

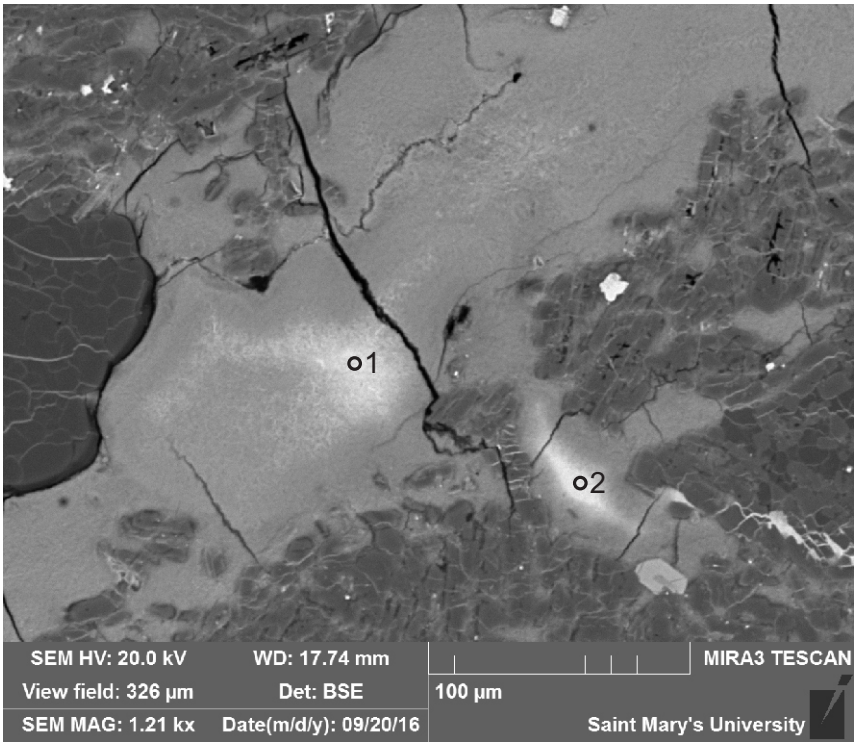

1:Ferrihollandite
2:Ferrihollandite

Figure 1-2.1: Sample 806 site 1 (EMP).

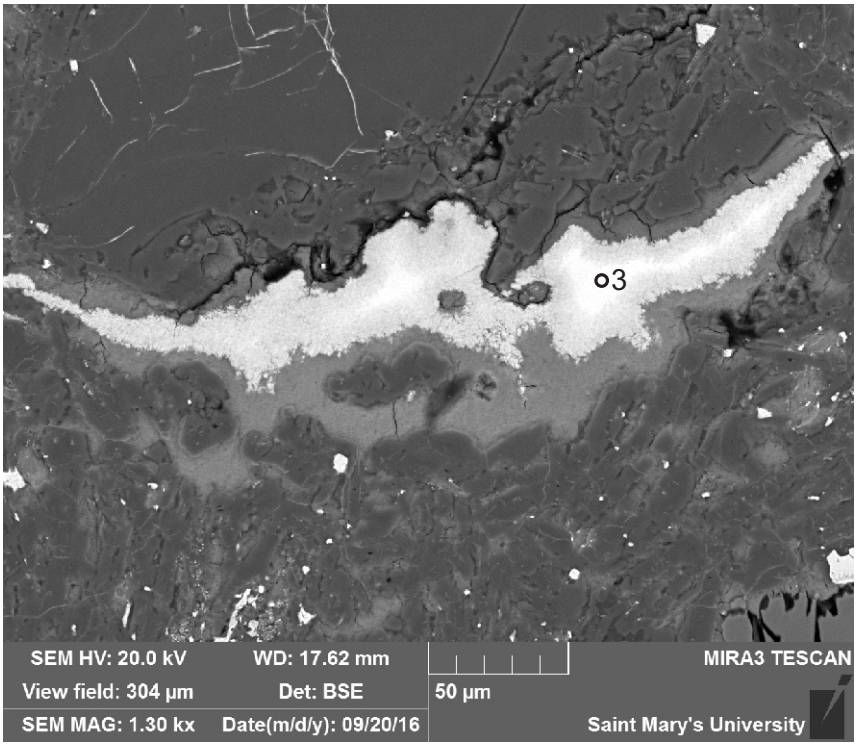

3:Romanechite

Figure 1-2.2: Sample 806 site 2 (EMP).

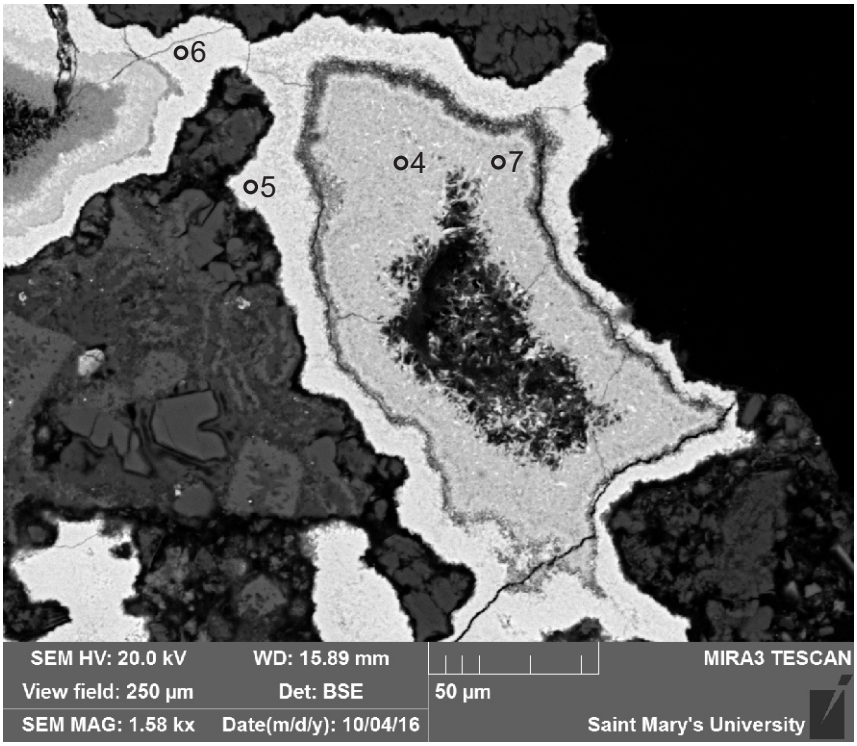

4:Romanechite
5:Romanechite
6:Romanechite
7:Romanechite

Figure 1-2.3: Sample 846a site 3 (EMP).

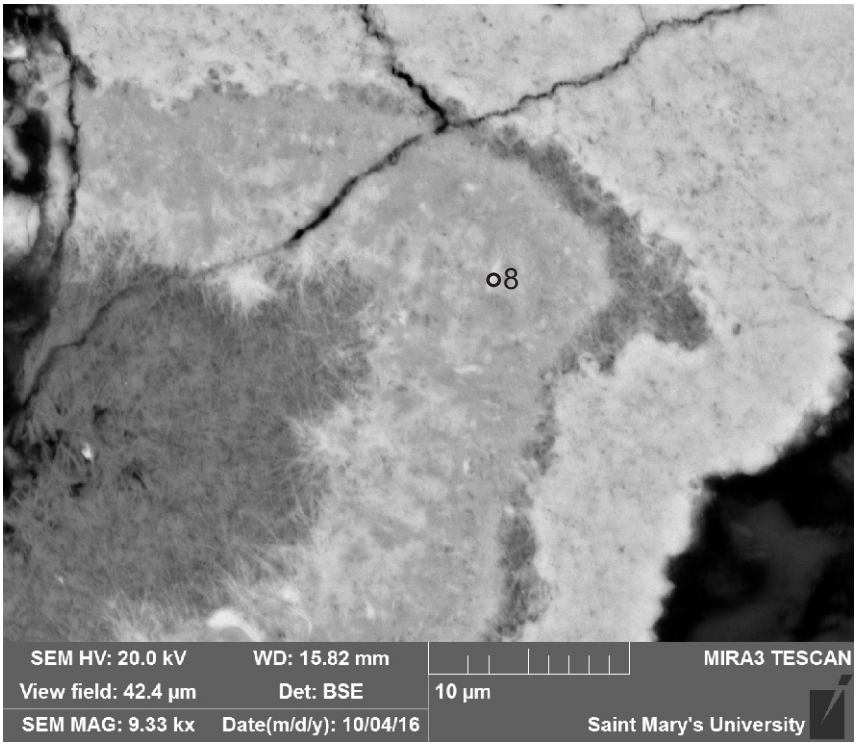

8:Romanechite

Figure 1-2.4: Sample 846a site 4 (EMP).

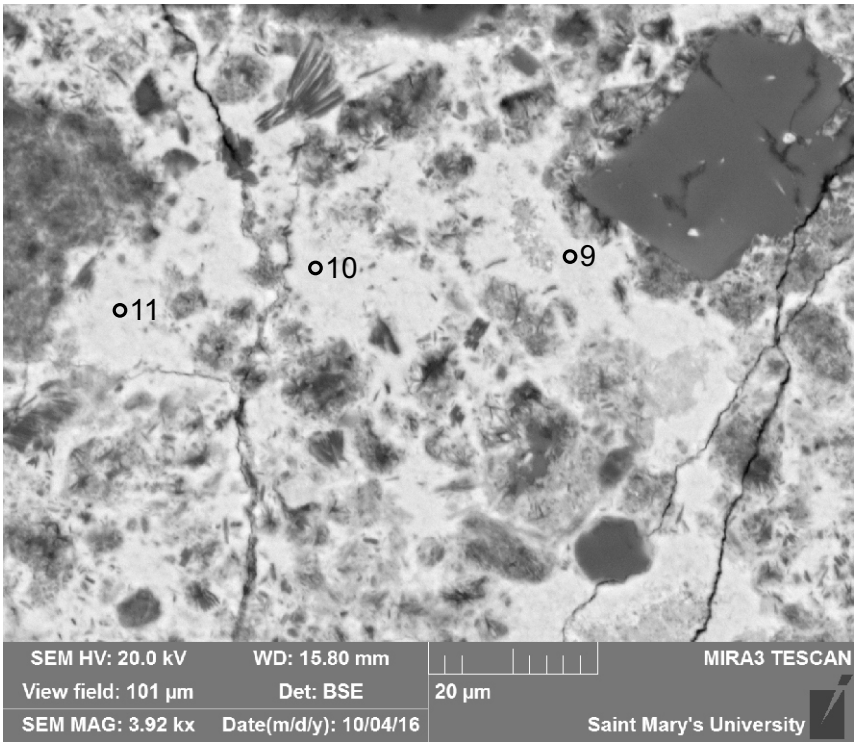

9:Romanechite
10:Romanechite
11:Romanechite

Figure 1-2.5: Sample 846a site 5 (EMP).

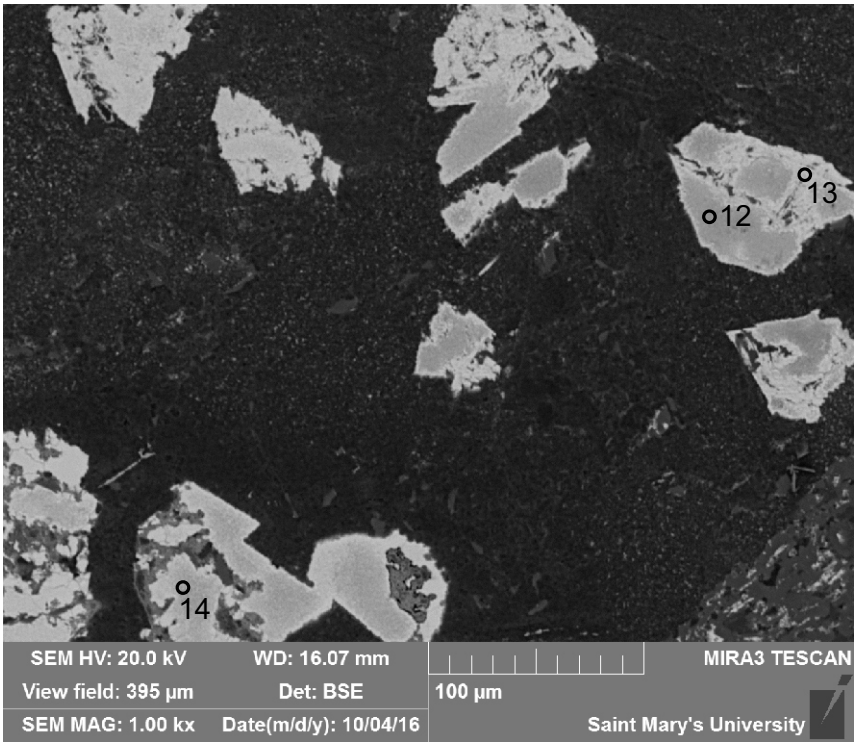

12:Romanechite
13:Romanechite
14:Romanechite

Figure 1-2.6: Sample 846a site 6 (EMP).

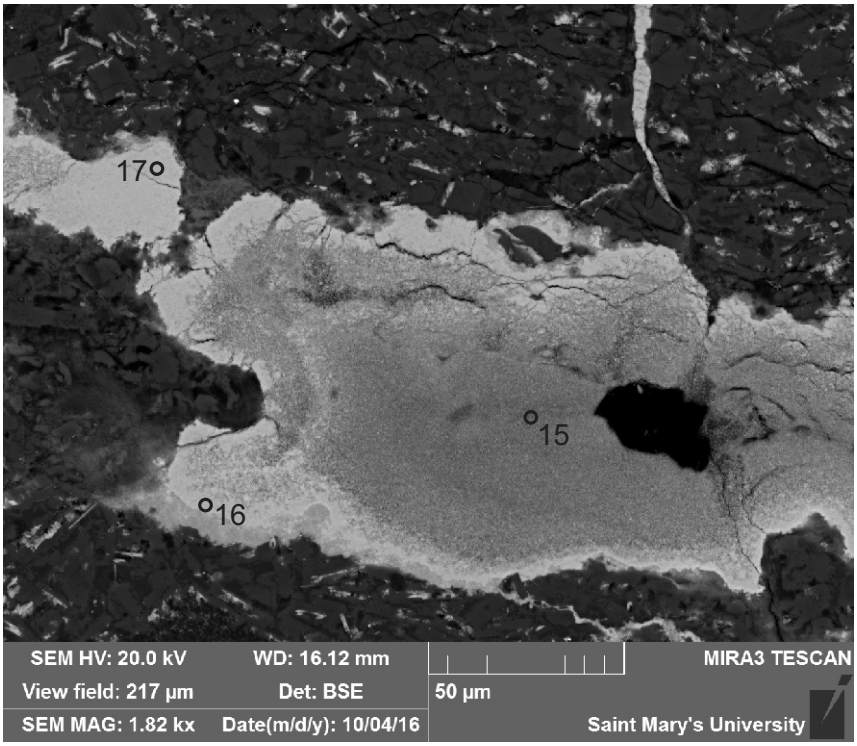

15:Romanechite
16:Romanechite
17:Romanechite

Figure 1-2.7: Sample 846a site 7 (EMP).

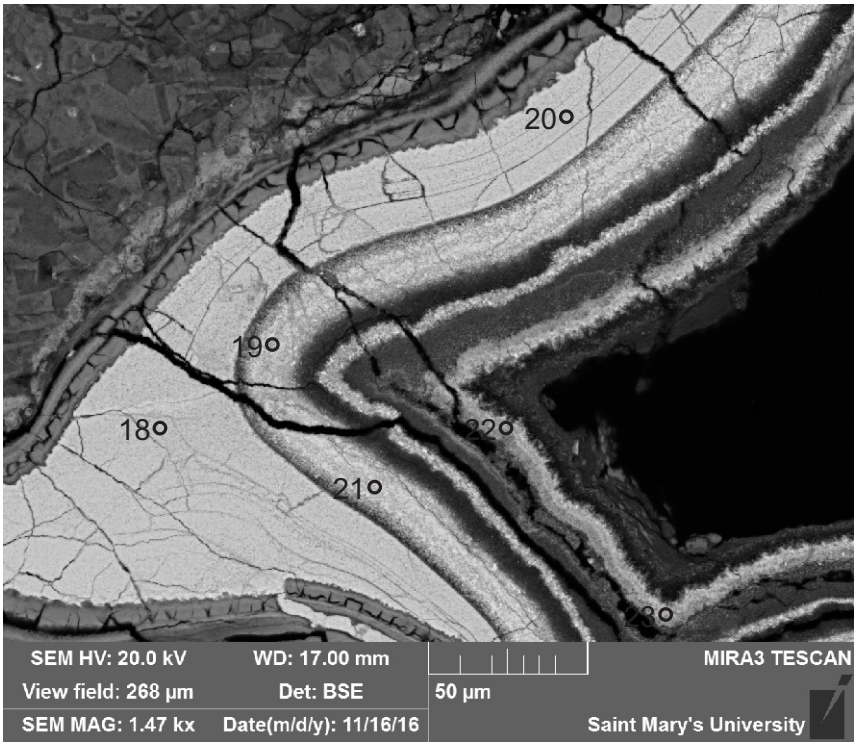

18:Romanechite
19:Romanechite
20:Romanechite
21:Romanechite
22:Romanechite
23:Romanechite

Figure 1-2.8: Sample 846a site 8 (EMP).

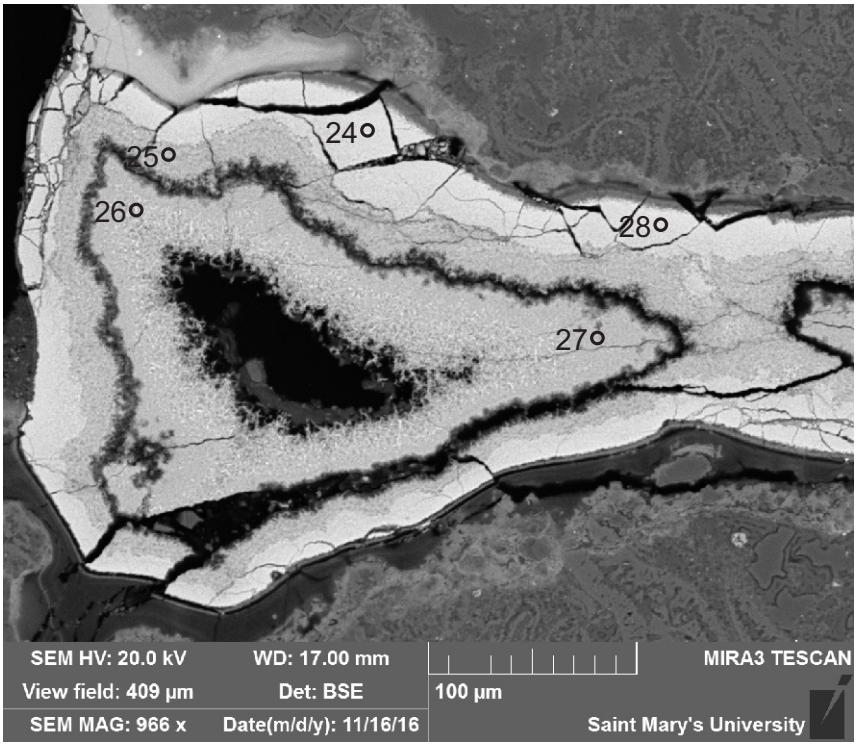

24:Romanechite
25:Romanechite
26:Romanechite
27:Romanechite
28:Romanechite

Figure 1-2.9: Sample 846a site 9 (EMP).

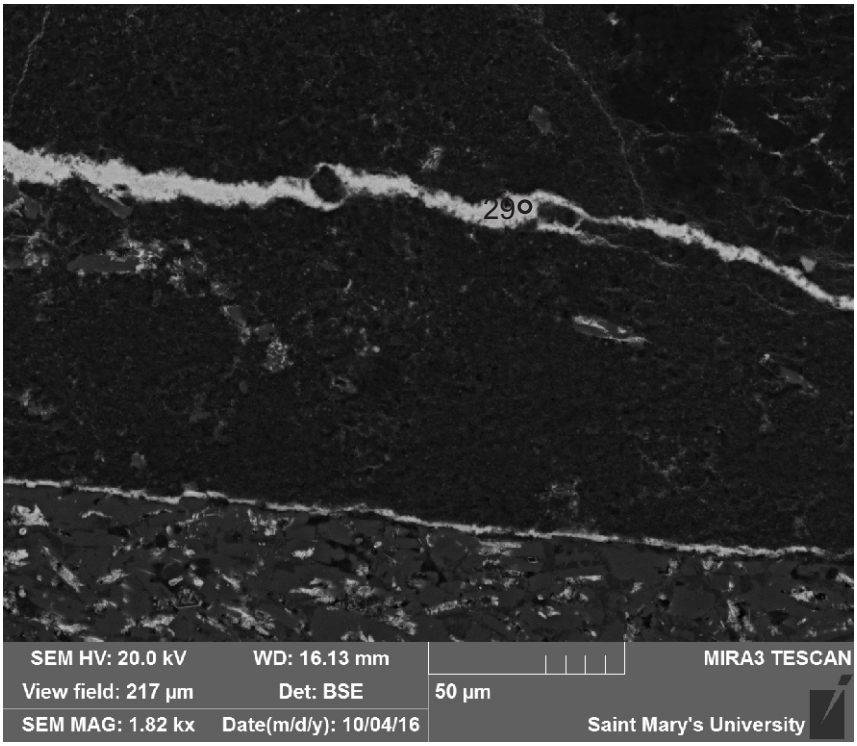

29:Romanechite

Figure 1-2.10: Sample 846a site 10 (EMP).

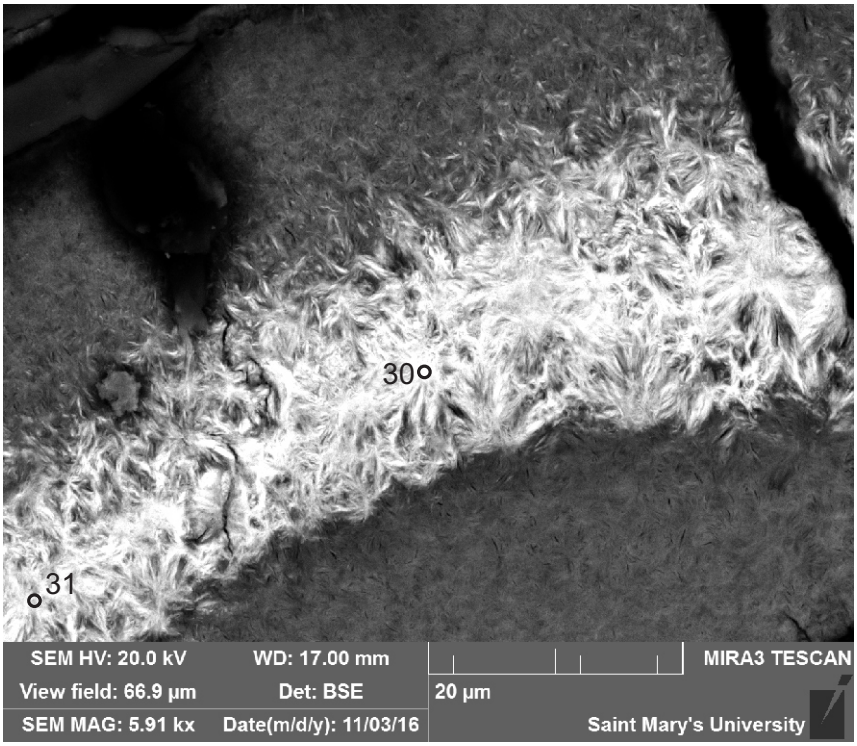

30:Ferrihollandite
31:Ferrihollandite

Figure 1-2.11: Sample 806 site 11 (EMP).

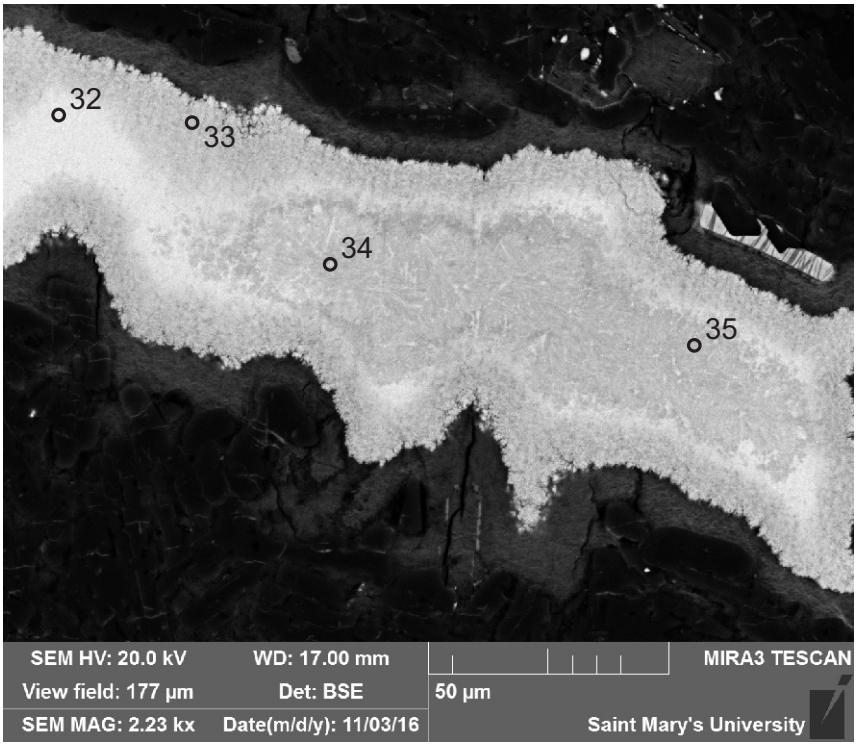

32:Romanechite
33:Romanechite
34:Romanechite
35:Romanechite

Figure 1-2.12: Sample 806 site 12 (EMP).

Table 1-2: Electron microprobe chemical analyses of the "Mn-oxide" in samples 806 and 846a.

Sample	Site	Pos.	Mineral	Al2O3	FeO	MnO	MgO	CaO	K2O	P2O5	SO3	As2O3	BaO	CoO	Ce2O3	SrO	TOTAL
806	1	1	Ferrihollandite	0.6765	19.0904	32.0244	1.0279	1.2946	0.4399	0.2219	0.0126	0.0055	6.6753	0.0688	-0.0381	0.1044	61.6039
806	1	2	Ferrihollandite	0.7259	15.3705	36.4003	1.1982	1.0692	0.4812	0.1148	-0.0098	-0.0235	7.6613	0.0709	-0.1025	0.1033	63.0600
806	2	3	Romanechite	0.2200	7.3148	50.5081	0.5101	0.6971	0.3005	0.1028	0.0042	0.0406	12.7494	0.0748	-0.0084	0.0498	72.5638
846a	3	4	Romanechite	0.5227	0.0032	68.5532	0.0933	0.4482	1.4557	0.1669	-0.0330	0.0020	2.8602	0.3508	0.2536	-0.0285	74.6482
846a	3	5	Romanechite	0.9124	0.1657	66.5335	0.0549	0.4330	1.9280	0.3547	0.0261	-0.0092	6.5167	0.2572	0.0480	-0.0678	77.1532
846a	3	6	Romanechite	1.2231	0.4177	64.5744	0.0982	0.5896	1.7813	0.5216	0.0509	-0.0221	7.0408	0.2853	0.1244	-0.0495	76.6359
846a	3	7	Romanechite	0.9550	0.0255	68.2352	0.1062	0.5828	1.2856	0.3845	0.0247	-0.0252	3.5569	0.1499	0.1211	-0.0631	75.3392
846a	4	8	Romanechite	1.3434	0.0812	66.6165	0.1075	0.6118	1.3376	0.4556	-0.0249	-0.0024	4.8377	0.1949	0.2272	-0.0878	75.6985
846a	5	9	Romanechite	0.6517	0.1528	66.7926	0.0811	0.3357	2.1670	0.2776	0.0027	0.0302	5.9070	0.3186	-0.0011	-0.0098	76.7062
846a	5	10	Romanechite	2.2147	1.1679	61.3792	0.1432	0.6841	1.2818	0.5735	0.0083	0.0155	7.2170	0.3987	0.1100	0.0375	75.2311
846a	5	11	Romanechite	0.6551	0.2783	65.4560	0.0562	0.3942	1.8846	0.3297	-0.0097	0.0033	7.2664	0.2688	0.0639	-0.0083	76.6386
846a	6	12	Romanechite	3.2981	0.0757	59.8284	0.0804	0.3292	1.4807	0.5970	0.0138	0.0038	6.5007	0.2829	0.1949	-0.0145	72.6712
846a	6	13	Romanechite	0.5895	0.0823	64.6173	0.0750	0.4524	1.6216	0.1863	0.0192	-0.0433	7.1467	0.2948	-0.0205	-0.0537	74.9676
846a	6	14	Romanechite	1.8450	0.1212	61.0328	0.0697	0.3195	1.8039	0.6198	0.0289	-0.0588	6.6871	0.1404	-0.0317	-0.0653	72.5125
846a	7	15	Romanechite	4.9279	0.1035	54.4153	0.1206	0.2854	1.1386	0.6520	0.0222	-0.0115	4.5464	0.6519	0.3821	-0.0355	67.1988
846a	7	16	Romanechite	0.3330	0.5321	64.3601	0.0953	0.4190	1.4207	0.1646	-0.0083	-0.0347	7.9919	0.3099	-0.0023	-0.0023	75.5789
846a	7	17	Romanechite	0.7363	0.1550	64.9263	0.0525	0.2934	2.1416	0.2093	-0.0179	-0.0115	7.1857	0.1053	0.1014	0.0126	75.8898
846a	8	18	Romanechite	1.6700	0.0974	66.3665	0.0685	0.3607	2.9163	0.3164	0.0630	0.0061	4.1751	0.4057	0.1231	0.0075	76.5763
846a	8	19	Romanechite	2.0196	0.1703	62.4517	0.0977	0.5577	1.7369	0.5991	0.0578	0.0212	6.3894	0.3341	0.0676	-0.0357	74.4673
846a	8	20	Romanechite	1.3394	0.2799	66.1619	0.1022	0.4649	2.5095	0.2742	0.0288	0.0049	4.2007	0.4916	0.1955	-0.0211	76.0324
846a	8	21	Romanechite	1.7556	0.1047	62.7746	0.0684	0.5667	1.7552	0.5250	0.0426	0.0223	6.6256	0.3715	-0.0786	-0.0262	74.5072
846a	8	22	Romanechite	0.4740	0.0408	67.8020	0.1390	0.8033	1.8664	0.0797	-0.0041	-0.0726	1.9127	0.7030	0.2436	-0.0248	73.9629
846a	8	23	Romanechite	0.5238	0.0327	67.4619	0.1119	0.6704	1.5042	0.1415	0.0436	-0.0631	1.8132	0.6583	0.2022	-0.0342	73.0665
846a	9	24	Romanechite	0.7986	0.3418	65.6196	0.0674	0.4428	1.6112	0.3124	-0.0179	-0.0131	6.9840	0.4234	0.0323	-0.0262	76.5762
846a	9	25	Romanechite	0.4982	0.0018	69.1350	0.1495	0.6109	1.0345	0.1221	0.0969	-0.0591	2.2810	1.1770	0.0587	-0.0565	75.0501
846a	9	26	Romanechite	0.8154	0.0049	68.5916	0.1659	0.5881	0.8661	0.2421	0.0137	-0.0405	2.7972	0.3147	0.1516	-0.0486	74.4623
846a	9	27	Romanechite	0.3945	0.0235	69.3796	0.1238	0.5331	0.8192	0.1390	0.0314	-0.0066	1.8624	0.2390	0.2640	-0.0382	73.7646
846a	9	28	Romanechite	0.5544	0.4277	65.1236	0.0689	0.4243	1.6009	0.2845	-0.0110	0.0074	7.0924	0.3385	-0.0159	-0.0133	75.8825
846a	10	29	Romanechite	0.4082	0.0994	64.2985	0.0669	0.3240	1.7082	0.1729	0.0178	-0.0602	7.5513	0.1730	-0.1061	-0.0177	74.6361
806	11	30	Ferrihollandite	0.7024	12.9065	38.0642	1.2327	0.8137	0.5484	0.1057	0.0195	0.0393	8.7530	0.0117	0.0386	0.1617	63.3974
806	11	31	Ferrihollandite	0.8630	13.4190	33.5313	1.5081	0.7188	0.8143	0.0508	0.0028	0.0260	8.1311	0.0588	-0.0266	0.2113	59.3088
806	12	32	Romanechite	0.1015	4.0059	55.1317	0.4234	0.4987	0.2111	0.1978	0.0221	-0.0321	14.4851	0.0842	-0.1963	0.0706	75.0037
806	12	33	Romanechite	0.3666	7.9738	47.6989	1.1108	0.7633	0.3839	0.1057	0.0069	0.0215	11.7558	0.0306	-0.2280	0.1457	70.1355
806	12	34	Romanechite	0.0022	0.3845	59.3137	1.7445	0.5823	0.3350	0.0337	-0.0125	0.0138	9.6279	0.0460	-0.0227	-0.0174	72.0311
806	12	35	Romanechite	0.0647	2.2274	57.3475	1.9876	0.5810	0.2893	0.0853	-0.0153	-0.0099	10.1458	0.1366	-0.0788	-0.0233	72.7382

Appendix 2: SEM-BSE images, energy dispersive (EDS) mineral analyses and electron microprobe (EMP) chemical analyses of silica in sample 856-1 (petrified wood)

Appendix 2-1: SEM-BSE images and energy dispersive (EDS) mineral analyses of silica in sample 856-1 (petrified wood)

Figure 2-1.1. Scanned thin section of sample 856-1 showing areas of analysed sites. Petrified wood. In sites 2,3,4 and 5, the silica contains Zn-oxide (0.1-0.7%) with or without As-oxide (0.6-1.4%).

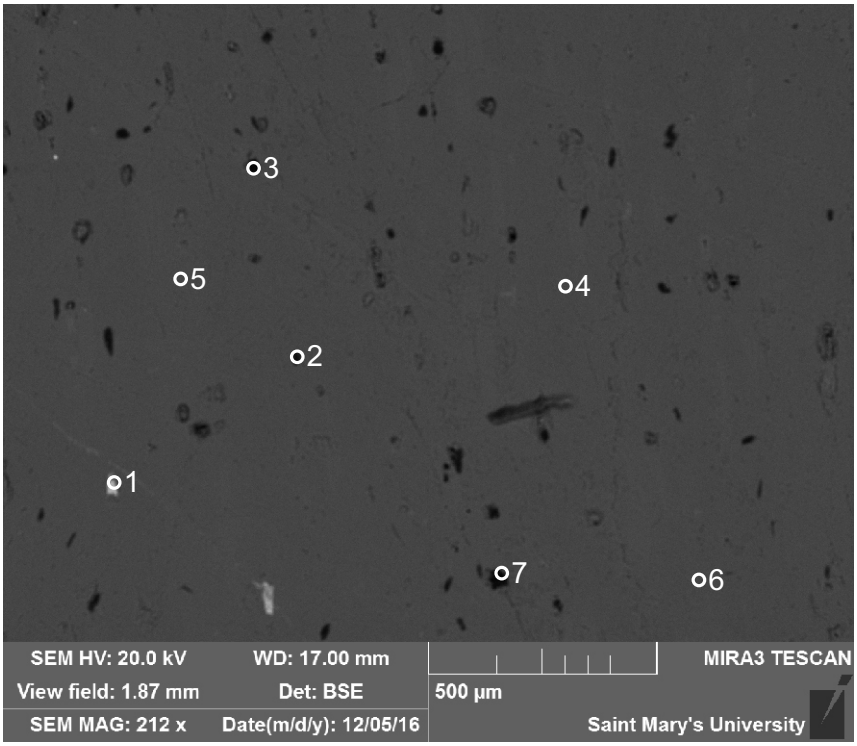

1:"Fe-oxide"+Silica
2:Silica+
3:Void
4:Silica
5:Silica
6:Silica
7:Void

Figure 2-1.2. Sample 856-1 site 1 (SEM). From a black layer of the sample is mostly made up of silica (4-6) with tiny specks of "Fe-oxide" (1).

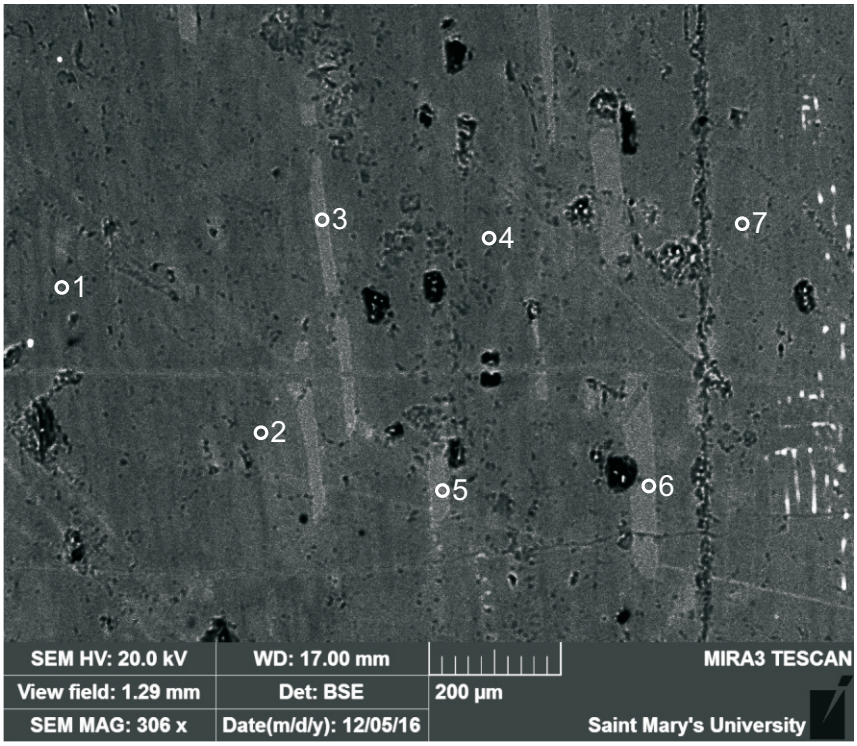

1:Silica
2:Silica
3:Silica
4:Silica
5:Silica
6:Silica
7:Silica

Figure 2-1.3. Sample 856-1 site 2 (SEM). Similar to Fig. 2, another black layer is predominantly silica (1-7) with small amounts of FeO, CaO and ZnO. The difference in color on the BSE images may be because of porosity. Positions 3,5 and 6 appears to have higher actual totals.

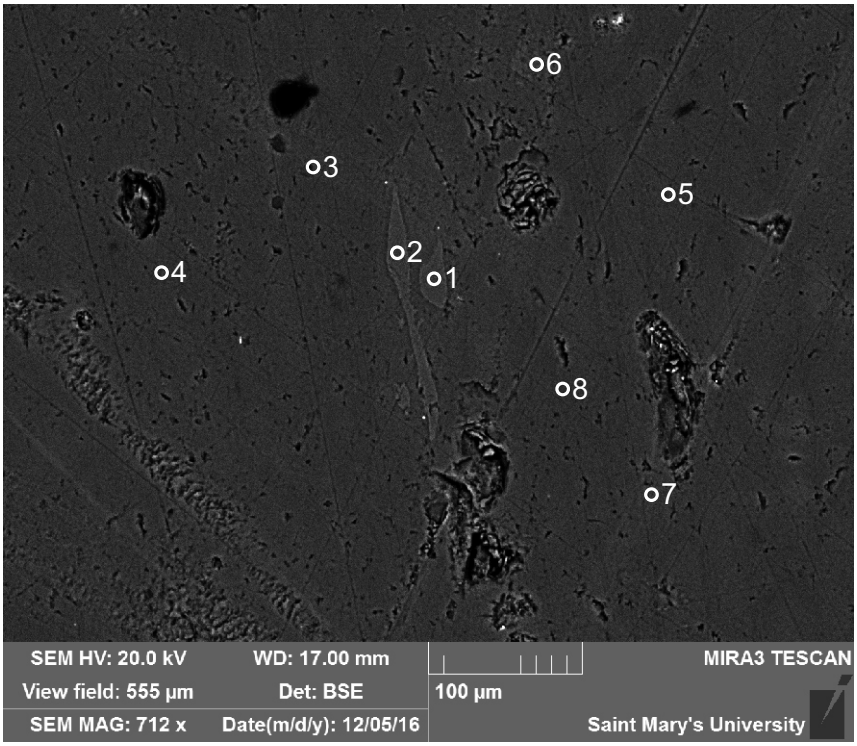

1:Silica
2:Silica
3:Silica
4:Silica
5:Silica
6:Silica
7:Silica
8:Silica

Figure 2-1.4. Sample 856-1 site 3 (SEM). A site showing the black layer predominantly made up of silica and small amounts of FeO, CaO, ZnO.

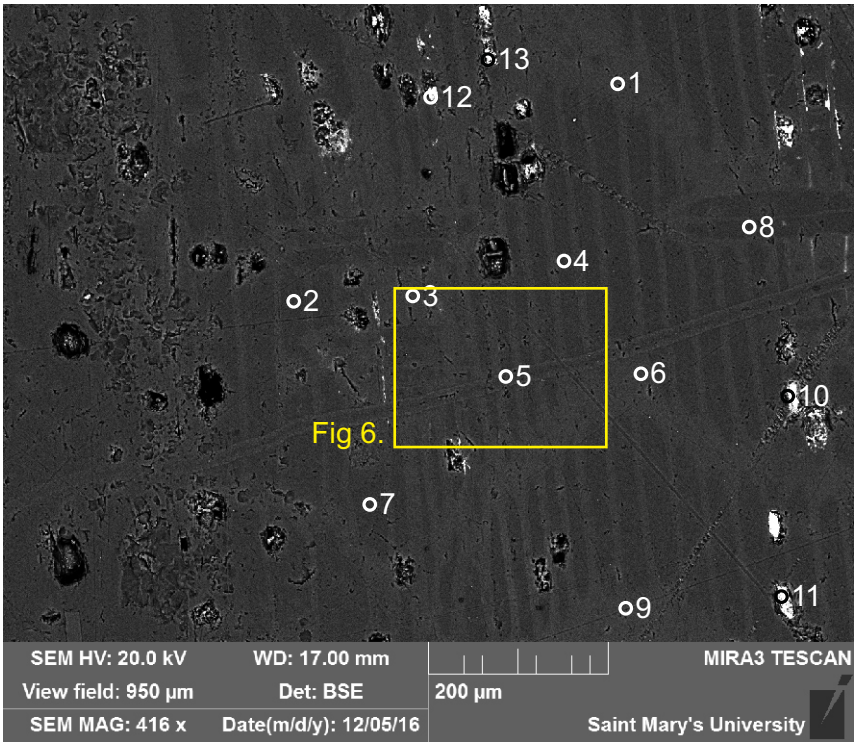

1:Silica
2:Silica
3:Silica
4:Silica
5:Silica
6:Silica
7:Silica
8:Silica
9:Silica
10:"Fe-oxide"+Silica
11:Mixture 2
12:Mixture 2
13:"Fe-oxide"+Silica

Figure 2-1.5. Sample 856-1 site 4 (SEM). This site is from the greenish-yellow layer and shows wood vessels that contain higher FeO in the brighter areas (1,6,9) and lower in the darker areas (2,4,8). In spots (10-13) where SiO_2 + FeO (Mixture 2) are mixed in addition to small amounts of CaO and ZnO, there is also As_2O_3 (up to 1.2%).

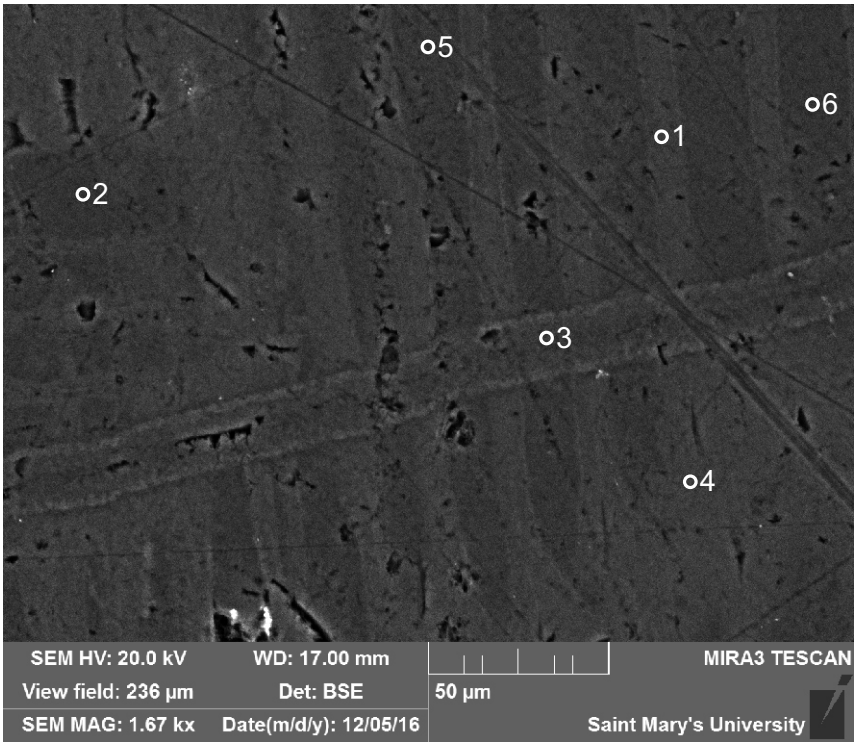

1:Silica
2:Silica
3:Silica
4:Silica
5:Silica
6:Silica

Figure 2-1.6. Sample 856-1 site 5 (SEM). The wood vessels appears to be cut by a vein (3) with similar composition, silica and small amounts of FeO and ZnO.

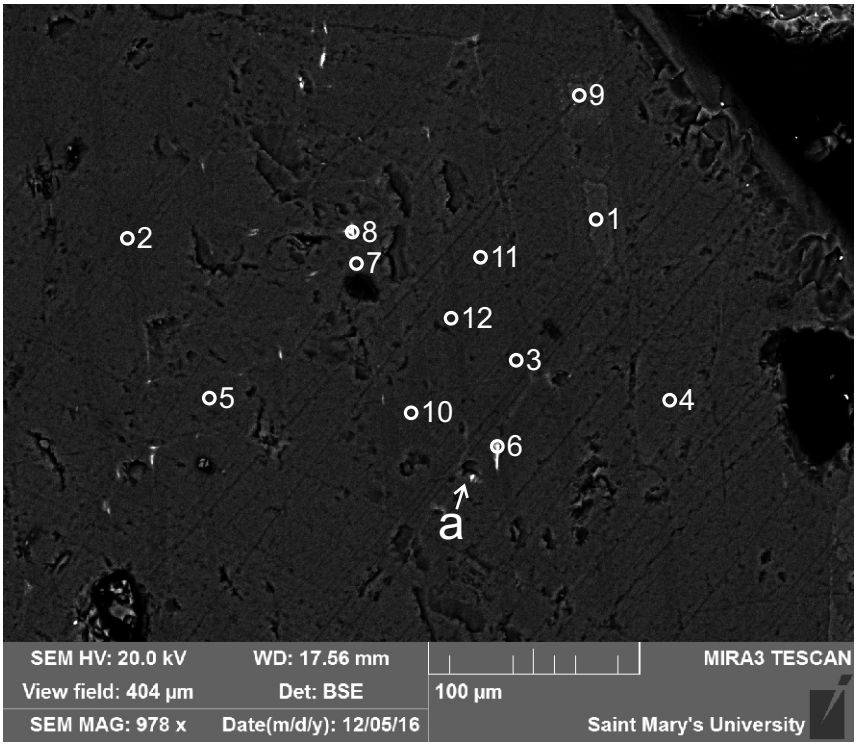

1:Silica
2:Silica
3:Silica
4:Silica
5:Silica
6:Mixture 2
7:Silica
8:Mixture 2
9:Silica+TiO2
10:Silica
11:Silica
12:Silica

Figure 2-1.7. Sample 856-1 site 6 (SEM). This site shows a yellowish layer with little pieces of red-orange color. The scattered bright spots of "Fe-oxide" are what appears to give off the red-orange hue and they often seems to be filling in the voids (e.g. position a).

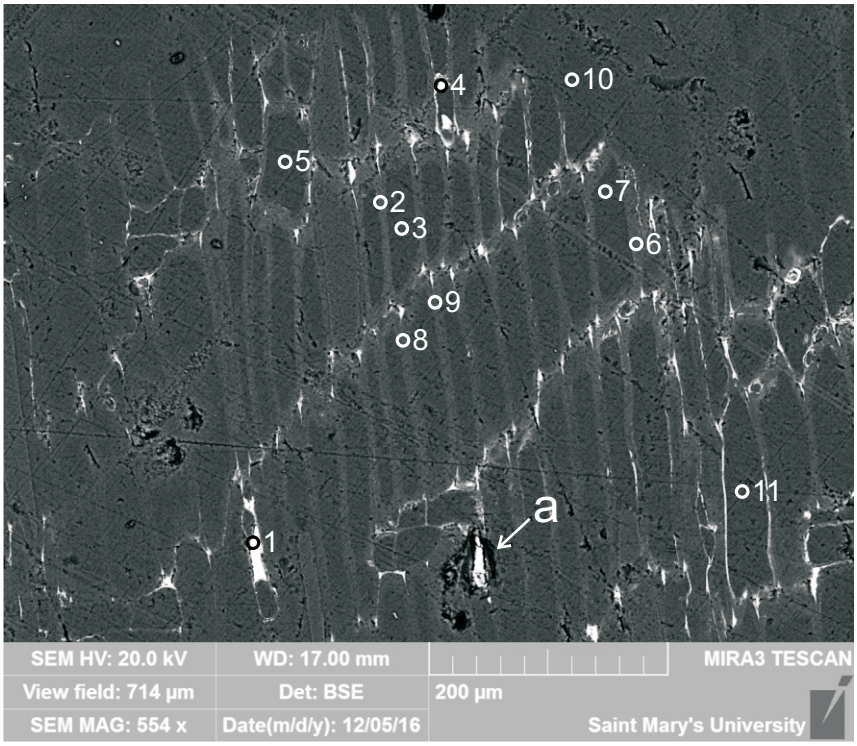

1:"Fe-oxide"+Silica
2:Mixture 2
3:Silica
4:"Fe-oxide"+Silica
5:Silica
6:Mixture 2
7:Silica
8:Mixture 2
9:Mixture 2
10:Silica
11:Silica

Figure 2-1.8. Sample 856-1 site 7 (SEM). Another site from a yellowish layer. In this site, "Fe-oxide" grains are filling in wood vessels (e.g. 1) or voids (position a). The SiO_2 + FeO (Mixture 2) again contains As_2O_3 (up to 1.5%), V2O5 (up to

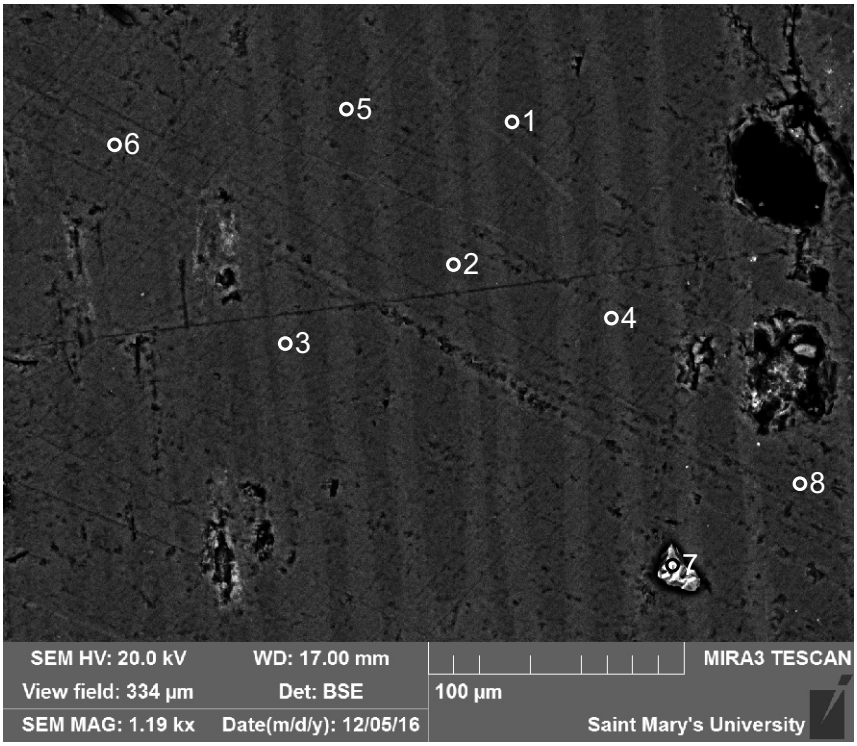

1:Silica
2:Mixture 2
3:Mixture 2
4:Mixture 2
5:Silica
6:Silica
7:Epidote
8:Silica

Figure 2-1.9. Sample 856-1 site 8 (SEM). A site showing a yellow layer with high Fe in the brighter areas and low Fe in the darker areas. Epidote (7) has been seen in a void.

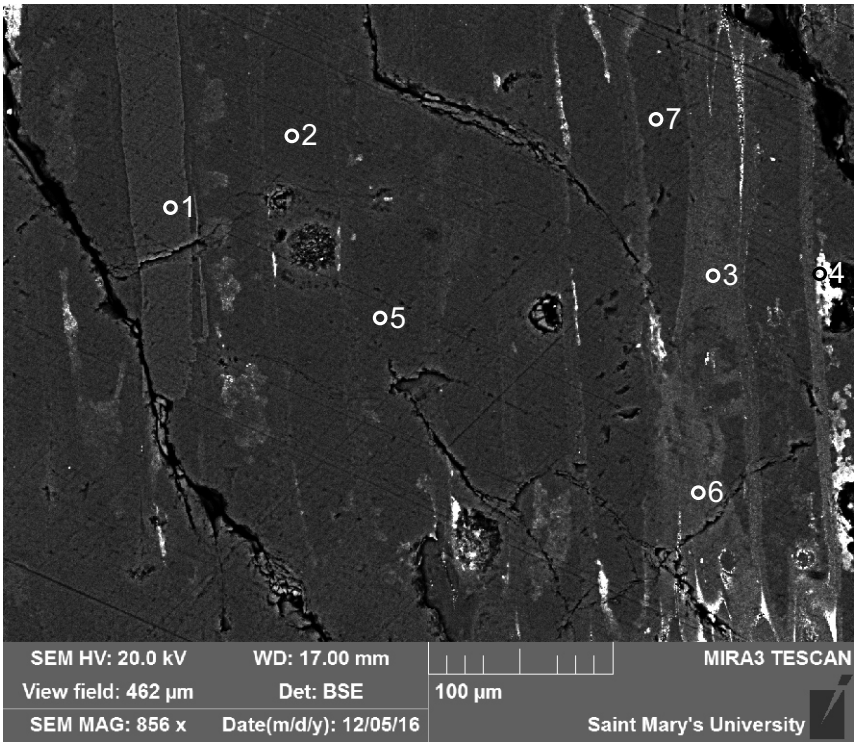

1:Silica
2:Silica
3:Mixture 2
4:"Fe-oxide"+Silica
5:Silica
6:Mixture 2
7:Silica

Figure 2-1.10. Sample 856-1 site 9 (SEM). This site is from a yellowish layer and similar to Fig. 8, Mixture 2 and "Fe-oxide" are seen to be filling wood vessels (3,6) or void (4).

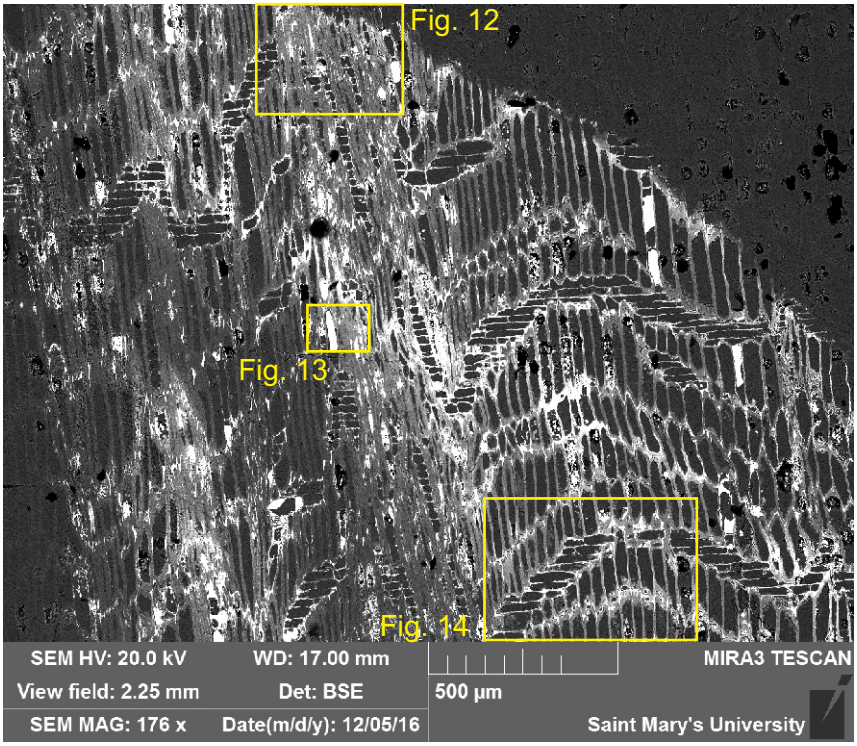

Figure 2-1.11. Sample 856-1 (SEM). An image from a dark orange-red layer of the sample.

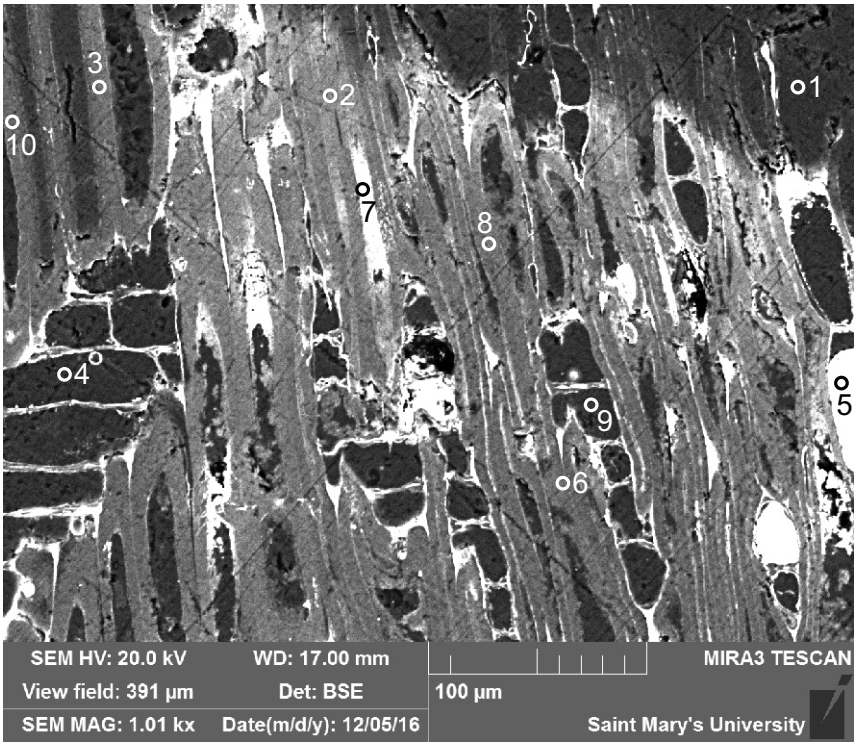

1:Silica
2:Mixture 2
3:Mixture 2
4:Silica
5:"Fe-oxide"+Silica
6:Mixture 2
7:"Fe-oxide"+Silica
8:Mixture 2
9:Silica
10:Mixture 2

Figure 2-1.12. Sample 856-1 site 10 (SEM). Mixture 2 fills wood vessel walls and cross-cut the vessels that have probably been silicified earlier (e.g. 4,9). Some of the mixture appears to have precipitated in to “Fe-oxide” (bright spots)The same mixture also fills the areas connecting the vessels.

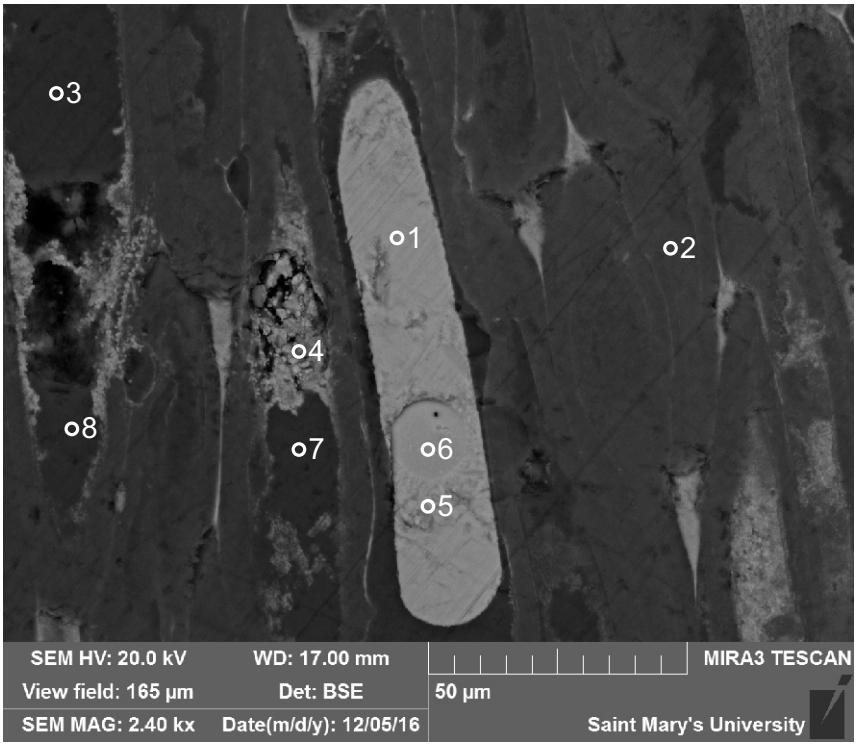

1:"Fe-oxide"+Silica
2:Mixture 2
3:Silica
4:Mixture 2
5:"Fe-oxide"+Silica
6:"Fe-oxide"+Silica
7:Silica
8:Silica

Figure 2-1.13. Sample 856-1 site 11 (SEM). Large wood vessel completely filled with "Fe-oxide" (1,5,6) however traces of SiO_2 is still present.

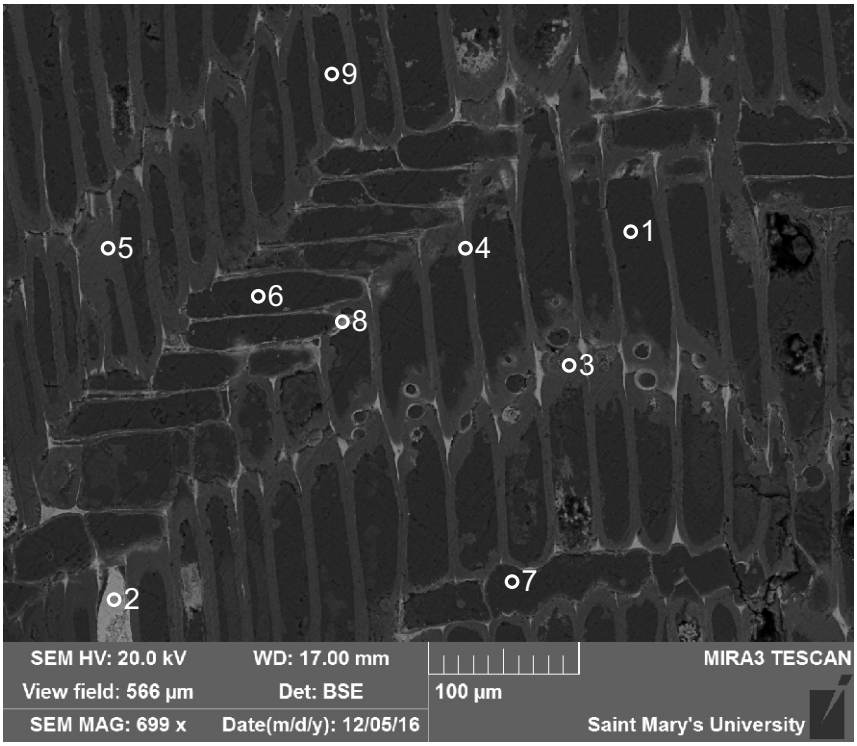

1:Silica
2:"Fe-oxide"+Silica
3:Mixture 2
4:Mixture 2
5:Mixture 2
6:Silica
7:Silica
8:"Fe-oxide"+Silica
9:Silica

Figure 2-1.14. Sample 856-1 site 12 (SEM). A site showing mixture 2 following the weakness pathways that are defined by the wood structure of the vessels.

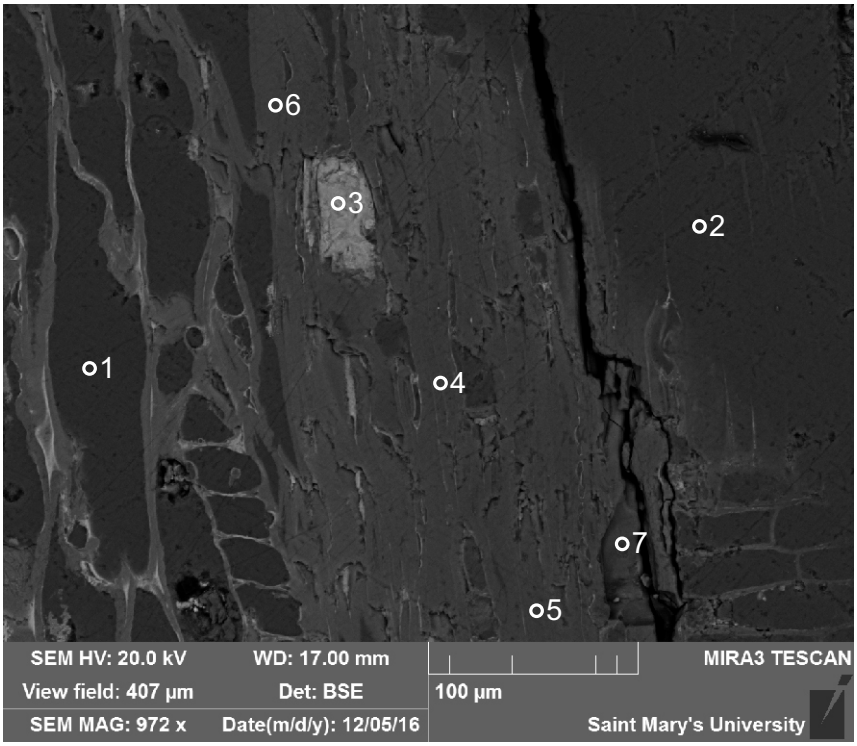

1:Silica
2:Silica
3:"Fe-oxide"+Silica
4:Mixture 2
5:Mixture 2
6:Mixture 2
7:Mixture 2

Figure 2-1.15. Sample 856-1 site 13 (SEM). Another site from the dark orange-red layer showing a mixture of SiO_2 + FeO (4-7) filling wood vessels.

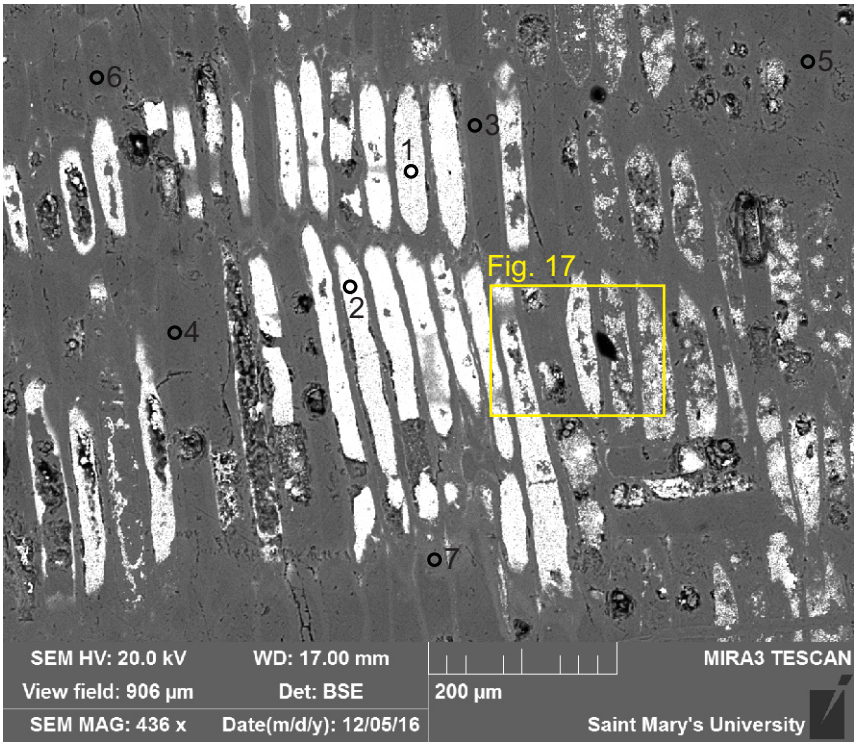

1:"Fe-oxide"+Silica
2:"Fe-oxide"+Silica
3:Silica
4:Silica
5:Silica
6:Silica
7:Silica

Figure 2-1.16. Sample 856-1 site 14 (SEM). Site from a yellow-orange layer showing silicified wood (3-7) with vessels mostly or completely filled with mixture of SiO_2 + FeO.

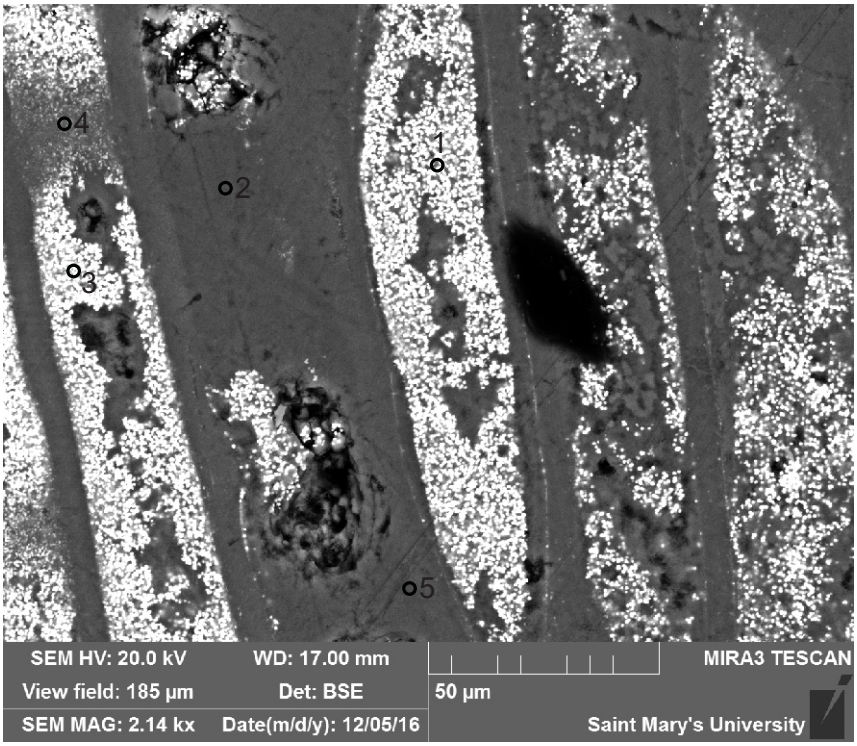

1:"Fe-oxide"+Silica
2:Silica
3:"Fe-oxide"+Silica
4:Mixture 2
5:Silica

Figure 2-1.17. Sample 856-1 site 15 (SEM). Zoomed in image of Fig. 16 shows "Fe-oxide" as dots in the wood vessels.

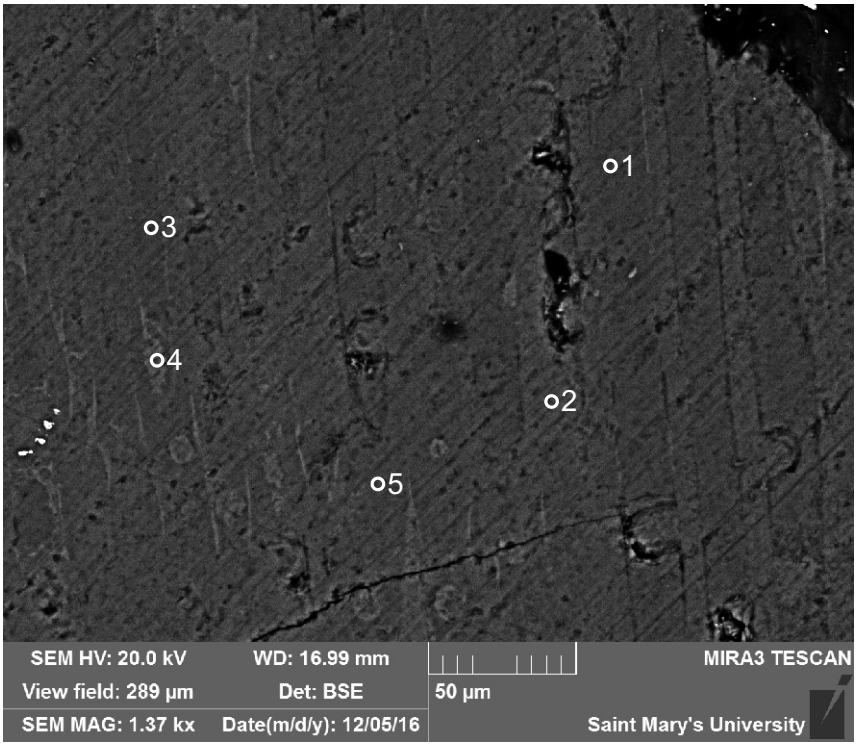

1:Silica
2:Silica
3:Silica
4:Silica
5:Silica

Figure 2-1.18. Sample 856-1 site 16 (SEM). Site from a white layer is completely made up of silicified wood.

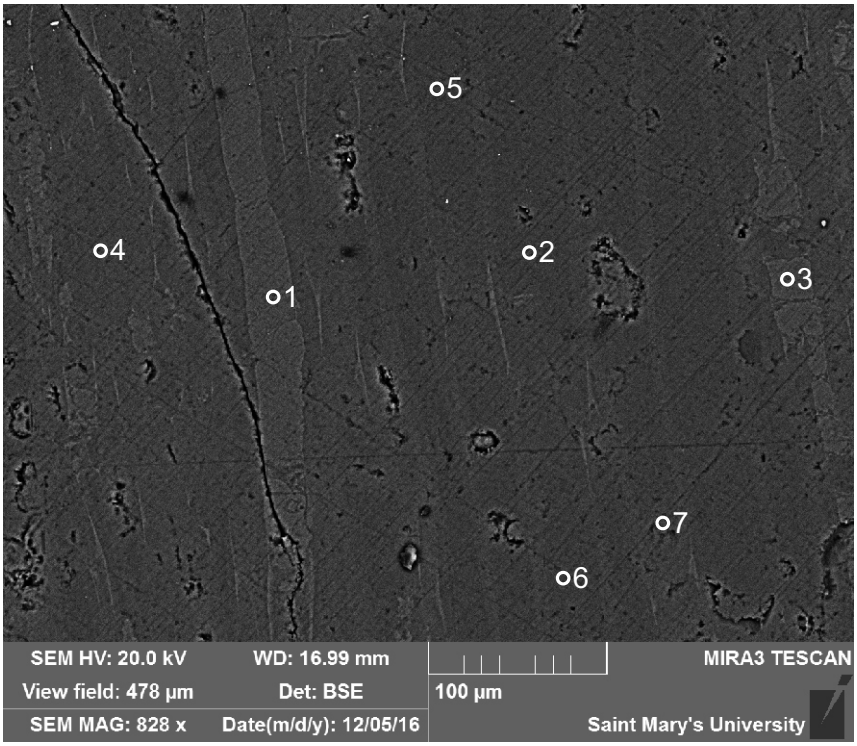

1:Silica
2:Silica
3:Silica
4:Silica
5:Silica
6:Silica
7:Silica

Figure 2-1.19. Sample 856-1 site 17 (SEM). Similar to Fig. 18, this site from a white layer is silicified wood.

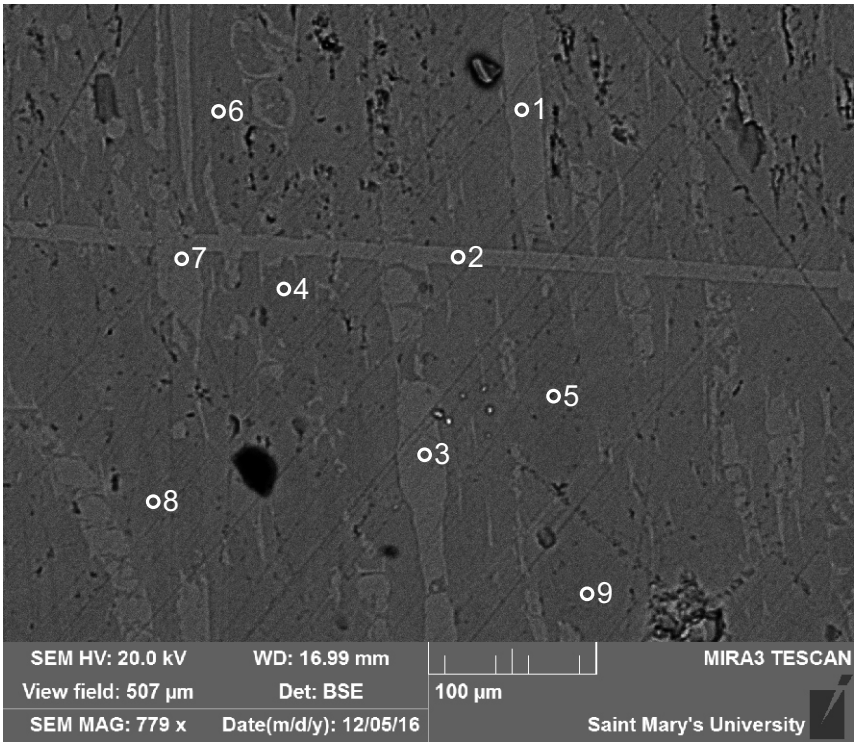

1:Silica
2:Silica
3:Silica
4:Silica
5:Silica
6:Silica
7:Silica
8:Silica
9:Silica

Figure 2-1.20. Sample 856-1 site 18 (SEM). Another site from a white layer. This site shows a silica veinlet (2) cuts across already silicified wood.

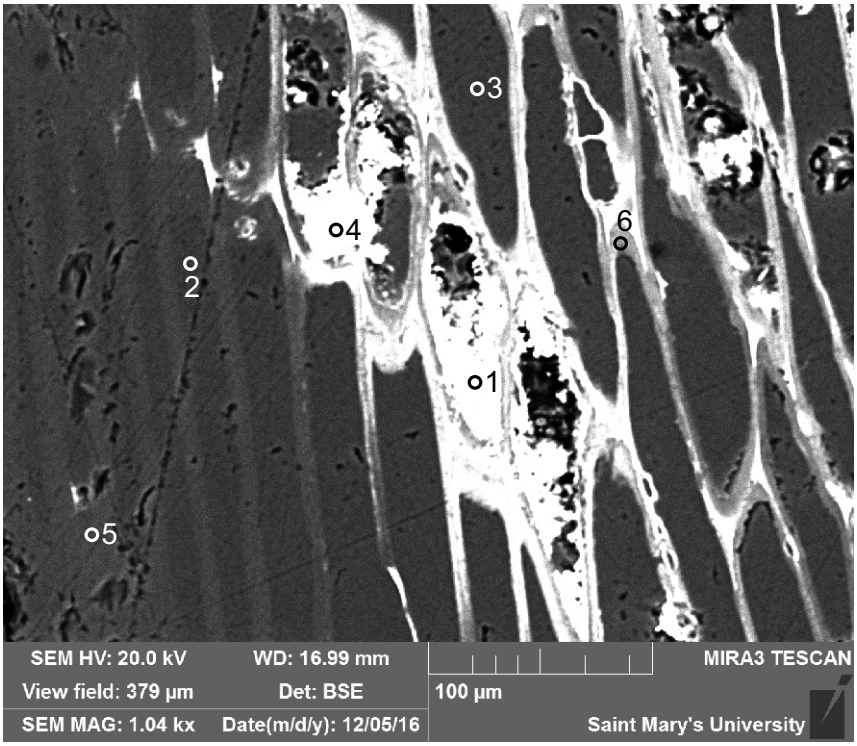

1:"Fe-oxide"+Silica
2:Silica+
3:Silica
4:"Fe-oxide"+Silica
5:Mixture 2
6:Mixture 2

Figure 2-1.21. Sample 856-1 site 19 (SEM). A site from a yellowish-red layer showing a complex pattern of wood vessels defined by the Fe-rich fluid circulation and crystallization.

Table 2-1. EDS chemical analyses of silica and/or silica mixtures from sample 856-1.

Sample	Site	Position	Mineral	SiO2	TiO2	Al2O3	FeO	MgO	CaO	Na2O	K2O	P2O5	SO3	Cl	V2O5	ZnO	As2O3	Nb2O5	Total	Actual Total
856-1	1	1	"Fe-oxide"+Silica	6.36	3.54	0.19	87.59	0.2	0.48	0.35		0.87			0.41				100	100
856-1	1	2	Silica+	92.19	0.34	1.09	0.83	0.36	0.89	0.48			3.35	0.47					100	64
856-1	1	3	Void	71.7	1.51		1.41		1.51					23.87					100	10
856-1	1	4	Silica	99.84					0.16										100	131
856-1	1	5	Silica	100															100	130
856-1	1	6	Silica	99.4			0.21		0.38										100	131
856-1	1	7	Void	90.81			0.51		0.54					8.14					100	28
856-1	2	1	Silica	99.22					0.49							0.29			100	121
856-1	2	2	Silica	99.2					0.5							0.29			100	123
856-1	2	3	Silica	99.71												0.29			100	132
856-1	2	4	Silica	99.05			0.4		0.22							0.34			100	125
856-1	2	5	Silica	99.6												0.4			100	136
856-1	2	6	Silica	99.7												0.3			100	137
856-1	2	7	Silica	99.3			0.12		0.22							0.36			100	128
856-1	3	1	Silica	99.29					0.42							0.17		0.11	100	115
856-1	3	2	Silica	99.75												0.25			100	115
856-1	3	3	Silica	99.14			0.14		0.47							0.25			100	107
856-1	3	4	Silica	99.1			0.16		0.45							0.29			100	107
856-1	3	5	Silica	99.43					0.06							0.19		0.31	100	110
856-1	3	6	Silica	99.78												0.22			100	113
856-1	3	7	Silica	99.83												0.17			100	115
856-1	3	8	Silica	99.34			0.16		0.4							0.1			100	107
856-1	4	1	Silica	98.68			0.92									0.22		0.19	100	113
856-1	4	2	Silica	99.4			0.01									0.35		0.24	100	112
856-1	4	3	Silica	98.98			0.67									0.34			100	114
856-1	4	4	Silica	99.69			0.08									0.23			100	111
856-1	4	5	Silica	99.68			0.12									0.19			100	113
856-1	4	6	Silica	98.85			0.86									0.3			100	115
856-1	4	7	Silica	99.7			0.07									0.22			100	112
856-1	4	8	Silica	99.57			0.11									0.32			100	110
856-1	4	9	Silica	98.95			0.83									0.22			100	118
856-1	4	10	"Fe-oxide"+Silica	36.96	0.49	0.32	59.43		0.35			0.67				0.54	1.24		100	93
856-1	4	11	Mixture 2	71.16	0.27		28.03		0.18								0.36		100	84
856-1	4	12	Mixture 2	52.65	0.84	0.18	44.88		0.33							0.35	0.77		100	93
856-1	4	13	"Fe-oxide"+Silica	31.68	0.63		65.75		0.24			0.38				0.72	0.6		100	83
856-1	5	1	Silica	99.17			0.56									0.26			100	114
856-1	5	2	Silica	99.7			0.04									0.26			100	110
856-1	5	3	Silica	99.54			0.04									0.37		0.05	100	114
856-1	5	4	Silica	98.91			0.82									0.27			100	114
856-1	5	5	Silica	99.63			0.04									0.33			100	112
856-1	5	6	Silica	99.72			0.05									0.24			100	110
856-1	6	1	Silica	99.97			0.03		0										100	104

Table 2-1. EDS chemical analyses of silica and/or silica mixtures from sample 856-1.

Sample	Site	Position	Mineral	SiO2	TiO2	Al2O3	FeO	MgO	CaO	Na2O	K2O	P2O5	SO3	Cl	V2O5	ZnO	As2O3	Nb2O5	Total	Actual Total
856-1	6	2	Silica	99.15			0.54		0.31										100	100
856-1	6	3	Silica	99.33			0.14	0.1	0.34									0.09	100	99
856-1	6	4	Silica	99.95			0.01		0.04										100	104
856-1	6	5	Silica	99.92			0.01		0.07										100	104
856-1	6	6	Mixture 2	62.99	0.61		35.28		0.38			0.46					0.29		100	104
856-1	6	7	Silica	99.73			0.08		0.03									0.16	100	105
856-1	6	8	Mixture 2	55.87	0.71	0.09	42.2	0.22	0.3			0.6							100	103
856-1	6	9	Silica+TiO2	98.63	1.22		0.14												100	105
856-1	6	10	Silica	99.76			0.03		0.21										100	101
856-1	6	11	Silica	99.94			0.06												100	103
856-1	6	12	Silica	99.52			0.12		0.36										100	99
856-1	7	1	"Fe-oxide"+Silica	6.11	0.84	0.61	88.05		0.62	0.52		1.43	0.26				1.55		100	83
856-1	7	2	Mixture 2	97.42			2.47		0.11										100	113
856-1	7	3	Silica	99.81			0.19												100	113
856-1	7	4	"Fe-oxide"+Silica	5.64	0.18		90.69		0.45			1.04			0.46		1.55		100	85
856-1	7	5	Silica	99.91			0.09		0										100	109
856-1	7	6	Mixture 2	97.8			2.2												100	114
856-1	7	7	Silica	100															100	112
856-1	7	8	Mixture 2	97.8	0.11		2.01		0.09										100	114
856-1	7	9	Mixture 2	97.97	0.13		1.9												100	114
856-1	7	10	Silica	99.9														0.1	100	111
856-1	7	11	Silica	99.89														0.11	100	115
856-1	8	1	Silica	99.92			0.04		0.01									0.04	100	111
856-1	8	2	Mixture 2	98.59			1.28		0.05								0.08		100	114
856-1	8	3	Mixture 2	98.8			1.2												100	113
856-1	8	4	Mixture 2	97.78			2.22												100	114
856-1	8	5	Silica	100															100	111
856-1	8	6	Silica	99.32			0.68												100	111
856-1	8	7	Epidote	44.14		23.21	10.11		21.71	0.52	0.3								100	111
856-1	8	8	Silica	100															100	119
856-1	9	1	Silica	99.93			0.04		0.03										100	117
856-1	9	2	Silica	100															100	111
856-1	9	3	Mixture 2	97.28			2.72												100	114
856-1	9	4	"Fe-oxide"+Silica	41.51	0.2		56.79		0.35			0.34	0.14				0.67		100	88
856-1	9	5	Silica	100															100	112
856-1	9	6	Mixture 2	96.68			3.11		0.06									0.15	100	114
856-1	9	7	Silica	100															100	113
856-1	10	1	Silica	99.73			0.16		0									0.11	100	114
856-1	10	2	Mixture 2	88.32			11.46		0.06								0.15		100	112
856-1	10	3	Mixture 2	90.81			9.13		0.06										100	112
856-1	10	4	Silica	99.53			0.42		0.05										100	115
856-1	10	5	"Fe-oxide"+Silica	4.66	0.5		91.46		0.5			1.35			0.39		1.14		100	87

Table 2-1. EDS chemical analyses of silica and/or silica mixtures from sample 856-1.

Sample	Site	Position	Mineral	SiO2	TiO2	Al2O3	FeO	MgO	CaO	Na2O	K2O	P2O5	SO3	Cl	V2O5	ZnO	As2O3	Nb2O5	Total	Actual Total
856-1	10	6	Mixture 2	91.02			8.98												100	115
856-1	10	7	"Fe-oxide"+Silica	36.68			60.76		0.32			0.72			0.35		1.16		100	91
856-1	10	8	Mixture 2	90.63			9.37												100	113
856-1	10	9	Silica	99.46			0.54												100	114
856-1	10	10	Mixture 2	91.47			8.34		0.01								0.18		100	113
856-1	11	1	"Fe-oxide"+Silica	4.24		0.33	91.84		0.37			1.09	0.23		0.45		1.44		100	86
856-1	11	2	Mixture 2	85.93			13.73	0.15	0.1									0.09	100	110
856-1	11	3	Silica	99.63			0.37												100	111
856-1	11	4	Mixture 2	55.17	0.22		43.21		0.22			0.48					0.71		100	101
856-1	11	5	"Fe-oxide"+Silica	4.81	0.2	0.3	91.16		0.49			1.22	0.2		0.45		1.15		100	86
856-1	11	6	"Fe-oxide"+Silica	3.96	0.14	0.49	91.88		0.4			1.16	0.14		0.41		1.41		100	87
856-1	11	7	Silica	99.29			0.59											0.12	100	114
856-1	11	8	Silica	99.4			0.45											0.15	100	112
856-1	12	1	Silica	99.55			0.39		0.06										100	113
856-1	12	2	"Fe-oxide"+Silica	4.37		0.24	91.17		0.48			1.38	0.2		0.58		1.58		100	86
856-1	12	3	Mixture 2	85.23			14.65		0.12										100	111
856-1	12	4	Mixture 2	86.72			13.21		0.07										100	110
856-1	12	5	Mixture 2	85.23			14.7		0.07										100	108
856-1	12	6	Silica	99.31			0.5		0.03									0.17	100	114
856-1	12	7	Silica	99.53			0.42											0.05	100	115
856-1	12	8	"Fe-oxide"+Silica	25.84			71.14		0.35			0.94			0.39		1.35		100	93
856-1	12	9	Silica	99.61			0.37		-0.01									0.03	100	111
856-1	13	1	Silica	99.39			0.5		0.05									0.06	100	114
856-1	13	2	Silica	99.87			0.08		0.05										100	114
856-1	13	3	"Fe-oxide"+Silica	3.53	0.48	0.53	91.33		0.69			1.88	0.34				1.21		100	79
856-1	13	4	Mixture 2	89.28			10.67		0.05										100	113
856-1	13	5	Mixture 2	90.87			9.13												100	115
856-1	13	6	Mixture 2	85.8			14.2												100	109
856-1	13	7	Mixture 2	80.52			19.48												100	35
856-1	14	1	"Fe-oxide"+Silica	41.44	0.17		57.79	0.27	0.14							0.19			100	100
856-1	14	2	"Fe-oxide"+Silica	28.09	0.27		70.56	0.23	0.22			0.46	0.17						100	101
856-1	14	3	Silica	99.23			0.6											0.17	100	116
856-1	14	4	Silica	99.6			0.28											0.11	100	116
856-1	14	5	Silica	99.42			0.56		0.03										100	115
856-1	14	6	Silica	99.35			0.46		0.07									0.11	100	116
856-1	14	7	Silica	98.12			1.78									0.09		0	100	118
856-1	15	1	"Fe-oxide"+Silica	47.46	0.26		51.12		0.14			0.26				0.33	0.43		100	104
856-1	15	2	Silica	99.55			0.45												100	114
856-1	15	3	"Fe-oxide"+Silica	40.58	0.29		58.76									0.37			100	97
856-1	15	4	Mixture 2	91.26			8.74												100	109
856-1	15	5	Silica	99.68			0.32												100	114
856-1	16	1	Silica	100															100	112

Table 2-1. EDS chemical analyses of silica and/or silica mixtures from sample 856-1.

Sample	Site	Position	Mineral	SiO2	TiO2	Al2O3	FeO	MgO	CaO	Na2O	K2O	P2O5	SO3	Cl	V2O5	ZnO	As2O3	Nb2O5	Total	Actual Total
856-1	16	2	Silica	100															100	117
856-1	16	3	Silica	100															100	112
856-1	16	4	Silica	100															100	117
856-1	16	5	Silica	100															100	115
856-1	17	1	Silica	99.88														0.12	100	118
856-1	17	2	Silica	100															100	112
856-1	17	3	Silica	99.92														0.08	100	122
856-1	17	4	Silica	100															100	115
856-1	17	5	Silica	100															100	112
856-1	17	6	Silica	100															100	116
856-1	17	7	Silica	100															100	116
856-1	18	1	Silica	99.8												0.2			100	123
856-1	18	2	Silica	99.83														0.17	100	123
856-1	18	3	Silica	99.7														0.3	100	124
856-1	18	4	Silica	99.91														0.09	100	117
856-1	18	5	Silica	99.86														0.14	100	120
856-1	18	6	Silica	99.84														0.16	100	116
856-1	18	7	Silica	99.85														0.15	100	123
856-1	18	8	Silica	99.77														0.23	100	117
856-1	18	9	Silica	99.89														0.11	100	121
856-1	19	1	"Fe-oxide"+Silica	16.37	0.35		80.48		0.32			0.77	0.27			0.38	1.06		100	92
856-1	19	2	Silica+	99.45			0.15									0.23		0.17	100	118
856-1	19	3	Silica	99.05			0.56									0.14		0.25	100	118
856-1	19	4	"Fe-oxide"+Silica	10.62	0.61	0.4	85.33		0.32			0.71	0.24			0.61	1.15		100	90
856-1	19	5	Mixture 2	98	0		1.67		0.03							0.16		0.14	100	121
856-1	19	6	Mixture 2	89.97			9.53		0.06							0.44			100	112

Appendix 2-2: Electron microprobe (EMP) chemical analyses of silica in sample 856-1 (petrified wood)

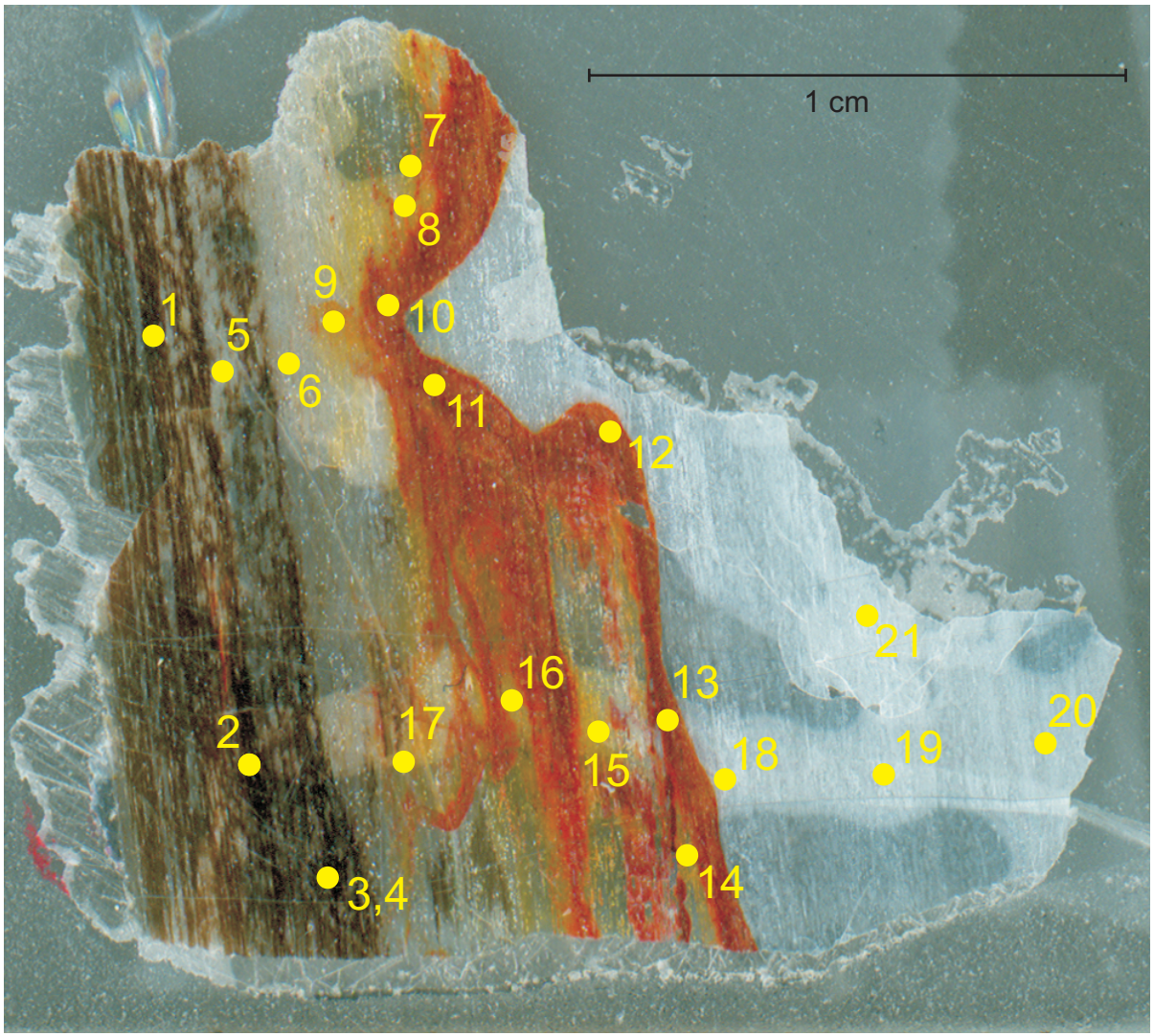

Figure 2.1. Scanned thin section of petrified wood (sample 856-1) showing spots of microprobe analyses.

Table 2-2. Electron microprobe chemical analyses of silica and/or silica mixtures in sample 856-1 (petrified wood).

Sample	Site		Mineral	SiO2 (wt%)	FeO (%wt)	TiO2 (ppm)	Al2O3 (ppm)	MgO (ppm)	CaO (ppm)	Na2O (ppm)	P2O5 (ppm)	As2O3 (ppm)	SO3 (ppm)	CoO (ppm)	V2O5 (ppm)	ZnO (ppm)	BaO (ppm)	Nb2O5 (ppm)	SrO (ppm)	TOTAL
856-1	Black	1	Silica	97.37	0.04	2			50		285		267	90		839		609	358	97.4871
856-1	Black	2	Silica	94.80	0.01			48	313	137	65				100	499			378	94.8209
856-1	Black	3	Silica	92.87	0.14	524		203	2911	203	251		184	76	625	658		154	87	93.5247
856-1	Black'	4	Silica	97.08	0.05				486	72	198	9	134	8	110	507		337		97.197
856-1	white (in black)	5	Silica	94.55	0.20	745		233	2944	226		221	300	181	46	234	165		344	95.2489
856-1	white (in black)	6	Silica	92.76	0.49	960	50	434	2756	434	4	222	783		181	242		263	818	93.867
856-1	yellow	7	Silica+Fe-oxide	77.40	11.80	768	447	299	747	619	814	1172	164		420	291			177	89.5587
856-1	yellow	8	Silica+Fe-oxide	75.94	9.28	230	758	60	648	462	364	650	131	35	583	374		4	227	85.6512
856-1	yellow	9	Silica+Fe-oxide	88.34	6.18	637	145	90	604	291	208	289	116	6	530	458		193	50	94.8366
856-1	orange	10	Fe-oxide+Silica	24.29	57.82	3016	2858	1500	3680	757	5320	8292	1034	244	2104	1046				84.8333
856-1	orange	11	Fe-oxide+Silica	2.90	78.50	4978	1783	233	4014	473	7878	7726	648		2835	824	7	101		84.4475
856-1	orange	12	Fe-oxide+Silica	1.66	71.04	4276	3037	899	7075	791	13211	7306	1741	407	1741	1427				76.6492
856-1	orange	13	Fe-oxide+Silica	8.06	70.15	3278	2874	1309	3232	665	4397	9764	990		1861	654	44	396		81.0454
856-1	yellow(in orange)	14	Silica+Fe-oxide	78.45	10.84	260	645	232	854	476	492	907	49		129	254			532	89.6766
856-1	yellow(in orange)	15	Silica+Fe-oxide	62.52	24.83	330	1958	759	1386	1409	1397	1881	336		1068				429	88.3608
856-1	yellow(in orange)	16	Silica+Fe-oxide	82.64	6.71	126	499	257	573	298	296	747	546					877	429	89.7284
856-1	yellow(in orange)	17	Silica+Fe-oxide	82.79	4.47	51	353	122	565	422	84	435	116			113			430	87.3542
856-1	white	18	Silica	95.76	0.04	97			253	19	42				78	485		383	987	95.9021
856-1	white	19	Silica	97.93	0.02	218			202	58	56	37	84			386			456	97.8933
856-1	white	20	Silica	96.96	0.02	48			181	298			67	56	102	560			237	97.0249
856-1	white	21	Silica	96.02	0.03	402	187		103	236	316		67			477		382		96.1336

Appendix 3: Representative table of EDS mineral analyses from each of the studied samples

Appendix 3. Representative mineral EDS analyses for each of the studied samples.

Sample	Site	Position	Mineral	SiO2	TiO2	Al2O3	FeO	MnO	MgO	CaO	Na2O	K2O	P2O5	SO3	F	Cl	As2O3	CoO	CuO	V2O5	ZnO	ZrO2	BaO	La2O3	Ce2O3	Nd2O3	ThO2	HfO2	WO3	Total	Actual Total
800a	8	8	"Fe-oxide"	0.37			98.03	1.17		0.23						0.21														100	58
800a	11	6	Apatite	4.02	0.45	0.65	3.77		0.27	44.94	0.25	0.25	38.89		5.83	0.67														100	119
800a	14	2	Ilmenite	1.06	41.02	0.93	53.04	0.57	3.38																					100	87
800a	11	4	Ilmenite	1.23	36.82	0.44	60.95	0.56																						100	102
800a	11	5	K-feldspar	68.1		17.78	1.67			1.22	4.35	6.88																		100	120
800a	12	6	K-feldspar	66.77		19.2	0.4			1.67	7.51	4.46																		100	116
800a	2	5	Mixture 1	32.05			10.25	47.06	6.65	0.7		0.21											3.07							100	89
800a	5	1	Mixture 1	43.51		0.44	14.19	34.08	4.02	0.93													2.83							100	91
800a	1	1	Silica (Am)	100																										100	115
800a	1	3	Silica (Am)	100																										100	115
800a	1	2	Silica (Mc)	100																										100	123
800a	1	4	Silica (Mc)	100																										100	127
800a	14	1	Ti-Magnetite	0.61	7.99	0.89	84.73	1.15	4.63																					100	83
800a	14	3	Ti-Magnetite	0.67	11.28	0.91	78.64	1.34	7.15																					100	83
800a	19	1	Fluorapatite	0.58			0.8			45.96			43.46	0.69	6.96	0.43													1.13	100	141
800a	20	4	Fluorapatite	0.78			0.7			45.54			43.84		7.44	0.49													1.21	100	140
806	12	1	"Fe-oxide"+Silica	30.83		1.65	64.14		1.99	0.69		0.7																		100	77
806	10	1	"Fe-oxide"+Silica	32.57		3.48	59.74		2.34	0.63		1.06									0.19									100	79
806	19	3	Romanechite					81.23	2.86	0.82		0.5							0.74				13.86							100	87
806	13	1	"Mn-oxide"+	7.47			8.83	64.64	0.79	0.9		0.4											16.97							100	73
806	13	8	"Mn-oxide"+	8.25			9.92	63.26	0.75	0.91		0.45											16.45							100	73
806	4	10	Andesine	58.98		25.35	0.76			7.73	6.72	0.46																		100	101
806	5	12	Andesine	58.04		25.91	0.93			8.48	6.21	0.43																		100	100
806	9	4	Diopside	53.98	0.42	2.15	7.76	0.44	15.32	19.45	0.46																			100	99
806	11	3	Hornblende	44.79	3.57	10.97	12.01	0.23	13.96	10.78	2.62	1.07																		100	95
806	17	2	Ilmenite	0.55	47.54		45.58	3.21	3.12																					100	114
806	5	13	K-feldspar	65.61		18.71	0.68			1.13	4.77	8.33											0.77							100	99
806	7	4	K-feldspar	65.12		18.01	2.79			1.04	4.94	8.11																		100	101
806	3	1	Labradorite	55.25		28.4	0.59			10.53	4.9	0.33																		100	99
806	6	8	Oligoclase	60.45		23.85	1.16			6.19	7.06	1.3																		100	101
806	1	7	Silica (Am)	98.19		0.95	0.25				0.61																			100	93
806	8	8	Silica (Am)	98.25		1.07					0.68																			100	104
806	9	7	Ti-Magnetite		4.82		92.52	0.76	1.9																					100	78
806	10	7	Ti-Magnetite		5.59		91.03	0.67	2.39												0.32									100	79
806	17	6	Zirconolite?	2.33	28.42	0.75	8.56			6.15												42.29				4.8	2.13		4.57	100	111
807	19	4	"Fe-oxide"+silica	27.64	0.73	69.45		1.51	0.68																					100	94
807	19	5	"Fe-oxide"+silica	37.17	0.87	58.67		2.3	0.71		0.27																			100	104
807	1	1	Mixture 1	16.72		14.94	50.47	1.19	0.72														15.96							100	47
807	4	1	Mixture 1	24.5		12.51	46.29	1.76	1.08		0.25												13.61							100	51
807	19	2	Mixture 2	66.88	1.28	27.17		3.07	1.27		0.34																			100	110
807	20	3	Mixture 2	68.09	1.77	25.54		2.76	1.35		0.47																			100	108
807	6	3	Silica	99.66		0.34																								100	56
839	2	4	Andesine	58.32		25.84	0.87			8.95	5.1	0.92																		100	113
839	3	6	Andesine	58.92		25.81	0.75			8.66	5	0.87																		100	113
839	8	3	Apatite	1.02			0.5			48.76			43.93		2.58	0.64									1				1.57	100	109
839	13	1	Apatite	0.48			0.26			48.4			44.13		4.62	0.48													1.63	100	116
839	7	3	Biotite	44.34	6.21	15.15	12.33		12.88			9.08																		100	103
839	8	2	Biotite	47.31	4.56	14.85	11.37		13.55		0.58	7.78																		100	99
839	11	9	Ilmenite	2.46	51.12	0.97	40.81	1.03	3.3	0.32																				100	96
839	11	2	Ilmenite (altered)	12.52	76.77	1.92	4.83		0.44	1.05												2.46								100	94
839	11	8	K-feldspar	65.81		19.27	0.46			1.29	4.36	7.84											0.96							100	111
839	18	3	K-feldspar	67.41		17.95	0.78			0.69	2.67	9.08											1.42							100	106
839	9	1	Labradorite	55.84		27.47	0.66			10.68	4.62	0.73																		100	109

Appendix 3. Representative mineral EDS analyses for each of the studied samples.

Sample	Site	Position	Mineral	SiO2	TiO2	Al2O3	FeO	MnO	MgO	CaO	Na2O	K2O	P2O5	SO3	F	Cl	As2O3	CoO	CuO	V2O5	ZnO	ZrO2	BaO	La2O3	Ce2O3	Nd2O3	ThO2	HfO2	WO3	Total	Actual Total
839	1	3	Oligoclase	62.34	0.29	23.03	2.44		2.18	5.54	2.06	0.66		1.47																100	87
839	7	1	Oligoclase	60.95		24.22	0.38			6.47	6.96	1.01																		100	114
839	14	7	Silica	97.05		2.33				0.62																				100	102
839	14	2	Silica	96.74		2.29	0.2			0.61		0.16																		100	103
839	12	7	Silica+Smectite	78.71		14.38	3.55		2.11	0.88		0.19				0.18														100	68
839	13	9	Silica+Smectite	79.52		12.01	4.94		2.04	1.17		0.32																		100	75
839	1	6	Smectite+Silica	69.75		21.3	2.5		4.38	1.72	0.35																			100	90
839	2	2	Smectite+Silica	68.61		21.59	2.8		3.08	2.16	1.34	0.43																		100	87
839	13	2	TiO2	6.73	86.56	1	1.91			1.05												2.76								100	96
839	6	2	Zircon	31.49																		67.22						1.29		100	117
842	4	1	Andesine	57.72		26.26	0.45			9.16	5.52	0.89																		100	132
842	4	6	Andesine	61.47		24.04	0.26			6.17	7.47	0.6																		100	137
842	7	2	Biotite	41.48	4.45	14.9	8.3		17.11			8.3			5.46															100	130
842	12	4	Ilmenite	3.11	68.74		26.84		1.3																					100	93
842	9	1	Ilmenite	1.04	68.41		30.35			0.21																				100	107
842	6	4	K-feldspar	65.99	0.65	21.48	1.74			0.51	2.98	6.65																		100	131
842	7	3	K-feldspar	66.13	0.42	20.13	1.61		0.79	0.48	2.36	7.49		0.59																100	131
842	7	1	Silica (Qz)	99.36		0.42	0.22																							100	136
842	5	1	Silica (Qz)	99.67		0.33																								100	134
842	6	6	Smectite	62.51	0.92	29.02	5.12		0.72	0.61	0.25	0.85																		100	122
842	9	2	Smectite	65.44	0.83	26.28	4.79		0.82	0.82	0.26	0.75																		100	123
842	6	1	Ti-Magnetite	0.54	5.48	0.65	89.62	0.86	2.85																					100	107
842	13	1	Organic	58.33												41.67														100	2
842	15	9	Organic	29.41		11.76	47.06									11.76														100	1
843	1	9	Biotite	43.76	3	17.78	12.34		15.08		1.15	6.9																		100	176
843	7	1	Biotite	39.71	4.33	14.76	17.81		13.51		0.81	9.08																		100	137
843	5	8	Ilmenite	0.52	59.12		40.36																							100	130
843	6	6	Ilmenite	0.54	58.86		40.6																							100	131
843	1	3	Ilmenite+Chlorite	6.92	55.3	2.4	32.24	0.69	2.45																					100	127
843	3	7	K-feldspar+	63.31	0.71	24.25	3.05		0.38		1.64	6.66																		100	118
843	8	3	Muscovite+other	54.12	3.66	24.88	6.35		7.18	0.29	0.47	3.05																		100	171
843	6	9	Silica	99.26		0.51						0.23																		100	159
843	8	1	Silica	98.82		0.71	0.27				0.2																			100	162
843	5	3	Smectite	58.22	0.5	32.14	7.15		0.73	0.36	0.38	0.34				0.17														100	124
843	8	4	Smectite	63.16	0.65	28.94	5.06		0.85	0.33	0.48	0.52																		100	161
843	11	3	Smectite+Hematite	49.65	0.63	13.17	34.36		0.35	0.43	0.49	0.41	0.5																	100	127
843	6	2	Smectite+Hematite	47.3	0.89	14.45	35.28		0.51	0.4	0.38	0.19	0.59																	100	129
843	4	3	Ti-Magnetite	0.91	17	2.1	75.37		2.44	0.74			0.65							0.79										100	127
843	9	3	Ti-Magnetite	2.04	10.08	1.77	82.54	0.48	2.56												0.54									100	131
844a	12	11	Albite	67.9		19.85				1.57	10.01	0.66																		100	119
844a	10	2	Apatite				0.33		0.4	47.14			44.02		6.17	0.22													1.73	100	127
844a	3	1	Apatite	0.54						47.97	0.37		42.77	0.56	5.76	0.26													1.77	100	154
844a	7	7	Biotite (C)	43.15	5.67	14.64	11.08		16.55		0.72	8.19																		100	111
844a	6	1	Biotite (C)	40.39	7.36	14.95	9.32		18.06		0.82	9.1																		100	109
844a	11	6	Biotite (CAI)	44.93		14.64	3.68		19.5	0.42	0.52	7.45			8.87															100	110
844a	14	8	Biotite (CAI)	47.44		19	3.84		15.99	0.47	0.37	6.08			6.82															100	107
844a	1	3	Biotite (CS)	57.94	0.95	14.45	7.27		12.65	0.88	0.58	5.08				0.19														100	118
844a	13	8	Biotite (CS)	47.87	0.45	18.84	3.76		16.1		0.41	6.38			6.18															100	106
844a	5	4	Biotite (CV)	41.94	9.29	14.46	7.49		17.89		0.57	8.36																		100	113
844a	15	5	Glass	73.35		18.36	0.35				1.66	6.27																		100	94
844a	1	8	Glass	73.55		14.74	0.88		0.31	0.48	2.67	7.37																		100	138
844a	8	14	Kaolinite	77.33		21.97	0.53									0.18														100	84
844a	12	8	Kaolinite	55.03		36.06	1.77		4.87			2.27																		100	84

Appendix 3. Representative mineral EDS analyses for each of the studied samples.

Sample	Site	Position	Mineral	SiO2	TiO2	Al2O3	FeO	MnO	MgO	CaO	Na2O	K2O	P2O5	SO3	F	Cl	As2O3	CoO	CuO	V2O5	ZnO	ZrO2	BaO	La2O3	Ce2O3	Nd2O3	ThO2	HfO2	WO3	Total	Actual Total
844a	2	5	K-feldspar	68.18		17.09					2.81	11.93																		100	124
844a	5	3	K-feldspar	66.88	0.3	18.61	0.23			0.83	5.97	7.18																		100	116
844a	4	1	Rutile	1.54	95.2	0.74	1.02			0.35			1.14																	100	102
844a	2	3	Silica	99.36		0.42					0.22																			100	154
844a	10	1	Silica	99.64		0.36																								100	125
844a	3	2	Zircon	31.12																		68.88								100	152
844b	9	1	Apatite				0.41			48.42			43.84	0.86	4.07	0.55													1.84	100	145
844b	15	1	Apatite							48.15			42.84	0.56	6.43	0.32													1.71	100	147
844b	11	1	Biotite	42.77	5.75	16.72	12.34	0.27	13.45		0.53	8.17																		100	126
844b	7	5	Biotite (altered)	45.55		14.49	5.21		19.09		0.34	7.23			7.84	0.26														100	128
844b	11	2	Glass	74.31		14.61	0.24			0.5	3.99	6.35																		100	140
844b	2	4	Glass	71.22		18.93					2.65	7.2																		100	107
844b	8	1	Illite	53.49	2.19	16.5	6.24		14.09	0.71	0.39	6.04				0.35														100	89
844b	7	8	Illite	53.06	4.48	15.76	5.07		13.34		0.7	7.34				0.26														100	93
844b	11	3	Kaolinite	57.87		41.69	0.44																							100	92
844b	12	11	Kaolinite	59.77		40.23																								100	110
844b	12	3	K-feldspar	68.58		17.5					3.79	10.13																		100	141
844b	7	11	K-feldspar	66.56		18.07	0.33		0.31		2.93	11.12											0.67							100	132
844b	7	3	Silica	100																										100	141
844b	5	1	Silica	99.53		0.47																								100	144
844b	12	13	TiO_2	7.04	84.11	2.35	1.56		1.26	0.63		0.77										2.28								100	121
844b	6	2	Zircon	31.32																		68.68								100	141
844b	19	2	Monazite	10.25		2.45	0.79		4.18		1.02	33.22	1.08	0	0.57							1.94	2.3	12.43	23.07	6.72				100	65
846a	3	1	"Mn-oxide"			0.91		90.59		0.7		1.77						1.06			1.09		3.88							100	94
846a	5	9	"Mn-oxide"	0.65		1.09		84.61		0.52	0.86	2.61						0.47					9.19							100	102
846a	2	1	Biotite	40.31	7.65	14.14	12.12		16.17		0.76	8.84																		100	138
846a	7	9	Glass	70.66		17.3		1.34		0.6	3.36	6.74																		100	141
846a	10	1	Glass	74.91		14.31				0.49	3.22	7.07																		100	143
846a	25	5	Glass (altered)	68.93		16.82				0.57	2.92	10.75																		100	133
846a	25	6	Glass (altered)	71.16		15.86					2.47	10.5																		100	123
846a	2	5	Kaolinite	54.7		40.18	2.88	2								0.24														100	105
846a	9	3	Kaolinite	56.61		43.39																								100	117
846a	13	3	K-feldspar	66.9		19.11	0.26			1.42	6.53	5.78																		100	140
846a	5	1	K-feldspar	66.91		18.44	0.28	0.75		0.6	5.62	7.39																		100	147
846a	11	2	Silica	99.28		0.37	0.35																							100	144
846a	16	7	Silica	99.62		0.38																								100	146
846a	13	3	K-feldspar	66.9		19.11	0.26			1.42	6.53	5.78																		100	140
846a	5	1	K-feldspar	66.91		18.44	0.28	0.75		0.6	5.62	7.39																		100	147
846a	26	12	"Mn-oxide"+"Fe-oxide"	2.95		6.55	51.5	29.88		0.41			5.54			0.38							2.8		1.04					100	59
846a	26	13	"Mn-oxide"+"Fe-oxide"	29.43	5.27	9.58	23.98	23.73		0.44	0.85	3.19	2.49																	100	86
846b	21	9	Andesine	59.64		24.65	0.63			6.96	6.8	0.79											0.54							100	129
846b	6	5	Glass	72.53		15.29	0.31				3.13	8.73																		100	125
846b	22	3	Glass	72.52	5.03	12.48	1.23			0.36	2.34	6.04																		100	121
846b	1	2	Hematite	2.93		4.27	81.88			0.57			3.43	1			5.92													100	85
846b	20	3	Hematite	4		4.84	83.02			0.39			3.55	0.88			3.32													100	90
846b	5	3	Jarosite			0.82	45.54					9.54	3.1	39.2			1.81													100	93
846b	6	6	Jarosite			0.9	45.89					9.11	3.49	39			1.61													100	93
846b	11	5	Kaolinite	57.11		42.21	0.69																							100	111
846b	12	1	Kaolinite	56.78		42.42	0.54			0.26																				100	109
846b	10	3	K-feldspar	65.06		18.04	1.32			0.61	5.32	7.69		0.73									1.22							100	132
846b	11	3	K-feldspar+	69.38	0.42	16.63	0.59			0.52	4.36	8.1																		100	131
846b	4	6	K-feldspar+ (H)	69.48		15.89	1.48				2.81	9.34		1																100	120

Appendix 3. Representative mineral EDS analyses for each of the studied samples.

Sample	Site	Position	Mineral	SiO2	TiO2	Al2O3	FeO	MnO	MgO	CaO	Na2O	K2O	P2O5	SO3	F	Cl	As2O3	CoO	CuO	V2O5	ZnO	ZrO2	BaO	La2O3	Ce2O3	Nd2O3	ThO2	HfO2	WO3	Total	Actual Total
846b	16	6	K-feldspar+ (H)	69.21		17.43	0.41				2.63	10.32																		100	125
846b	25	13	K-feldspar+ (I)	65.34		18.5	0.37			0.57	4.42	8.64											2.16							100	123
846b	9	4	K-feldspar+ (I)	65.75		18.49	0.57			0.72	4.98	8.06											1.44							100	131
846b	19	1	Oligoclase	63.07		22.56	0.34			4.87	7.78	1.37																		100	128
846b	21	13	Oligoclase	59.74		24.68	1.11			6.85	6.81	0.81																		100	131
846b	30	6	Silica	99.76			0.24																							100	130
846b	22	11	Silica	99.08		0.6					0.32																			100	131
846b	24	1	Zircon	31.48																		68.52								100	128
847	3	1	Biotite	40.39	6.79	14.02	15.74		13.71		0.79	8.56																		100	67
847	8	1	Fe-hydroxide	1.78		2.48	94.61						1.13																	100	51
847	8	3	Fe-hydroxide	1.96		2.16	94.82						1.06																	100	50
847	4	4	Silica (Am)	99.19		0.56					0.26																			100	77
847	7	1	Silica (Am)	97.67		1.34	0.56			0.28		0.15																		100	75
847	3	5	Silica+Smectite	88.74		5.29	2.56		0.3	0.51	1	1.6																		100	66
847	1	5	Silica+Smectite	76.59		11.23	9.34		0.97	1.58		0.28																		100	60